



Universitat Autònoma de Barcelona

ADVERTIMENT. L'accés als continguts d'aquesta tesi queda condicionat a l'acceptació de les condicions d'ús establertes per la següent llicència Creative Commons:  http://cat.creativecommons.org/?page_id=184

ADVERTENCIA. El acceso a los contenidos de esta tesis queda condicionado a la aceptación de las condiciones de uso establecidas por la siguiente licencia Creative Commons:  <http://es.creativecommons.org/blog/licencias/>

WARNING. The access to the contents of this doctoral thesis it is limited to the acceptance of the use conditions set by the following Creative Commons license:  <https://creativecommons.org/licenses/?lang=en>



Universitat Autònoma de Barcelona

***In vivo* interactions between food availability and
nanoparticles in *Caenorhabditis elegans***

Zhongrui Luo

Doctoral Thesis

Doctoral studies in Materials Science

Director and Tutor: Dr. Anna Laromaine Sagué

Departament de Física

Facultat de Ciències

Acknowledgements

Firstly, I want to gratefully thank my supervisor Anna Laromaine whose advice, guidance, patience, and support through the PhD process. I also want to thank Dr. Anna Roig and Dr. Martí Gich from the Group of Nanoparticles and Nanocomposites for their support and encouragement during these years. Moreover, I want to thank all the ICMAB personnel and thank for the possibility of using the infrastructure in ICMAB.

Secondly, I want to thank my former and current groupmates for their friendship and assistance in my research. Dr. Laura González, thank you for leading me into the *C. elegans* research field and teaching me to start *C. elegans* work step by step. Her working style and way of lab organization really influenced me a lot. Maria Segarra and Gerrit Bredeck, thank them for their help in establishing experimental protocols. Genís Rabost, thank you for programming codes for spectral analysis and patiently teaching me. Natalia Martínez, thank you for teaching me how to efficiently prepare agar plates. Deyaa Youssef, thank you for good ideas for inspiring me to nicely design my experiment. Carlos Moya, thank you for teaching me everything about SPIONs.

Ma Zheng and Soledad Roig, thank you for all the support and patience for my work and life. Miquel Torras, thank you for enduring my complaints and helping me to amend the standard curve. Irene Anton, thank you for teaching me the statistical analysis. Amanda Muñoz, thank you for the great support for my thesis writing and the journey to my paradise place, La Rioja. Yajie Zhang, thank you for the guidance and advice for my research. I also want to thank all the other labmates: Jordi Floriach, Mónica Benito, Qianzhe Zhang, Dani beltrán, Olatz Arriaga, Valentin Natarov, Oriol Torrecilla, María Jesús, Remei Escudero, and Jan Grzelak, Gustavo Alberto, Maria del Mar Blanes, Pawel Cwynar, Sumithra Srinivasan, Wenchao Duan, Nerea Murugarren, Saúl Estandía who have been directly or indirectly involved in my research work.

Thirdly, I also want to thank our collaborators, Natascia Ventura and Silvia Maglioni from IUF-Leibniz; Núria Benseny from MIRAS beamline in ALBA synchrotron facility who patiently taught me how to make measurements and analyze data; Mariano Campoy and Alejandro Goñi from the NANOPTO group of ICMAB for their collaboration and support in photothermal assays; Esther Dalfo group from the faculty of Medicine of UAB; Dr. Patricia Horcajada and Dr. Sara Rojas from the APMU of IMDEA Energy. I also want to thank other worm researchers I met in Spanish worm meetings and was in touch with during these years.

I also want to thank my previous bachelor and master classmates for their support and caring.

Finally, I acknowledge the funding from the Chinese Scholarship Council for pursuing my PhD degree.

Above all, I want to thank my parents, Lianshun Luo and Yuqing Jin, for their love, support, and encouragement. I also need to thank myself for self-development and being tough.

Abstract

During the last decades, nanoparticles (NPs) have been widely used in various fields, especially in medical applications such as drugs, imaging agents, and drug-delivery carriers. However, they also raised public concerns regarding the potential adverse influences on human health. Collective efforts from worldwide researchers in materials and biological science have been invested in investigating the toxicity mechanisms of different NPs.

In this thesis, we dedicated major efforts to apply (*Caenorhabditis elegans*) *C. elegans* as a robust and simple model organism for toxicity assessments of assorted NPs. The general objective of this thesis was to study effects of food availability on nano-bio interactions between superparamagnetic iron oxide nanoparticles (SPIONs) or 10 nm AuNPs and *C. elegans*, and prove that this small animal can be used to study alimentary effects.

Firstly, we studied the effects of food availability on toxicities induced by exposure to SPIONs after 24 h (acute exposure) or 72 h (prolonged exposure). We found that food provided some protection to *C. elegans* determined by measuring multiple toxicity endpoints such as survival and reproduction. Worms in the acute exposure condition had a higher uptake efficiency of SPIONS facilitated by food compared with the condition without the addition of food. The utilization of synchrotron Fourier transform infrared microspectroscopy (SR- μ FTIR), allowed us to demonstrate that long-exposure (24 h versus 4 h) and high concentrations of SPIONs (500 μ g/mL versus 100 μ g/mL) induce more severe oxidative stress determined by increased levels of lipid oxidation.

Secondly, we investigated food's influences on worms after 24 h exposure to 10 nm AuNPs. The protective role of food was identified in reducing toxic effects, such as survival and reproduction. Using SR- μ FTIR, we found that small-sized AuNPs (10 nm versus 150 nm) or long-exposure (24 h versus 4 h) caused an increased level of lipid oxidation which was related to responses against oxidative stress. On the other hand, we preliminarily evaluated the possibility of performing the photothermal therapy in worms containing 150 nm AuNPs. We found photoablated damages on the laser irradiation spots of worms, suggesting that multiple experimental settings needed to be optimized.

At the end of the thesis, also we presented some collaborations where we performed some experiments with different nanomaterials such as lutein and (metal-organic frameworks) MOFs and evaluated them on *C. elegans*. We studied antioxidative properties of lutein in *C. elegans* disease models associated with Leigh Syndrome and demonstrated the possibility to apply synchrotron Fourier transform infrared microspectroscopy (SR- μ FTIR) on this topic. On the other hand, we performed the preliminary toxicity assessment of MOFs, MIL-127 and chitosan (CS) coated MIL-127 (CS-MIL-127). Additionally, we investigated about effects of the chitosan (CS) coating on *C. elegans*' uptake and excretion efficiencies of MIL-127 and CS-MIL-127. We reported the potential of applying *C. elegans* as an oral administration model of studying

metal-organic frameworks' (MOFs') *in vivo* toxicities.

In summary, food availability could decrease adverse effects, partially associated with oxidative stress, induce by SPIONs or AuNPs on *C. elegans*. It also suggested that *C. elegans* has a great potential of being employed as an oral administration model of testing various materials. Furthermore, combined with other advanced techniques, we could have a more general understanding of the toxicity mechanism and broaden the application range of material science techniques for biological research.

Resumen

Durante las últimas décadas, las nanopartículas (NPs) se han utilizado ampliamente en distintos campos, especialmente en aplicaciones médicas como fármacos, agentes de formación de imágenes y como liberadores de fármacos. Sin embargo, también han planteado dudas respecto a las posibles reacciones adversas sobre la salud humana. Así, se han realizado grandes esfuerzos de investigación en el campo de las ciencias biológicas para elucidar los mecanismos de toxicidad de distintas NPs.

En este trabajo de Tesis, hemos dedicado esfuerzos a aplicar el (*Caenorhabditis elegans*) *C. elegans* como un organismo modelo robusto y simple para las evaluaciones de toxicidad de NPs. El objetivo general de esta tesis ha sido estudiar la interacción de la comida de estos gusanos con las NPs. En particular, el estudio de las interacciones nano-bio entre nanopartículas de óxido de hierro superparamagnéticas (SPIONs) o AuNPs de 10 nm en *C. elegans* alimentados o no; así demostrar que este pequeño animal puede utilizarse para estudiar efectos alimentarios.

En primer lugar, estudiamos los efectos de la disponibilidad de alimento sobre las toxicidades inducidas por la exposición de SPIONs tras 24 h - exposición aguda - o 72 h - exposición prolongada. Descubrimos que la comida brinda cierta protección a los *C. elegans*, la cual se determinó midiendo la supervivencia y la reproducción. Los gusanos en la exposición aguda tuvieron una mayor eficiencia de absorción de SPIONs facilitada por la comida en comparación con la condición sin alimento. La utilización de la microespectroscopía infrarroja de Síncrotrón (SR- μ FTIR) nos permitió demostrar que la exposición prolongada (24 h versus 4 h) y altas concentraciones de SPIONs (500 μ g/mL versus 100 μ g/mL) inducen un estrés oxidativo más severo debido a el aumento de la oxidación de lípidos.

En segundo lugar, investigamos las consecuencias de la ingesta de comida sobre los gusanos después de 24 h de exposición a AuNP de 10 nm. Se identificó el papel protector de los alimentos en la reducción de efectos tóxicos. Usando SR- μ FTIR, encontramos que las AuNPs de pequeño tamaño (10 nm frente a 150 nm) o la exposición prolongada (24 h frente a 4 h) causaron un mayor nivel de oxidación de lípidos que se relacionó con las respuestas contra el estrés oxidativo. Por otro lado, evaluamos preliminarmente la posibilidad de realizar la terapia fototérmica en gusanos que contenían AuNP de 150 nm. Encontramos daños por fotoablación en los puntos de irradiación láser sobre los gusanos, sugiriendo que se podría usar este gusano para evaluar NPs, pero para ello es necesario optimizar la configuración experimental.

En la parte final, presentamos algunas colaboraciones donde realizamos experimentos con diferentes nanomateriales como luteína y *metal-organic frameworks* (MOFs), evaluados empleando *C. elegans*. Estudiamos las propiedades antioxidantes de la luteína en *C. elegans* modificados para ser modelos de enfermedades asociadas con el síndrome de Leigh y demostramos la posibilidad de aplicar microscopía de infrarrojo (SR- μ FTIR) en estos estudios. Por otro lado, realizamos la evaluación preliminar de toxicidad de MOF, MIL-127 y CS-MIL-127 recubierto de quitosano (CS). Además, investigamos los efectos del

recubrimiento de CS en la absorción y excreción por los *C. elegans*.

En resumen, hemos encontrado que la disponibilidad de comida puede disminuir los efectos adversos, parcialmente asociados con el estrés oxidativo, inducidos por SPIONs o AuNPs en *C. elegans*. Nuestros resultados también sugieren que los *C. elegans* tienen un gran potencial como modelo de administración oral ya que pueden emplearse para probar diferentes materiales. Además, en combinación con otras técnicas avanzadas, nos pueden ayudar a comprender de forma más general los mecanismos de toxicidad y ampliar el rango de aplicación de las técnicas de ciencia de materiales para la investigación biológica.

Resum

Durant les darreres dècades, les nanopartícules (NP) s'han utilitzat en diversos camps, especialment en aplicacions mèdiques com ara medicaments, agents d'imatge i d'alliberament de fàrmacs. No obstant això, també es van plantejar preocupacions sobre les possibles reaccions adverses sobre la salut humana. Així, s'han invertit esforços d'investigació a nivell global en la ciència dels materials i la biologia per determinar els mecanismes de la toxicitat de diferents NPs.

En aquest treball de tesi, hem dedicat grans esforços a aplicar el (*Caenorhabditis elegans*) *C. elegans* com un organisme model robust i simple per a avaluacions de toxicitat de NPs. L'objectiu general d'aquesta tesi ha estat la interacció de l'alimentació dels cucs amb les NPs. En específic, les interaccions nano-bio entre nanopartícules d'òxid de ferro superparamagnètiques (SPION) o AuNPs de 10 nm en *C. Elegans* alimentats o no, així demostrar que aquest petit animal es pot utilitzar per estudiar els efectes alimentaris.

En primer lloc, hem estudiat els efectes de la disponibilitat de menjar sobre les toxicitats induïdes per l'exposició de SPIONs després de 24 h (exposició aguda) o 72 h (exposició perllongada). Hem trobat que el menjar proporcionava certa protecció als *C. elegans* determinada per la supervivència i la reproducció. Els cucs en la condició d'exposició aguda van tenir una eficiència de captació de SPIONS més alta facilitada pel menjar en comparació amb la condició sense menjar. La utilització de la microspectroscòpia infraroig en el sincrotró (SR- μ FTIR), ens va permetre demostrar que l'exposició llarga (24 h versus 4 h) i les altes concentracions d'SPIONs (500 μ g/mL versus 100 μ g/mL) indueixen un estrès oxidatiu més sever determinat per l'augment dels nivells d'oxidació dels lípids.

En segon lloc, vam investigar les conseqüències de la ingesta de menjar sobre els cucs després de 24 h d'exposició a AuNPs de 10 nm. El paper protector del menjar es va identificar en la reducció dels efectes tòxics, com la supervivència i la reproducció. Utilitzant SR- μ FTIR, vam trobar que les AuNPs de mida petita (10 nm versus 150 nm) o la exposició perllongada (24 h versus 4 h) provocaven un augment del nivell d'oxidació dels lípids que es relacionava amb les respostes a l'estrès oxidatiu. D'altra banda, vam avaluar preliminarment la possibilitat de realitzar la teràpia fototèrmica en cucs que contenien AuNPs de 150 nm. Hem trobat danys degut a la fotoablació a les zones d'irradiació làser dels cucs, cosa que suggereix que és possible utilitzar els cucs, però cal optimitzar els diversos paràmetres experimentals.

Al final de la tesi, també presentem col·laboracions on vam realitzar experiments amb diferents nanomaterials com luteïna i MOFs (metal-lo-organic framework) i els vam avaluar en els *C. elegans*. Vam estudiar les propietats antioxidants de la luteïna en *C. elegans* models de malaltia associades al síndrome de Leigh i vam demostrar la possibilitat d'aplicar la microscòpia d'infraroig (SR- μ FTIR) en aquests estudis. Així, també vam realitzar l'avaluació preliminar de la toxicitat de MOFs, MIL-127 i CS-MIL-127 recoberts de quitosà (CS). A més, hem investigat els efectes del recobriment de quitosà (CS) sobre la captació i eficiència d'excreció en els *C. elegans*.

En resum, la disponibilitat d'aliments podria disminuir els efectes adversos, parcialment associats a l'estrès oxidatiu, induïts per SPION o AuNPs a *C. elegans*. També suggerim que els *C. elegans* tenen un gran potencial d'utilitzar-se com a model d'administració oral per diversos materials. A més, combinat amb altres tècniques avançades, podríem tenir una comprensió més general del mecanisme de toxicitat i ampliar la gamma d'aplicacions de tècniques de ciència de materials per a la investigació biològica.

Attributions

I would like to thank people who had contributed to my thesis

- Miquel Torras synthesized SPIONS that the SPIONS I used in my thesis.
- Dr. Carlos Moya helped me to measure the concentration of SPIONS in liquid solutions by UV-Vis.
- Dr. Silvia Maglioni led and performed the main experiments in studying anti-oxidative behaviors of lutein in *C. elegans*' disease models.
- Dr. Núria Benseny helped us and assist me in the study of tissue-oxidation in nanoparticles-treated *C. elegans* and anti-oxidative behaviors of lutein in *C. elegans*' disease models by SR- μ FTIR.
- Dr. Patricia Horcajada and Dr. Sara Rojas assisted me in the project of studying *in vivo* toxicities of MOFs in *C. elegans* and chitosan's effects on the uptake and excretion rate of MOFs determined by HPLC.
- Dr. Mariano Campoy, Dr. Alejandro Goñi, and Xabier Rodriguez assisted me in the photothermal trials by performing the laser irradiation in *C. elegans*.
- Dr. Bernat Bozzo (ICMAB-CSIC) conducted magnetometry experiments.
- Dr. Judit Oró (ICMAB-CSIC) conducted the TEM visualization of synthesized and internalized SPIONS.
- Dr. Ignasi Villarroya (Servei d'Anàlisi Química, UAB) conducted the ICP-MS analysis of SPIONS-treated *C. elegans* for studying the uptake amount of SPIONS.

Table of contents

Acknowledgements	i
Abstract	iii
Resumen	v
Resum	vii
Attributions	ix
Table of contents	xi
List of Abbreviations	xv
List of Figures	xvii
List of Tables	xxi
Chapter 1 Introduction to Nanomaterials and nano-bio interactions	1
1.1 Nanomaterials and Nanomedicine	2
1.1.1 Nanomaterials	2
1.1.2 Nanomedicine	3
1.2 The administration route of nanomedicine	3
1.2.1 Oral administration	4
1.2.2 Food-drug interplay	4
1.3 <i>C. elegans</i> as a model animal for NPs' toxicity assessment	4
1.3.1 Experimental advantages of <i>C. elegans</i>	5
1.4 Toxicity study of NPs in <i>C. elegans</i>	7
1.5 Bio-evaluation of NPs in <i>C. elegans</i>	8
1.5.1 Essential role of metals in <i>C. elegans</i>	8
1.5.2 Literature review	8
1.5.3 Major factors regulating NPs' toxicity in <i>C. elegans</i>	9
1.5.3.1 Factors of the exposure system	9
1.5.3.2 Physicochemical properties of NPs.....	13
1.5.4 Uptake, biodistribution and translocation	15
1.5.5 Recovery and excretion of NPs from <i>C. elegans</i>	16
1.5.6 Evaluation of toxicity mechanism of NPs in <i>C. elegans</i>	16
1.5.6.1 Oxidative stress.....	16
1.5.6.2 Signaling pathway	17
1.6 Analytical techniques with potential to assess nano-bio interactions	17
1.7 Conclusions	18
1.8 Objectives and hypothesis	18
Chapter 2 Protocols applied to assess the nano-bio interaction	19
2.1. Introduction	20
2.2. Worms exposure conditions	20
2.3. Multiple toxicity endpoints	22
2.4. NPs uptake in <i>C. elegans</i>	24
2.4.1. Sample preparation	24
2.4.2. Physical analysis by magnetometry	25
2.4.3. Chemical analysis by ICP-MS.....	25

2.5. NPs status after exposure to <i>C. elegans</i>	25
2.5.1. Physical analysis by magnetometry	25
2.5.2. TEM analysis of internalized NPs	26
2.5.3. Excretion of ingested NPs	26
2.6. Qualitative analysis of oxidative stress	26
2.6.1. Sample preparation	27
2.6.2. Spectral optimization and data analysis	27
2.7. Photothermal effect	28
2.7.1. Sample preparation	28
2.7.2. Raman spectra analysis.....	29
2.8. Statistical analysis.....	30
2.9. Chapter conclusion	30
Chapter 3 Evaluation of SPIONs applying <i>C. elegans</i>. The influence of food availability and varied exposure durations	31
3.1. Introduction of superparamagnetic iron oxide nanoparticles	32
3.2. Aims.....	32
3.3. SPIONs synthesis and characterization	33
3.4. Toxicity analysis.....	34
3.4.1. Acute exposure.....	35
3.4.2. Prolonged exposure.....	39
3.5. Biodistribution of SPIONs.....	41
3.6. SPIONs uptake in <i>C. elegans</i>	42
3.6.1. Magnetometry.....	42
3.6.2. Inductively Coupled Plasma Mass Spectrometry (ICP-MS).....	43
3.7. NPs status inside <i>C. elegans</i>	44
3.7.1. Zero Field Cooled/ Field Cooled Magnetometry (ZFC-FC)	44
3.7.2. Transmission electron microscopy (TEM)	44
3.8. Qualitative analysis of oxidative stress	45
3.8.1. Study of exposure time.....	46
3.8.2. Study of oxidative stress	47
3.8.3. FPA mapping	47
3.9. Chapter conclusions.....	49
Chapter 4 Evaluation of gold nanoparticles applying <i>C. elegans</i>. The influence of food availability	51
4.1 Introductions to the gold nanoparticles.....	52
4.2 Aims.....	53
4.3 Toxicity analysis.....	53
4.4 Biodistribution of AuNPs.....	57
4.5 Photothermal effect	57
4.5.1 Feasibility of performing laser irradiation (Preliminary trial)	58
4.5.2 Effects of laser irradiation conditions	60
4.6 Qualitative analysis of oxidative stress	62
4.6.1 Study of exposure duration	63
4.6.2 Study of oxidative stress	63
4.6.3 Focal Plane Array mapping	64
4.7 Chapter conclusions.....	65
Chapter 5 Evaluation of Lutein’s antioxidative effects and MOFs toxicity in <i>C. elegans</i>	67

5.1. Collaboration work in <i>C. elegans</i> research	68
5.2. The assessment of lutein in <i>C. elegans</i>.....	68
5.2.1. Aims.....	69
5.2.2. Lutein’s antioxidative behaviors	69
5.2.3. Conclusions and future work.....	70
5.3. The assessment of MOFs in <i>C. elegans</i>.....	72
5.3.1. Aims.....	72
5.3.2. The effect of chitosan coating	73
5.3.3. Conclusions and future work	73
Chapter 6 Conclusions.....	75
6.1. Conclusions... ..	76
6.2 Future work.....	77
6.2.1. Exposure routes	77
6.2.2. Assayed materials	77
6.2.3. Advanced techniques	78
6.3 Prospects and challenges	78
References	79
Curriculum vitae	97

List of Abbreviations

MUA	11-mercaptoundecanoic acid
AD	Alzheimer's disease
AALL	Ambient artificial laboratory light
AAS	Atomic absorption spectrophotometry
BOW	Bag of worm
BAC-C16	Benzylcetyldimethylammonium chloride
BSA	Bovine serum albumin
<i>C. elegans</i>	<i>Caenorhabditis elegans</i>
CM	Carboxymethyl dextran
CI	Chemotaxis index
CS	Chitosan
CNGG	Component nematode growth gellan gum
DEX	Dextran
DEAE	Diethylaminoethyl dextran
DMSA	Dimercaptosuccinic acid
<i>E. coli</i>	<i>Escherichia coli</i>
EMA	European medicine agency
EU	European union
FND	Fluorescent nanodiamonds
FUdR	Fluorodeoxyuridine
FPA	Focal plane array
FDA	Food and Drug Administration
FTIR	Fourier transform infrared
GI	Gastrointestinal tract
AuNPs	Gold nanoparticles
AuNPs	Gold nanoparticles
GCeCP	Good <i>C. elegans</i> culture practice
GA-AgNPs	Gum Arabic coated silver nanoparticles
HPLC	High performance liquid chromatography
HA	Humic acid
HD	Huntington's disease
ICP-MS	Inductively coupled mass plasma spectrometry
IIS pathway	Insulin/Insulin-like signaling pathway
IV	Intravenous
FeO _x	Iron oxides
IONPs	Iron-oxide nanoparticles
LA-ICP-MS	Laser ablation inductively coupled plasma-mass spectrometry
LD	Leigh disease
LDs	Lipid droplets
LN	Lymph node
LB	Lysogeny broth
MRI	Magnetic resonance imaging
MCT	Mercury cadmium telluride
MOFs	Metal-organic frameworks
CI	Mitochondrial complex I
MAPKs	Mitogen-activated protein kinases
MnSOD	Mn superoxide dismutase
NCs	Nanocrystals
NMs	Nanomaterials
NPs	Nanoparticles

NOM	Natural organic matter
NIR	Near-infrared
NGG	Nematode growth gelrite
NGM	Nematode growth medium
OXPPOS	Oxidative phosphorylation
PD	Parkinson's disease
PIXET	Particle-induced X-ray emission tomography
PBS	Phosphate-buffered saline
PBST	Phosphate-buffered saline (PBS) + 0.01% Triton X-100
PTT	Photothermal therapy
PEG	Polyethylene glycol
PLFA	Pony Lake fulvic acids
PCA	Principal component analysis
PCs	Principal components
PC	Protein-corona
ROS	Reactive oxygen species
R-mie	Resonant mie scattering
AgNPs	Silver nanoparticles
SSPW	Simulated soil pore water
siRNA	Small interfering RNA
sAgNPs	Sulfidized silver nanoparticles
SQUID	Superconductive quantum interference device
SPIONs	Superparamagnetic iron oxide nanoparticles
SPR	Surface plasmon resonance
SR- μ FTIR	Synchrotron Fourier transform infrared microspectroscopy
SR	Synchrotron radiation
SRXRF	Synchrotron radiation X-ray fluorescence
TS	Topic search
TEM	Transmission electron microscope
UPR	Unfolded protein response
XFM	X-ray fluorescence microscopy
ZFC-FC	Zero-field-cooled/field-cooled magnetization

List of Figures

Figure 1 Bibliometric analysis of research in 2011-2019 from Web of Science Core Collection (Web of Science, Clarivate Analytics) on Nanoparticles (search strategy: topic search (TS)=(Nanoparticles*) (containing “nanoparticles” in the topic of articles)) and The nanoparticles in nanomedicine (search strategy: (TS)=(Nanoparticles* and Nanomedicine*)).	2
Figure 2 (A) <i>C. elegans</i> bridge the gap between <i>in vitro</i> and <i>in vivo</i> toxicity assays, (B) Bibliometric analysis of research in 2011-2020 from Web of Science Core collection (Web of science, Clarivate Analytics) on studies of nanoparticles in <i>C. elegans</i> . (search strategy: (TS)=(Caenorhabditis elegans* AND nanoparticles*)).	5
Figure 3 Adult hermaphrodite, schematic drawing of the alimentary and reproductive systems within an intact animal. Adapted from Altun ⁶⁹	6
Figure 4 The developmental stages of <i>C. elegans</i> . (Worms were cultured on the bacterial lawn) The scale bar represented 0.1 mm. Adapted from AK Corsi ⁹⁸	9
Figure 5 Confirmation of <i>E. coli</i> inactivation efficiency in 48 h, 4 drops of alive <i>E. coli</i> were put on the left part of the LB agar. 4 drops of heat-killed <i>E. coli</i> were put on the right part. The scale bar represents 20 mm.	21
Figure 6 Schematic diagram of toxicological studies relevant to the different stages of <i>C. elegans</i> development, adapted from Wu ⁵⁷	22
Figure 7 Chemotaxis assay (A) Chemotaxis index calculation equation, (B) Chemotaxis assay plate.	24
Figure 8 Anatomical evaluations of NPs biodistribution inside <i>C. elegans</i>	24
Figure 9 Magnetization measurements of <i>C. elegans</i> treated by SPIONs. (A) Raw data, (B) Hysteresis curve by making the subtraction of the diamagnetic signal, (C) Enlarged image of the curve to determine the $M_{R(C. elegans)}$ value.	25
Figure 10 (A) Equations used to calculate the size decrease. V is the NP volume; T_B is the blocking temperature; r is the NP radius, (B) ZFC-FC measurement of internalized SPIONs at 4-300K.	26
Figure 11 Visual images of <i>C. elegans</i> on the CaF ₂ window for the SR- μ FTIR measurement.	27
Figure 12 (A) The scheme flow of the spectral optimization, (B) Raw data, (C) Remaining spectra after the removal of spectra with signs of low signal to noise ratio or saturation, (D) The spectra of C with the R-mie correction, (E) The application of 2 nd derivative on the spectra shown in D, The peaks used for calculating lipid oxidation ratios are marked.	28
Figure 13 Sample preparation for photothermal effect study.	29
Figure 14 (A) Raman microscopy (apyron [∞] , WITec company), (B) The screenshot of the video recorded by the infrared camera. The red square showed the location where the temperature was monitored, within the chamber of the Raman microscope. The bright spot within the red square is the spot of laser irradiation. The value was the instant temperature of the red square.	29
Figure 15 (A) The square zone with red boundary was set on the AuNPs, (B) The image of the zone before laser irradiation, (C) The image of the zone after laser irradiation.	29
Figure 16 Microwave-assisted synthesis of SPIONs (A) The CEM Focused Microwave Synthesis System, (B) The temperature ramp indicating three steps: 1) 5 min at 60 °C, 2) 10 min reaction at 180 °C, 3) cooling down to 50 °C in 3 min.	33
Figure 17 Structural characterization of SPIONs. (A) TEM image, (B) TEM size distribution, (C) SAED pattern indexed to an inverse spinel structure, (D) SPIONs stability in MilliQ water and M9 medium, (E) M(H) measurement at 300K up to 6 Tesla.	34

Figure 18 Graphical representations to describe the acute/prolonged exposure conditions and studies toxicity endpoints.	35
Figure 19 Effects of food availability on the survival (A) and reproduction (B) of <i>C. elegans</i> (n=3) exposed to increasing concentrations of SPIONs. Bars indicate the mean \pm S.E.M. $p < 0.0332$ (*), $p < 0.0021$ (**), $p < 0.0002$ (***).....	36
Figure 20 Effects of food availability on the lifespan of <i>C. elegans</i> after acute exposure upon SPIONs. (n=3). Bands represented SD.	36
Figure 21 Nile red staining images of worms treated in control and 300 $\mu\text{g}/\text{mL}$ SPIONs conditions.	37
Figure 22 Effects of food availability on intestinal integrity (A) and lipid content (B) of <i>C. elegans</i> after acute exposure upon SPIONs (n=3). Bars indicate mean \pm S.E.M. $p < 0.0332$ (*), $p < 0.0021$ (**), $p < 0.0002$ (***).....	37
Figure 23 Effects of food availability on body bending frequency (A) and chemotaxis (B) of <i>C. elegans</i> after acute exposure upon SPIONs (n=3). Groups with and without food availability were separately analyzed. Bars indicate mean \pm S.E.M. $p < 0.0332$ (*), $p < 0.0021$	38
Figure 24 Effects of SPIONs on survival (A) and reproduction (B) of <i>C. elegans</i> after prolonged exposure with food availability (n=3). Bars indicate mean \pm S.E.M.(C) The L1 larva after prolonged exposure to SPIONs with <i>E. coli</i> . The scale bar represented 30 μm	39
Figure 25 Effects of SPIONs on Nile red staining results (A) and Oil Red O staining results (B) of <i>C. elegans</i> after prolonged exposure with food availability (n=3). Bars indicate mean \pm S.E.M.	39
Figure 26 Effects of SPIONs on the lifespan (A) and body bending frequency (B) of <i>C. elegans</i> after prolonged exposure with food availability (n=3). Bars indicate mean \pm S.E.M. $p < 0.0332$ (*), $p < 0.0021$ (**), $p < 0.0002$ (***).....	40
Figure 27 Prussian blue-stained worms after acute exposure to 500 $\mu\text{g}/\text{mL}$ SPIONs with <i>E. coli</i> . Scale bar represents 30 μm	42
Figure 28 Biodistribution of SPIONs in <i>C. elegans</i> after acute exposure to varying concentrations of SPIONs with <i>E. coli</i> (50 worms per sample). The upper simplified graph showed the division of the alimentary system: pharynx, anterior gut, central gut, and posteri	42
Figure 29 (A) Enlarged magnetic hysteresis of SPIONs at 5 K showing the remanence magnetization MR(SPIONs), and (B) Enlarged magnetic hysteresis of treated worms at 5 K showing the remanence magnetization MR (<i>C. elegans</i>).....	43
Figure 30 ZFC-FC graphs of synthesized SPIONs and internalized SPIONs inside <i>C. elegans</i>	44
Figure 31 (A) Gaussian distribution of synthesized SPIONs and internalized SPIONs inside <i>C. elegans</i> , (B) TEM image of SPIONs after the recovery process.	45
Figure 32 The peaks used for calculating lipid oxidation ratios are marked in the spectra with the application of the 2 nd derivative. The peak 1745 cm^{-1} corresponded to the carbonyl group of the ester bond. The peak 2921 cm^{-1} corresponded to the asymmetric stretch from CH_2	46
Figure 33 Box and whiskers plot of the lipid oxidation ratio (1745 cm^{-1} / 2921 cm^{-1}) of all spectra, for control, 4 h and 24 h exposure of wild-type and <i>sod-3</i> mutant worms to 100 $\mu\text{g}/\text{mL}$ and 500 $\mu\text{g}/\text{mL}$ SPIONs. $p < 0.0332$ (*), $p < 0.0021$ (**), $p < 0.0002$ (***).....	47
Figure 34 Merged Box and whiskers plots of the lipid oxidation ratio (1745 cm^{-1} / 2921 cm^{-1}) from the whole body and head zone of wild-type and <i>sod-3</i> worms exposed to 100 $\mu\text{g}/\text{mL}$ and 500 $\mu\text{g}/\text{mL}$ SPIONs for 24 h. $p < 0.0332$ (*), $p < 0.0021$ (**).....	48
Figure 35 FTIR mapping of <i>sod-3</i> mutants treated with 500 $\mu\text{g}/\text{mL}$ SPIONs for 24 h with the lipid oxidation ratio (1745 cm^{-1} / 2921 cm^{-1}). Dark blue color corresponds to the level of lipid oxidation measured in regions	

away from the worm. Color scale bar: dark blue means low, red means high.	48
Figure 36 Structural characterization of 10 nm AuNPs. (A) TEM image, (B) TEM size distribution, (C) UV-vis spectrum.....	54
Figure 37 Graphical representations to describe the acute exposure condition and studies toxicity endpoints.	54
Figure 38 Effects of food availability on the survival exposed to increasing concentrations of AuNPs of <i>C. elegans</i> (n=3). Bars indicate the mean \pm S.E.M. $p < 0.0332$ (*), $p < 0.0021$ (**), $p < 0.0002$ (***).....	54
Figure 39 Effects of food availability on reproduction (A) intestinal integrity (B) and lipid content (C) of <i>C. elegans</i> after acute exposure upon 100 $\mu\text{g}/\text{mL}$ AuNPs (n=3). Bars indicate mean \pm S.E.M. $p < 0.0332$ (*), $p < 0.0021$ (**), $p < 0.0002$ (***).....	55
Figure 40 Effects of food availability on body bending frequency (A) and life span (B, C) of <i>C. elegans</i> after acute exposure upon AuNPs (n=3). Groups with and without food availability were separately analyzed. Bars indicate mean \pm S.E.M. $p < 0.0332$ (*), $p < 0.0021$ (**), $p < 0.0002$ (***).. Bands represented SD.....	56
Figure 41 Worms after acute exposure to 500 $\mu\text{g}/\text{mL}$ 10 nm AuNPs with <i>E. coli</i> . Scale bar represents 100 μm	57
Figure 42 Biodistribution of 10 nm AuNPs in <i>C. elegans</i> after acute exposure to varying concentrations of AuNPs with <i>E. coli</i> (50 worms per sample). The upper simplified graph showed the division of the alimentary system: pharynx, anterior gut, central gut, and post gut. The lower color legend depicted the percentage of observed locations of AuNPs.	57
Figure 43 (A) A line-scan of 150 nm AuNPs on the glass slide. The red dot represented AuNPs, and the blue dot represented the glass. (B) Raman spectra of two locations showed in A. The colors of the spectra correspond to the colors of locations. (C) A white light image of <i>C. elegans</i> containing AuNPs. (D) Principle component analysis (PCA) was performed on the average spectra obtained from the large-scale-image-scan of the worm in C. 3 clusters were resolved and colored differently.	58
Figure 44 (A) Two positions of line-scan on the worm containing varied contents of AuNPs. (B) The average spectra of positions with high or low loadings of AuNPs. The colors of spectra corresponding to the colors were marked in 44A. (C) Raman mapping image of high loading of AuNPs with a Z-axis scan. (D) Raman mapping image of low loading of AuNPs with a Z-axis scan. The color scale bar illustrates the intensity of the band at 47 cm^{-1}	59
Figure 45 Snapshots of the video recording temperature variation during the line-scan irradiation.	60
Figure 46 Snapshots of the video recording temperature variation during the pulsed irradiation on the fix-point with varied laser power.	60
Figure 47 (A) A white light image of worms containing AuNPs with colored icons representing the irradiation positions. (B) The Raman intensity spectrum with time shifts of position 1. The laser power applied in each time interval was showed above the spectrum. (C) The Raman spectrum of continuous irradiation on position 2. (D) The Raman spectrum of line-scan under the continuous irradiation on position 3. (E) The enlarged reflected microscopy image of position 1, 2 and 3 after varied types of irradiation. Scale bar 10 μm	61
Figure 48 Snapshots of the video recording temperature variation during the continuous irradiation on the fix-point with the laser power of 30 mW.	62
Figure 49 Snapshots of the video recording temperature variation during the continuous irradiation of line-scan with the laser power of 30 mW.	62
Figure 50 Box and whiskers plot of the lipid oxidation ratio (1745 cm^{-1} / 2921 cm^{-1}) of all spectra, for control, 4 h and 24 h exposure of wild-type (A) and <i>sod-3</i> mutant (B) worms to 100 $\mu\text{g}/\text{mL}$ of 10 nm and 150 nm AuNPs. $p < 0.0332$ (*), $p < 0.0021$ (**), $p < 0.0002$ (***).....	63

Figure 51 FTIR mapping of *sod-3* mutants in the control condition (A) and treated with 100 µg/mL of 10 nm AuNPs for 4 h (B) and 24 h (C) with the lipid oxidation ratio (1745 cm⁻¹ / 2921 cm⁻¹). Dark blue color corresponds to the level of lipid oxidation measured in regions away from the worm. Color scale bar: dark blue means low, red means high. 64

Figure 52 The chemical structure of lutein, adapted from Koushan K et al³⁴³. 69

Figure 53 The spectrum showed biomolecular peak assignments from 3000–800 cm⁻¹. Adapted from Baker et al³⁴⁴. 69

Figure 54 Bar plot of the lipid oxidation (1745 cm⁻¹/2921 cm⁻¹) and amide oxidation (1745 cm⁻¹/1654 cm⁻¹) of all spectra for control, *nuo-5*, and *lpd-5*. N=3, n=15-20. p < 0.0332 (*), p < 0.0021 (**), p < 0.0002 (***), and p < 0.0001 (****)..... 70

Figure 55 Bar plot of lipid oxidation (1745 cm⁻¹/2921 cm⁻¹), amide oxidation (1745 cm⁻¹/1654 cm⁻¹), and lutein absorbance (1515 cm⁻¹/2921 cm⁻¹) of all spectra for control, *nuo-5*, and *lpd-5*. N=3, n=15-20. p < 0.0332 (*), p < 0.0021 (**), p < 0.0002 (***), and p < 0.0001 (****) versus respective control conditions. 70

Figure 56 The structure of MIL-127 (Fe), adapted from Roja S et al³⁶⁰. 72

Figure 57 Effects of CS coating on the Survival (A) of *C. elegans* (n=3) exposed to increasing concentrations of MIL-127 and CS-MIL-127. Bars indicate the mean ± S.E.M. (B) The worm after acute exposure to 500 µg/mL of MIL-127, (C) The worm after acute exposure to 500 µg/mL of CS-MIL-127. The scale bar represents 100 µm..... 73

List of Tables

Table 1 Techniques used in the investigation of interactions between NPs and <i>C. elegans</i>	20
Table 2 The summary of diverse toxicity endpoints of <i>C. elegans</i> after acute or prolonged exposure upon SPIONs with and without food.	41
Table 3 Comparison of the SPIONs uptake results by SQUIDs and ICP-MS. The relative error was indicated.	43
Table 4 Size decrease of internalized SPIONs and synthesized SPIONs estimated from ZFC-FC and TEM techniques.	45

Chapter 1 Introduction to Nanomaterials and nano-bio interactions

1.1 Nanomaterials (NMs) and Nanomedicine

1.1.1 Nanomaterials

1.1.2 Nanomedicine

1.2 The administration route of nanomedicine

1.2.1 Oral administration

1.2.2 Food-drug interplay

1.3 *C. elegans* as a model animal for NPs' toxicity assessment

1.3.1 Experimental advantages of *C. elegans*

1.4 Toxicity study of NPs in *C. elegans*

1.5 Bio-evaluation of NPs in *C. elegans*

1.5.1 Essential role of metals in *C. elegans*

1.5.2 Literature review

1.5.3 Major factors regulating NPs' toxicity in *C. elegans*

1.5.3.1 Factors of the exposure system

1.5.3.2 Physicochemical properties of NPs

1.5.4 Uptake, biodistribution and translocation

1.5.5 Recovery and excretion of NPs from *C. elegans*

1.5.6 Evaluation of toxicity mechanism of NPs in *C. elegans*

1.5.6.1 Oxidative stress

1.5.6.2 Signaling pathway

1.6 Analytical techniques with potential to assess nano-bio interactions

1.7 Chapter conclusions

1.8 Objectives and hypothesis

1.1 Nanomaterials and Nanomedicine

1.1.1 Nanomaterials

Nanoscience is a continually developing research field, aiming to acquire desired properties of materials designed at the atomic and molecular scale^{1,2}. Nanomaterials (NMs) are generally referred to materials with one or more of their dimensions within the 1-100 nm range, according to International Organization for Standardization and the Commission of the European Union (EU) guidelines and the IUPAC recommendations¹, with distinct properties, significantly differing from their macroscale counterparts^{1,3}. Determined by the number of dimensions in the nanosized range, NMs could be categorized into four types as zero-dimensional (nanospheres, nanoclusters), one-dimensional (nanofibers, nanowires, nanotubes), two-dimensional (nanoplates, nanosheets), and three-dimensional objects (composed of individual blocks)¹.

Nanoparticles (NPs) as a subcategory of NMs, are attracting tremendous interests in almost every cutting-edge research field⁴, as evidenced by the growing number of scientific articles from Web of Science Core Collection (Web of Science, Clarivate Analytics)² during 2011–2019 (Figure 1). The unique physicochemical properties (size, shape, and surface chemistry) promote their widespread applications including biomedicine, energy, food industry, engineering, etc^{3,5}. They're frequently employed in nanomedicine (Figure 1), NPs have emerged as a promising tool for the diagnosis and treatment of diseases⁴, for instance, targeted drug delivery⁶, imaging agents⁷, and hyperthermia⁸, etc.

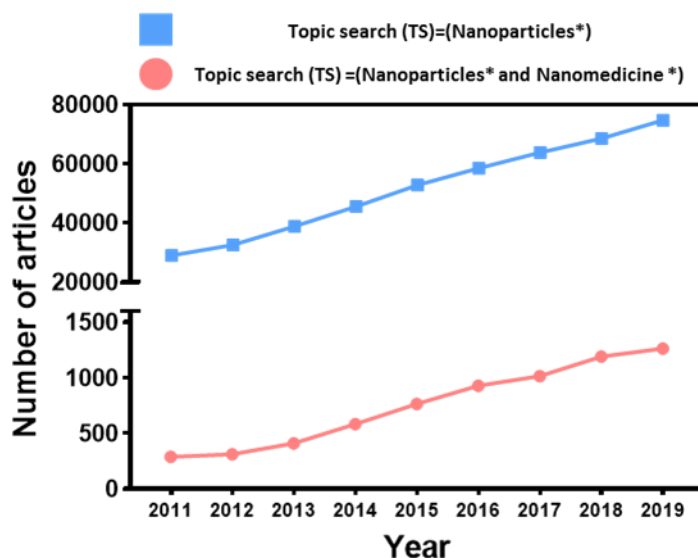


Figure 1 Bibliometric analysis of research in 2011-2019 from Web of Science Core Collection (Web of Science, Clarivate Analytics) on Nanoparticles (search strategy: topic search (TS)=(Nanoparticles*) (containing “nanoparticles” in the topic of articles)) and The nanoparticles in nanomedicine (search strategy: (TS)=(Nanoparticles* and Nanomedicine*)).

1.1.2 Nanomedicine

Nanomedicine, referring to biomedical and pharmaceutical applications of nanotechnology, aims to improve the quality of our healthcare and bring advanced therapeutics for patients¹. Due to the increased demand for developed therapeutics with enhanced safety and efficacy, the nanomedicine industry has thrived in the last decade, encompassing the development of NPs for diverse therapies⁶ and imaging agents⁷.

Therapeutic/diagnostic NPs are typically divided into two groups: organic NPs (e. g. liposomes, protein-based, polymeric, etc.) and inorganic NPs (e.g., iron oxide, gold, silica, etc.)⁶. For example, Doxil[®], the liposomal doxorubicin functionalized with polyethylene glycol (PEG), was the first FDA-approved (1995) medicine for cancer therapy⁹. For inorganic NPs, iron-oxide nanoparticles (IONPs) are employed in the iron-replacement therapy for iron-deficiency anemia^{10–12}. Ferumoxytol is the FDA-approved superparamagnetic iron oxide nanoparticles (SPIONs) used for the treatment of anemia^{13,14}. Alongside this, IONPs have also been clinically approved to be applied as magnetic resonance imaging (MRI) contrast agents for multiple cancers and pathologies^{15–18}. Ferrotran[®], currently, is the only MRI agent consisting of SPIONs for the detection of lymph node (LN) metastasis in patients with prostate cancer^{6,19}.

Besides the above-mentioned clinical applications, IONPs have been extensively studied in the preclinical stage of varied applications such as thermal ablation of tumors via hyperthermia^{20,21} and drug delivery^{22–24}. With an external changing magnetic field, SPIONs could also be applied to reach the target zone and damage the tumor by inducing an increased temperature²⁵. Gold nanoparticles (AuNPs) have also been applied in the photothermal therapy for cancer treatment^{26,27}. The Aurolase[®] therapy is a gold-silica particles-directed photothermal therapy that selectively targets and generates a lethal dose of heat to ablate tumor tissue when NPs are illuminated by NIR irradiation^{28,29}.

1.2 The administration route of nanomedicine

Nanomedicine, defined by Bobo et al., are drugs or biologics incorporating NPs (1-100 nm)³⁰. One of their uses is to achieve improved therapeutic efficacy or be applied as imaging agents *in vivo*³⁰. These biomedical applications mainly focus on the intravenous (IV) injection or oral administration routes^{30,31}, among other routes such as intramuscular injections, subcutaneous injections, pulmonary inhalation, etc^{32–34}. For the use of MRI contrast agents, IV injection is a commonly applied method for the administration of IONPs³⁵. It can also be used for anemia treatment in patients for whom oral administration of iron cannot be used because of intolerance, ineffectiveness or unresponsiveness^{35,36}. However, from a safety perspective, IV injection of iron supplement drugs could also be risky for inducing two main side effects which are hypersensitivity reactions and hypophosphatemia^{36,37}. Comprehensive guidelines have been published about the management if there are iron-induced hypersensitivity reactions after IV injections³⁶. Meanwhile, mainly in patients with preserved kidney function, IV iron could cause hypophosphatemia, apparent soon after the injection and lasting for two weeks at most³⁷. Therefore, the oral administration

route is a safer method.

1.2.1 Oral administration

In the NP-mediated drug delivery system, biocompatibility, biodegradability, and physicochemical properties of NPs are extremely important. However, the route of administration is also critical. The oral administration is the most preferred route of drug administration³⁸ which is widely accepted by patients. It's also the most favored route due to the convenience for self-administration, non-invasiveness, and ease of use which facilitate adherence from patients to therapies^{39–42}.

Regardless of the advantages offered by the oral-route administration for the patient or therapy, the complexity of the physicochemical environment in the gastrointestinal tract (GI) impacts on the efficacy of oral-delivery drugs^{41,42}. The GI fluids are complicated and heterogeneous, with a wide range of pH from 1 to 8 and^{42,43}. It also contains diverse types of biomolecules, bile salts, food components, digestive enzymes, etc⁴². Moreover, the GI tract is a dynamic environment related to internal (i.e., secretion) and external stimuli (i.e., food ingestion)⁴⁴. When NPs encounter with complex fluids, it's prone to form a protein-corona (PC) surrounding NPs due to interactions with the aforementioned biomolecules^{42,44}. The resulting PC would render NPs different *in vivo* fates and impact on the therapeutic efficacy^{33,45}. For this reason, the interaction deserves to be thoroughly studied, aiming to know all the final fates of the NPs and effects to improve curative effects and decrease adverse effects^{44,46}.

1.2.2 Food-drug interplay

The food-drug interaction refers to the physicochemical or physiological relationship between a drug and a product consumed as food or nutrient^{46,47}, within the environmental matrix (i.e., GI lumen)⁴⁸. The food can influence the absorption, bioavailability, and metabolism of drugs^{38,47}. In order to learn the food effects on the drug absorption, Food and Drug Administration (FDA) and European Medicine Agency (EMA) both recommend studying pharmacokinetics in the fed state after having a high-fat meal⁴⁹. The effects can be simply defined as “positive effects” of increased dissolution and solubilization or “negative effects” of reduced and delayed absorption⁵⁰. Additionally, since 1st January 2010, approximately 40% of medicines approved by FDA and EMA show food effects or contain suggestions of taking medications with or without food. These instructions are commonly devised to improve safety or tolerability and maximize clinical efficacy⁵⁰. Meanwhile, some research work demonstrated that co-ingested carbohydrates, proteins, or lipids in food could potentially alter the bioavailability of certain types of drugs^{51–55}. Therefore, in this thesis, we chose to study food effects on the toxicity evaluation of SPIONs and AuNPs in *C. elegans* and evaluate if this animal model can bring light to this type of research.

1.3 *C. elegans* as a model animal for NPs' toxicity assessment

Researchers have reported various toxic profiles of diverse NPs through *in vitro* or *in vivo* assays. However,

many times, there are discrepancies or gaps existing between data obtained from cell culture conditions and *in vivo* model animals which make it difficult to evaluate or predict toxicological outcomes of NPs in the clinical stage⁵⁶. Regarding the huge demand for toxicological studies of emerging NPs following their broad applications in our daily life, assays with good comparison to the real environment and of high simplicity that could be performed in any lab are needed. *Caenorhabditis elegans* (*C. elegans*) has emerged as a powerful and informative model for NPs' toxicity testing⁵⁷⁻⁵⁹ (Figure 2A).

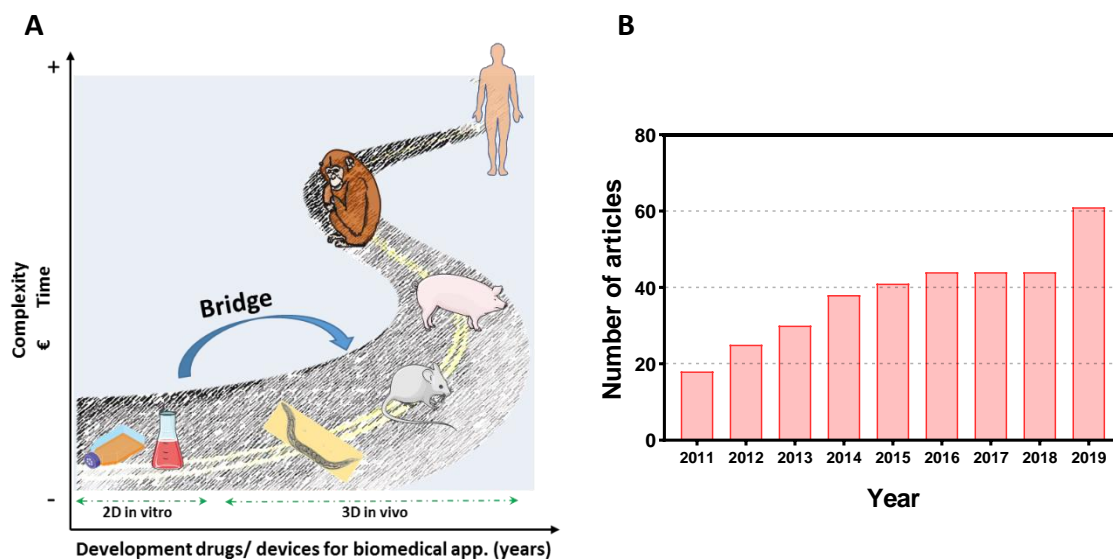


Figure 2 (A) *C. elegans* bridge the gap between *in vitro* and *in vivo* toxicity assays, (B) Bibliometric analysis of research in 2011-2020 from Web of Science Core collection (Web of science, Clarivate Analytics) on studies of nanoparticles in *C. elegans*. (search strategy: (TS=(*Caenorhabditis elegans** AND nanoparticles*))).

1.3.1 Experimental advantages of *C. elegans*

C. elegans is a non-parasitic⁶⁰ and free-living nematode, mainly found in the bacteria-rich soil⁶¹. It was first adopted as a model animal by Sydney Brenner in 1965 for studying the nervous system development⁶²⁻⁶⁴. Given that, it has been considered as a suitable and robust toxicity model for toxicological research⁶⁵, with an increased tendency of published articles (shown in Figure 2B). Its biological applications have prospered due to its small size, transparent body, short and prolific life cycle, ease of maintenance, invariant development, constant cell number, well-characterized genome, easy genetic manipulation, and abundant databases of *C. elegans*^{59,61,66,67}. Moreover, *C. elegans* has the relevance to biological systems of mammal, expressing homologs to 50%-80% of human genes^{63,66}. In terms of evaluating NPs' *in vivo* toxicities, their distribution within worms and clearance as well as their influences on tissues or organs are commonly studied⁵⁷. The anatomy of *C. elegans* includes four organ systems which are an alimentary system, a reproductive system, a neural system, and an immune system, which are the same as those in vertebrates^{57,68}.

The alimentary system

The *C. elegans* alimentary system is essentially a tube, composed of the pharynx, grinder, intestine, and hindgut (rectum) (shown in Figure 3)⁶⁹. Because of not having a circulatory system, *C. elegans* relies upon the passive diffusion for transporting O₂, CO₂, and nutrients⁶⁶. Food rapidly transits the digestive tract within a few minutes⁷⁰. The grinder, a circular structure, is the position of mechanically breaking up food particles. In the intestinal lumen, a weakly acidic compartment of around pH 4.4⁷¹, ground food particles are thoroughly broken down by digestive enzymes and uptaken⁷². In the end, with a set of muscular contractions, the debris of food is propelled out through the anus⁷³.

C. elegans feed themselves by collecting food components of the liquid phase from their surrounding environment into the pharynx by pumping and peristalsis⁶⁸. Additionally, some facets of the food digestion and uptake process of *C. elegans* are comparable to those of humans, for instance, the acidic microenvironment, the excretion of digestive enzymes, and uptake of digestive food components^{68,70}. Thus, *C. elegans* could be applied as an oral toxicity model for testing NPs' toxicity with the food supply⁶⁸. It can help to elucidate the role of food in the interaction between NPs and *C. elegans* following oral uptake⁷⁴.

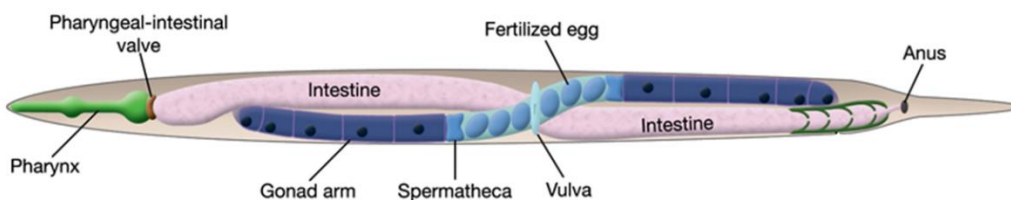


Figure 3 Adult hermaphrodite, schematic drawing of the alimentary and reproductive systems within an intact animal. Adapted from Altun⁶⁹.

The reproductive system

C. elegans has two sexes, self-fertilizing hermaphrodites and males of rare occurrence (0.1% of the time)^{62,66}. Only hermaphrodites have the space for fertilization and egg-laying which is mainly divided into three sections consisting of somatic gonad, germline, and egg-laying apparatus (vulva and uterine)^{62,75} (shown in Figure 4). Normally, by self-fertilizing, hermaphrodites can produce around 300 embryos. Reproduction is an important endpoint since it has been reported that reproduction is more sensitive to the relatively lower concentration of NPs which have an adverse influence on *C. elegans* than other toxicity endpoints⁵⁷. Several reproductive parameters are chosen for studying NPs' toxic effects on *C. elegans* including the number of offspring (also referred to as brood size), the number of oocytes, and embryonic lethality⁷⁶. Meanwhile, the egg-laying behavior is assisted by the muscular contraction which is under the regulation of the neural system⁷⁷. If certain neurons controlling the muscles of a well-developed vulva are impaired, it may lead to reduced progeny and bag of worm (BOW) phenomenon (hatching of larvae inside the paternal body)⁷⁸.

The neuronal system

Typically, an adult *C. elegans* has 302 neurons and 7000 synapses that constitute two independent nervous systems, a large somatic system and a small pharyngeal system⁷⁸, using the same neurotransmission systems (glutamatergic, cholinergic, serotonergic, and dopaminergic) which are phylogenetically conserved in worms and vertebrates^{57,63}. *C. elegans* exhibits varied types of behaviors containing locomotion, feeding, defecation, egg-laying, and mating⁷⁹. In addition, worms can sense and make responses to chemical, physical, or thermal stimuli. Benefitting from the laser ablation of neurons, we have an enhanced understanding of the connectivity of the neuronal network which is involved in those behaviors^{78,79}. Moreover, the transparent body allows us to observe the neuron damage, neuro-degeneration, or even neuron dynamics in the NP-treated worms with fluorescent markers⁸⁰⁻⁸².

The immune system

One of the major threats to any living organism is getting infected by a pathogen. Thus, it's essential to have an efficient immune system that can recognize and remove the pathogen, subsequently. Generally, in higher vertebrates, the immune defense systems are made of an innate response and an adaptive response⁸³. Different from humans and other vertebrates, *C. elegans* doesn't have an adaptive immunity which is delayed but highly specific and long-lasting⁸³. Alternatively, they have their own innate recognitions and immune activities to protect themselves from pathogenic bacteria⁸³. They can make use of secretion and action of antimicrobial molecules to break up or up-regulate expressions of catalases, superoxide dismutases, metallothioneins, etc. to detoxify pathogens^{67,83}. It has been stated that several signaling pathways involved in the innate immunity are conserved in worms and humans, for instance, a p38 mitogen-activated protein kinase, mitogen-activated protein kinases (MAPKs) and insulin signaling/DAF-2, etc^{66,67,83}. On the other hand, *C. elegans* can be easily manipulated to get infected by simply replacing the original food bacterium *Escherichia coli* (*E. coli*) with any pathogen. The affected phenotype such as survival, motility, and pathogen burden can be easily confirmed⁶⁷.

1.4 Toxicity study of NPs in *C. elegans*

In recent decades, NPs are becoming promising tools in the nanomedicine field^{62,84}, owing to their unique physicochemical properties^{8,57}. One of the main concerns about NPs applied as nanomedicines is whether they can induce adverse effects, partially due to their nano-bio interactions with different components (i.e., enzymes and ingested food components)⁴⁷ within the environmental matrix (i.e., GI lumen)⁴⁸ of the human body^{62,77,84}. To this end, extensive studies have been performed to study their toxicological profiles in the biological environment through toxicity tests from *in vitro* to *in vivo*⁸. NPs with a wide range of concentrations can be rapidly tested by *in vitro* assays. However, obtained results cannot be utilized to predict responses at the organism level. Moreover, it's highly possible to provide us false-positive

or -negative outcomes^{68,85}. On the other hand, it's not feasible to run all the toxicity tests in mammalian models regarding the fact that it's expensive and time-consuming together with ethical issues^{57,68}. Thus, *C. elegans* has gained popularity and gradually become a highly promising *in vivo* model for toxicity assessments and toxicological studies of NPs^{62,76}. NP-mediated toxicity data including lethal and sublethal endpoints can be easily generated in an intact animal model with assorted organ systems such as digestive, reproductive, endocrine, and neural systems^{62,68}. The oral uptake of NPs with *E. coli* and their fate in the intestinal digestive system of *C. elegans* can mimic the process of oral-administration of nanomedicine after food intake. Additionally, the availability and applicability of varied high-end techniques material science techniques would provide us a more comprehensive understanding of food-NPs interplay in *C. elegans*^{59,62}.

1.5 Bio-evaluation of NPs in *C. elegans*

1.5.1 Essential role of metals in *C. elegans*

Metals are critical components in organisms that can be generally divided into essential and nonessential groups. Metals are involved in multiple physiological processes; therefore, the occurrence of unbalanced metal metabolism may induce various pathological events⁸⁶. The model organism, the nematode *C. elegans*, has gradually become an important *in vivo* platform for toxicity assessment of substances including metal and metal oxide NPs⁷⁶. Although the common cause of toxicities induced by NPs is disrupted biological pathways, released metal ions of NPs could also generate adverse effects on *C. elegans*⁵⁹, more element-specific^{86,87}. In *C. elegans*, zinc, copper, iron, and manganese are essential elements that are involved in diverse metabolic pathways. As only trace amounts of these metals are required, a minimal release of any of those ions may disrupt the delicate balance of hemostasis and cause severe dysfunction within worms⁸⁶. In addition, based on the extensive gene homology (approximately 45%) to the human genome, *C. elegans* has potentials to study molecular mechanisms induced by exposure upon NPs^{68,76}.

1.5.2 Literature review

There has been a rapid increase in applying *C. elegans* as an *in vivo* assessment model in the toxicity study of NMs, including metal and metal oxide NPs, carbon nanomaterials, and other types of materials such as quantum dots^{59,88}, especially in the fields of ecological toxicity assessment and biomedical applications⁵⁷.

In the ecotoxicological assays, considering the important role in benthic food webs⁸⁹⁻⁹¹ with sensitivity properties to environmental toxicants, *C. elegans* is used as the animal model to test environmentally relevant concentrations of NPs. So far, acute exposure (≤ 24 h), prolonged exposure (≥ 48 h), chronic exposure (≥ 72 h), and transgenerational exposure have been applied as effective exposure systems to make the toxicity evaluation⁷⁶. Among these exposure systems, long-term exposure including prolonged and chronic exposure has shown good potential in estimating the possible toxicity in environmentally realistic

conditions⁵⁷. On the other hand, for biomedical applications, a wide range of concentrations and diverse toxicity endpoints measurements are normally performed. Additionally, a comprehensive study of the destiny of NPs inside worms including uptake, distribution, translocation, excretion, and recovery combined with genetic mechanisms triggered by exposure to NPs, is also performed⁷⁷.

In addition, *C. elegans* has also been taken as a tool to broaden the application range of certain techniques like atomic force microscopy^{92,93} or confirm the feasibility of NPs for a given application, for instance, drug delivery^{94–97}.

1.5.3 Major factors regulating NPs' toxicity in *C. elegans*

1.5.3.1 Factors of the exposure system

The appropriate exposure condition of worms to NPs is a crucial step in studying nano-bio interactions. Multiple variables including the developmental stage of worms, optimal exposure media, concentration ranges, exposure durations, and food availability would determine final interaction results. In this section, the previous work was reviewed by different factors of the exposure condition.

Effect of developmental stage

The development period of worms could be divided into four stages (shown in Figure 4)⁹⁸. Previous work showed that the level of NPs' toxicity was partially related to the developmental stage of worms. Generally, L3/L4 staged worms appear more resistant to toxic effects from NPs⁵⁹. For example, Zhao *et al.* reported that L1-larvae might be more sensitive to TiO₂-NPs than L4-larvae or adult nematodes⁹⁹. Collin *et al.* also reported that L3 stage worms were more resistant than younger L1 stage worms regarding LC₅₀ of 272 and 15.5 mg Ce L⁻¹ for L3 and L1, respectively¹⁰⁰. Gonzalez-Moragas *et al.* studied the influence of surface modification (citrate and bovine serum albumin) on toxicological profiles of SPIONs using larval and adult staged worms and observed that the higher sensitivity of larvae to SPIONs treatment suggested that the toxic effects of SPIONs are stronger in the early stages of worms¹⁰¹.

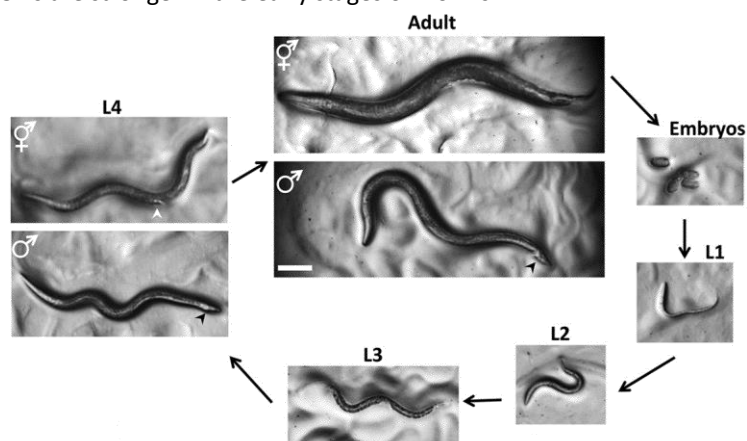


Figure 4 The developmental stages of *C. elegans*. (Worms were cultured on the bacterial lawn) The scale bar represented 0.1 mm. Adapted from AK Corsi⁹⁸.

Effect of exposure duration

The selection of suitable exposure conditions should be in accordance with the research purpose. Normally, prolonged (≥ 48 h) or chronic (≥ 72 h) exposure of worms to NPs could induce more harmful effects than acute (≤ 24 h) exposure, with the potential in studying possible toxicities of some environmental toxicants^{59,76}. Wu et al. evaluated the effects of Dimercaptosuccinic acid (DMSA) coated 9 nm Fe₂O₃-NPs in K-medium using three different assay systems: 24 h exposure of L4 nematodes, from L1 to adults and from L1 to day-8 adult. Adverse effects were observed at concentrations higher than 50 mg/L, 0.5 mg/L, and 0.1 mg/L corresponding to each exposure system indicating extended treatment duration inducing higher toxicity¹⁰². Zhao et al. investigated recovery responses of worms after acute or prolonged exposure to TiO₂-NPs (100 μ g/L). They found prolonged exposed nematodes could not recover to the level compared with that of worms under the normal condition, but acutely exposed worms could⁹⁹.

On the other hand, the chronic exposure system could also be applied to study the eco-toxicity⁷⁶. Yu et al. observed that chronic exposure (10-d) to Al₂O₃-NPs at concentrations of 8.1–30.6 mg/L induced severe stress response and oxidative damage in intestines, whereas acute exposure did not affect¹⁰³. To manifest the nano-bio interactions in the life of *C. elegans*, Piechulek et al. performed a chronic exposure over the entire life span (about 34 days) of worms to Ag, ZnO and CeO₂ -NPs. They found that silver nanoparticles (AgNPs) induced a shortened lifespan and locomotive deficits at concentrations of ≥ 10 μ g/mL, but didn't occur to worms in response to ZnO and CeO₂ -NPs (1-160 μ g/mL), indicating that chronic exposure to AgNPs induced premature neuromuscular defects in worms¹⁰⁴.

Effect of exposure in liquid media and ionic strength

Liquid media is commonly applied as the exposure system with various advantages such as homogeneous NPs exposure and maintained monodispersity of NPs, and regarded as an ideal system for diverse high-throughput studies^{57,59,62}. M9 buffer, S basal, and K-medium are three commonly used liquid media with varied ionic strengths to improve the stability of NPs⁵⁹. However, some studies discovered the occurrence of NPs aggregates in these media. For instance, Meyer et al. reported that, due to the relatively high ionic strength of the K-medium, the formation of AgNPs aggregates with diameters of 1–1.6 μ m that rapidly settled from suspension resulted in an elevated effective local “dose” of aggregated AgNPs at the bottom of wells. Ellegaard-Jensen et al. also observed an immediate agglomeration of AgNPs after addition to the K-medium¹⁰⁵. The incident of aggregation transformed nano-size into micro-size of studied NPs which could lead to a biased nanotoxicity result. For example, Yang et al. found that a lower ionic strength medium (moderately hard reconstituted water) resulted in greater toxicity of AgNPs compared with that of K-medium. It could be attributed to the formation of aggregation which facilitates the uptake of AgNPs aggregates since *C. elegans* feed on bacteria and large particles that have settled to the bottom of the water column¹⁰⁶. On the other hand, reported by Wang et al., even with high ionic strengths, the lower toxicity of

ZnO-NP was found in K-medium¹⁰⁷.

In order to optimize the stability and dispersion to truly reflect the toxicity of NPs, several newly established exposure systems have been employed. For example, Brinke et al. proposed a nematode growth gellan gum (CNGG) with a gel-like component that supported the three-dimensional distribution of worms and food bacteria with allowing free movement of the former. Moreover, CNGG offered advantages for long-term studies and testing other poorly soluble or insoluble NPs¹⁰⁸. Luo et al. found a semi-fluid nematode growth gelrite medium (NGG) with better distribution of AgNPs which can be regarded as a suitable and sensitive culture method for the evaluation of AgNPs toxicity in *C. elegans*¹⁰⁹ compared with other standard nematode growth medium (NGM) and K-medium¹¹⁰. Considering research purposes of eco-toxicity or biomedical applications of NPs which will likely occur in the environment or the human body, it's controversial to make tremendous efforts to establish an ideal exposure condition with homogeneous dispersion and stability of NPs. However, preliminary toxicological profiles of diverse NPs obtained from these artificially created conditions at the starting stage can provide us valuable information and potentially accelerate the research process⁵⁹.

Effect of natural organic matter

In the environmental toxicity study, natural organic matter (NOM) plays an important role in determining bioavailability and toxicity of NPs to the model soil organism *C. elegans*^{59,111}. Yang et al. reported that co-exposure to Pony Lake fulvic acids (PLFA) resulted in the formation of NOM–AgNPs composites and rescued NP-induced damage, potentially by declined intracellular uptake¹¹¹. Collin et al. reported a similar mitigated toxicity of CeO₂-NPs with the presence of humic acid (HA) as NOM. They found that the addition of HA to the exposure media significantly decreased the toxicity which might be related to partial HA adsorption by reducing the reactivity between cells and CeO₂-NPs surfaces¹⁰⁰. Sulfidation is one primary transformation of manufactured AgNPs in the wastewater treatment process. Starnes et al. observed greatly reduced toxicity of sulfidized AgNPs (sAgNPs) as compared to manufactured AgNPs suggesting that sulfidation transformation via the wastewater treatment plants (WWTPs) could mitigate the toxicity of AgNPs¹¹². Additionally, the low and negligible toxicity of sAgNPs in the presence of NOM regardless of NOM influence on dissolution was also reported by Collin et al¹¹³. Schultz et al. observed that increasing soil organic matter content significantly decreased the toxicity of 3–8nm unfunctionalized silver (Ag 3–8Unf)¹¹⁴.

The addition of NOM has the potential to mimic the environmental condition. For instance, Tyne et al. designed a new toxicity testing medium providing better representation of soil solution condition than other media, called simulated soil pore water (SSPW). The low ionic strength coupled with the existence of the dissolved organic component of SSPW make it a suitable environment for metal and NPs toxicity testing in *C. elegans*¹¹⁵.

Effect of food availability

The addition of *E. coli* is suggested to be performed in the exposure system, especially for long-term exposure, to ensure sufficient food supply and avoid starvation effects¹¹⁶. Interestingly, we found conflicting results from several studies about the influence of food availability. Ellegaard-Jensen et al. found that containing *E. coli* in the test medium as a food source increased AgNPs toxicity towards nematodes compared to without food presence condition¹⁰⁵. Likewise, Luo et al. reported that a mixture of AgNPs and *E. coli* would increase the uptake of NPs into worms resulting in increased cellular and organ toxicity¹⁰⁹. They further found that small-sized AgNPs (25 nm) could be more easily accumulated in *E. coli* and exhibited stronger toxicity to *C. elegans* in the food chain¹¹⁷. Even with the removal of potential accumulations of NPs in alive *E. coli*, CuO-NP could also interact with the organic bacterial lysate components into forming agglomerates which can be ingested by nematodes and released copper ions contributed to toxic effects, reported by Mashock et al.⁸¹. Kleiven et al. also demonstrated that *E. coli*, acting as vehicles, enhanced the bioavailability of Ag(I) from NM300K AgNPs and consequent the toxicity¹¹⁸. Oppositely, Yang et al. found that food had a strong mitigating effect on AgNPs toxicity¹¹¹. Moreover, a similarly beneficial influence from the addition of bacterial food was reported by Starnes et al. on decreasing the toxicity of sAgNPs and AgNPs¹¹². However, some researchers claimed that there were no clear relations between bioaccumulation and food presence. Collin et al. observed that the addition of *E. coli* did not modify the Ce accumulated by *C. elegans* exposed to CeO₂-NPs¹⁰⁰, and Yang et al. also reported that “biomagnification” effects were not observed in food-borne Fe⁰NP-exposed worms¹¹⁹. Different types of NPs studied in diverse exposure conditions may explain the discrepancy.

Effect of standard toxicity assays

Multiple types of exposure systems, mostly acute exposure, have been applied to study NPs’ potential toxicities or biomedical applications. But, within each exposure system, modification or optimization in methodological details is allowed due to special properties of certain NPs. But maybe these small variations allowed in the methodology affect NPs’ behaviors and toxicity the most¹²⁰. Hunt et al. demonstrated standardization factors for toxicology and good *C. elegans* culture practice (GCeCP) are essential to obtain reliable and repeatable results⁶⁸. Scanlan et al. developed a standardized counting protocol with maximizing counting accuracy and minimizing variability for *C. elegans* in liquid medium. They identified sources of variability and found three variables with significant effects on counting which were shaking of the culture, priming of pipette tips, and sampling location¹²¹. In addition, Hanna et al. studied experimental factors of six main branches including organism maintenance, protocol, bacteria etc. and found bacterial feed density and plate shaking had significant influences on growth inhibition by exposing to benzylcetyldimethylammonium chloride (BAC-C16), identified by cause-and-effect analysis¹²². Furthermore, they observed that hetero-agglomeration of *E. coli* with positively charged NPs caused growth inhibition of

C. elegans, whereas greatly reduced toxicity without the presence of *E. coli*, illustrating a key unexpected artifact which may occur in nanotoxicity assays¹²³.

Overall, this section displayed several key factors combined with standard toxicity assays, which are required to be considered to obtain reliable data and ensure comparability between studies for more accurate evaluations of nano-bio interaction.

1.5.3.2 Physicochemical properties of NPs

Effect of sizes

Multiple studies demonstrated the strong correlation between NP size and the magnitude of toxic effects⁵⁷. In the study of AgNPs, Meyer et al. observed growth inhibition by all test AgNPs (7, 21, and 75 nm) in low concentrations (0.5, 5, 50 mg/L). The bagging phenotype and intergenerational transfer were only detected for 7-nm citrate coated AgNPs, indicating that reprotoxicity was related to size difference¹²⁴. Furthermore, they continued to study several factors involved in the mechanism of AgNPs toxicity with several sizes of AgNPs (from 5 to 75 nm average diameter). There was no correlation between size and toxicity, but it was dependent on dissolved silver and coating¹⁰⁶. Ellegaard-Jensen et al. also observed higher toxicity of AgNPs28 (PVP coated 28 nm) than AgNPs1 (1 nm) and demonstrated that it might be due to a combination of effects of coating, Ag-solubility and higher uptake rates¹⁰⁵. On the other hand, some researchers reported that size-dependent adverse effects were observed on lifespan and fertility in the multigenerational exposure¹²⁵ in PVP-coated AgNPs^{117,126}. It was also reported in the study of AuNPs coated with 11-mercaptoundecanoic acid (MUA) that size-dependent toxic effects were observed in the declined worm population and mean body length reduction¹²⁷.

In the study of metal oxide NPs, Roh et al. reported that smaller sized CeO₂-NPs (15 nm) induced more toxic effects than larger sized (20 nm) on toxicity endpoints measured (survival, growth, and fertility)¹²⁸. Arnold et al. also stated that exposure to CeO₂-NPs caused more dramatic growth inhibition compared with bulk CeO₂¹²⁹. Additionally, findings that small-sized NPs are more toxic than larger-sized have been published for TiO₂^{130–132}, ZnO^{133,134}, Ni¹³⁵, or iron oxide NPs^{77,136}.

Effect of surface properties

Surface properties can make a profound influence on the toxicity induced by NPs, mostly in a positive way⁵⁷. For AgNPs, Yang et al. demonstrated that the mechanism of AgNPs toxicity was dependent on surface coating by using three types of AgNPs separately coated by citrate, polyvinylpyrrolidone (PVP) and gum arabic (GA)¹⁰⁶. Ahn et al. also found that bare AgNPs had toxicities, whereas PVP coating reduced the toxicity of the AgNPs significantly¹²⁶. Considering environmental toxicities, Schultz et al. found that the higher reproductive toxicity of unfunctional AgNPs compared with that of PVP-coated AgNPs may depend on the surface coating. They proposed that the extent of observed toxicity was related to the degree of

agglomeration, a more rapid attachment of organic molecules to the uncoated surface than to the PVP-coated AgNPs¹³⁷. Moreover, sulfidation of AgNPs can contribute to declined toxicity relative to their pristine counterparts by not only decreasing the solubility of AgNPs but also reducing the bioavailability of intact NPs^{57,112,138,139}.

Gonzalez-Moragas et al. demonstrated protective effects of bovine serum albumin (BSA) because of less degradation of SPIONs and declined toxicity to *C. elegans* even at 500 µg/mL^{101,140}. Wu et al. investigated the possible environmental safety concentrations of Fe₂O₃-NPs coated with DMSA in different assay systems with multiple toxicity endpoints and detected adverse effects on worms¹⁰². Höss et al. studied the toxicity of selected iron oxides (FeO_x) with variable aggregate sizes and compositions of FeO_x-associated organic matter (OM) on *C. elegans*. They reported that OM compositions determined the toxicity of mixed OM-FeO_x¹³⁶. Another type of NOM, HA, has also been reported of reducing the toxicity of CeO₂-NPs when it's added into the exposure system¹⁰⁰, by Collin et al. Kim et al. synthesized platinum nanoparticles conjugated with HIV-1 TAT-derived peptide via a platinum binding peptide and studied its anti-oxidative effects in *C. elegans*. The authors observed greatly improved internalization and enhanced antioxidant effects¹⁴¹. In contrast, Hu et al. found that, with higher ratios of MUA to AuNPs, more severe toxicity was observed in *C. elegans* compared with bare AuNPs¹²⁷.

On the other hand, it is broadly accepted that NPs with positive charges, especially due to surface functionalization, induce higher toxicity than ones with negative charges⁵⁷. For instance, Arndt et al. compared mortality and reproductive toxicity caused by identical CeO₂-NPs but differently coated by cationic (diethylaminoethyl dextran; DEAE), anionic (carboxymethyl dextran; CM) and non-ionic (dextran; DEX) polymers. They observed approximately an order of magnitude higher toxicity induced by DEAE coated CeO₂-NPs¹⁴². The same finding was also reported by Collin et al. that positively charged CeO₂-NPs were significantly more toxic to *C. elegans* with a greater extent of bioaccumulation than the neutral and negatively charged CeO₂-NPs¹⁰⁰. But Hanna et al. assessed the toxicity of Si, Au, and polystyrene NPs with different charged coatings in a standard *C. elegans* toxicity assay system with food supply and concluded that positively charged NPs were observed to form a hetero-agglomeration with *E. coli* which would lead to a false positive toxic effect on growth and reproduction¹²³.

Effect of ion release

The disintegration of NPs released metal ions that can be considered to make a partial contribution to the final toxicity of metal or metal oxide NPs⁶¹. Yang et al. reported that a linear relationship between dissolved silver and toxicity was discovered. Gum Arabic coated AgNPs (GA-AgNPs) are most toxic with the highest dissolved silver concentration, whereas citrate coated AgNPs are least toxic with the lowest dissolved silver¹⁰⁶. In addition, Ahn et al. and Maurer et al. demonstrated that relatively higher toxicity of bare AgNPs¹²⁶ and PVP-AgNPs^{61,143} could be partially due to dissolved silver ions, respectively. The occurrence of dissolved silver of PVP-AgNPs was also proposed in a modified toxicity assay medium¹⁰⁹ or in

a common toxicity testing medium with the addition of NOM¹¹³ which was regarded to be involved in the triggered toxicity of AgNPs. Considering metal oxide NPs, Mashock et al. concluded that released copper ions from CuO-NPs are a major factor contributing to the observed toxicity of neuronal health and stress response⁸¹. The study made by O'Donnell provided evidence that apoptosis in germ cells and enhanced apoptosis effects promoted by ZnO-NPs exposure was partially due to ionic zinc¹⁴⁴, correlated with the previous finding proposed by Ma et al¹⁴⁵. Gonzalez-Moragas et al. also demonstrated that toxicity effects exerted by SPIONs were partly explained by the release of iron ions¹⁰¹.

The dissolution of metal or metal oxide NPs could also occur under the light radiation condition for studying their phototoxicity. For instance, Nie et al. stated that full UV treatment enhanced AgNPs uptake which is also inclined to release more Ag⁺, a crucial factor influencing its toxicity¹⁴⁶.

Effect of radiation

Some studies demonstrated that UV irradiation, as an environmental factor, and laser radiation, for biomedical applications, may enhance the toxicity of studied metal or metal oxide NPs⁵⁷. Nie et al. reported that UV-radiation induced complex physicochemical changes of AgNPs which held a great impact on the toxicity on *C. elegans*¹⁴⁶. The phototoxicity of ZnO-NPs was demonstrated by Ma et al. that three times' increase of toxicity was detected under natural sunlight (NSL) compared to that under ambient artificial laboratory light (AALL) illumination¹⁴⁷. Angelstorf et al. noted that light-induced production of reactive oxygen species (ROS) by TiO₂-NPs increased their toxicity from a median effect concentration of 100 mg/L to 53 mg/L¹⁴⁸.

In view of biomedical applications, Foster et al. demonstrated that laser-induced photothermal, and accompanying nano- and microbubble phenomena, can injure or kill *C. elegans* containing gold nanoshells, gold nanospheres or magnetic (iron oxide) NPs at laser energies which are safe for humans. It has the potentiality of being applied to detect and physically eliminate small organisms and pathogen carriers¹⁴⁹.

In general, this section listed some factors related to physicochemical properties of NPs which are responsible for NP-induced toxicity effects. Some of them can be applied for the elucidation of the toxicity mechanism of SPIONs and AuNPs.

1.5.4 Uptake, biodistribution and translocation

C. elegans, especially young adults, could uptake particles of a size range of 0.5-3 μm ^{150,151}. The observed toxicity is partially correlated with the biodistribution of NPs inside worms. Benefiting from the transparency of *C. elegans*, applying multiple types of microscopy⁵⁹ and novel techniques such as synchrotron radiation X-ray fluorescence (SRXRF)¹⁵² and Raman imaging¹⁵³ techniques, we can localize NPs more easily and accurately. According to most of the research studying bio-distribution, metal and metal oxide NPs mainly distributed alongside the digestive tract, although some may translocate in the reproductive organ. For AgNPs, early studies stated that they were distributed alongside the digestive system¹⁵⁴, as the major uptake

site. Maurer et al.¹⁴³ and Yang et al.¹¹¹ also considered the possibility of endocytosis *in vivo* by the lysosome. Luo et al. reported that they found small AgNPs in the subcutaneous tissue, gut lumen, and gonad, demonstrating that AgNPs penetrated cells of various tissues through the intestinal wall¹¹⁷. A similar discovery for silica NPs was proposed that they were not only observed in the lumen of pharynx and intestine¹⁵⁵ but also in the egg-laying organ vulva and in spermathecae¹⁵⁶. Oppositely, CuNPs were found only in the alimentary region¹⁵². The confinement of AuNPs in the intestine without translocation to other cellular compartments was also reported^{157,158}. Gonzalez-Moragas et al.^{101,159} and Yu et al.¹⁴⁰ demonstrated that most SPIONs were located inside the intestinal lumen, and only a small number could be detected in the endosomal/lysosomal compartment. It's similar to the distribution pattern of CeO₂-NPs that they were present in the digestive tract as well as on the cuticle¹²⁹. On the contrary, TiO₂-NPs were detected in the digestive lumen, extending from the pharynx to the anal region¹⁶⁰. Additionally, more deposition was found in the tissue of the terminal bulb¹⁵³ and into intestinal cells⁹⁹ of passing through the biological membrane of the pharynx and intestine. Gupta et al. noted that 10 nm ZnO-NPs could be detected inside eggs with the main distribution inside the whole digestive tract¹³⁴.

1.5.5 Recovery and excretion of NPs from *C. elegans*

Researchers had stated that acutely exposed worms might undergo the recovery process when they were transferred to normal culture conditions with *E. coli*, whereas worms after prolonged or multigenerational exposure might have difficulties in recovery^{57,62}. One of the hypotheses is that NPs taken up inside worms in the liquid medium can be excreted with the resumption of food^{161,162}. Rare earth fluoride nanocrystals (NCs)¹⁶³ and fluorescent nanodiamonds (FND)¹⁶⁴ could be fully excreted out from worms when they were fed with *E. coli*. Moreover, Gonzalez-Moragas' work suggested that treated worms containing AuNPs or SPIONs could rapidly excrete them out with food resumption, confirming that the excretion process was regulated by the food availability^{101,158}. On the other hand, exposed worms obtained from prolonged exposure to TiO₂-NPs⁹⁹ or multigenerational exposure to AgNPs¹⁶⁵ or AuNPs^{166,167} couldn't fully recover under the normal condition.

1.5.6 Evaluation of toxicity mechanism of NPs in *C. elegans*

1.5.6.1 Oxidative stress

Oxidative stress, accumulation of molecular damage caused by byproducts called ROS, has been generally taken as the predominant cause for toxic effects on *C. elegans* induced by NPs exposure¹⁶⁸. It can result in higher mortality, reduced body length, shortened lifespan, impaired locomotive behaviors, and reproductive damage in a size-specific manner⁵⁷. Hu et al. and Kong et al. suggested that AuNPs¹²⁷ and Ni-NPs¹³⁵ are likely capable of inducing higher oxidative stress which is responsible for multiple toxicities and reproductive toxicity observed, respectively. It's also reported that AgNPs strongly enhanced the production

of oxidative stress with a dose-response effect¹⁶⁹, and the related mitochondrial and DNA damage was likely to be the mechanisms of toxicity¹²⁶. On the other hand, Pt-NPs, as an effective antioxidant, elicited strong resistance against excessive oxidative stress¹⁷⁰, especially conjugated with TAT¹⁴¹. The discovery that ROS accumulation was closely associated with adverse effects was also proposed for metal oxide NPs such as Fe₂O₃-¹⁷¹, TiO₂-^{130,172}, CeO₂-¹⁷³, and Al₂O₃-NPs¹⁰³.

Further studies demonstrated that more severe toxicity was observed in mutants with the deletion of certain genes involved in the ROS defense mechanism⁶¹. Multiples studies have proposed that *sod-1*^{134,174}, *sod-2*^{102,175-177}, *sod-3*^{102,106,129,174-178}, *sod-5*¹⁷⁴, *mev-1*¹⁰⁶, and *mtl-2*^{106,129,175,177} are susceptible genes which response to NPs-induced ROS accumulation⁵⁹. Moreover, Gonzalez-Moragas et al. not only identified several susceptible genes but also proposed key signaling pathways such as MAPK, Wnt, and Calcium pathway which may govern the response of *C. elegans* to SPIONs¹⁵⁹.

1.5.6.2 Signaling pathway

Through pathway analysis in exposed worms, we can identify certain genes involved in the defense process against NPs exposure, which may be extrapolated to higher organisms, even humans⁵⁷. Eom et al. found that the clathrin-mediated endocytosis pathway was a potential mechanism of SiO₂-NPs uptake in *C. elegans*, further resulting in toxic outcomes⁹⁴. Khare et al. indicated that exposure to ZnO-NPs induced altered gene expression which was related to Insulin/Insulin-like signaling (IIS) pathway in *C. elegans*¹³³. Meanwhile, Hu et al. stated that, during the multigenerational exposure to TiO₂-NPs, key genes in the IIS pathway actively regulated the expression of downstream genes with increased stress resistance¹⁷⁹. Furthermore, several pathways were reported to respond to NPs toxicity cooperatively. For AgNPs, the MAPK cascade integrated with the oxidative stress signaling pathway played a pivotal role in defense process¹⁸⁰⁻¹⁸². Kim et al. indicated that JAK/STAT together with TGF- β , crosstalk pathways, were involved in reproductive toxicity and phototoxicity caused by TiO₂-NPs¹⁸³. The finding of Li et al. indicated that innate immunity in *C. elegans* under the regulation of SKN-1/Nrf and the p38 MAPK signaling pathway was suppressed by the early-life long-term exposure to ZnO-NPs¹⁸⁴. Moreover, Tsyusko et al. stated that specific and more general pathways were induced by AuNPs in *C. elegans* including the clathrin-mediated endocytosis, the unfolded protein response (UPR), Ca signaling and amyloid processing pathways. Due to the fact that some pathways were evolutionarily conserved from *C. elegans* to humans, thus it paves a promising avenue for future study¹⁸⁵.

1.6 Analytical techniques with potential to assess nano-bio interactions

Diverse types of novel material science techniques have been adopted to study NPs' behaviors in *C. elegans*⁵⁹ to further understand their nano-bio interactions. For instance, the laser ablation inductively coupled plasma-mass spectrometry (LA-ICP-MS) method was developed for the elemental imaging and distribution of platinum¹⁸⁶ and manganese¹⁸⁷ in *C. elegans*. With LA-ICP-MS, Wang et al. found the increased

cadmium burden in gonads and embryos by concurrent exposure to TiO₂-NPs, indicating the multigenerational reproductive toxicity of Cd¹⁸⁸. Seznec's group reported that particle-induced X-ray emission tomography (PIXET), the advanced version of particle-induced X-ray emission (PIXE)¹⁶⁰, could give us defined information about ionic content and distribution of TiO₂-NPs¹⁸⁹. Raman spectroscopy has been applied to study the spatial distribution of ZnO-NPs¹⁹⁰ and TiO₂-NPs¹⁵³ in *C. elegans*. McColl's group conducted a series of research about the abundance and spatial localization of essential elements in *C. elegans* with synchrotron-based X-ray fluorescence microscopy (XFM)^{191–196}. Additionally, other researchers investigated the aquatic toxicity of cadmium¹⁹⁷, lanthanum¹⁹⁸, cobalt NPs¹⁹⁹, or CuNPs¹⁵² by XFM with the resulting disruption of metals distribution. Fourier transform infrared (FTIR) microspectroscopy has also been used to monitor the change of biochemical compositions of *C. elegans* such as carbohydrates, proteins, and lipids^{159,200–202}. FTIR combined with focal plane array (FPA) allows us to differentiate different anatomical regions by varied IR spectra⁶⁰.

1.7 Conclusions

Given the fact that nanomaterials are continuing to be widely used in all aspects of our life, studies of diverse types of NPs, complemented with advanced techniques including material science techniques, have been conducted in *C. elegans* to obtain comprehensive toxicity results to evaluate their nano-bio interactions. However, limited efforts have been taken to explore their toxic effects on *C. elegans* with the presence of food, with the consideration of potential clinical applications or environmental pollutions via the food chain. Due to the existing gap knowledge, there is a need to study the behavior and fate of NPs with food availability. We treat synchronized worms with SPIONs or citrated-AuNPs with the addition of heat-killed *E. coli* as the food⁶⁸ and measure multiple toxicological endpoints. Moreover, we plan to use the synchrotron-based FTIR to study the relation between lipid oxidation and oxidative stress in treated worms and Raman spectroscopy to explore the laser-induced photothermal phenomenon with AuNPs inside *C. elegans*.

1.8 Objectives and hypothesis

The purposes of this thesis were to acquire general toxicological profiles of SPIONs and AuNPs in *C. elegans* and stress the importance of food presence in the toxicity evaluation system. The parameters were selectively chosen to approve our hypothesis among these known toxicity mechanisms caused by NPs' treatments including lipid storage and lifespan (dysregulation of iron storage), locomotion behaviors and chemotaxis (neurotoxicity), the biodistribution and uptake amount of NPs (potential accumulation pattern), and characterization of NPs' *in vivo* status (ionic release)²⁰³. The brief hypothesis was that food availability would positively decrease toxic effects of SPIONs and AuNPs on *C. elegans*.

Chapter 2 Protocols applied to assess the nano-bio interaction

2.1. Introduction

2.2. Worm exposure conditions

2.3. Multiple toxicity endpoints

2.4. NPs uptake in *C. elegans*

2.4.1. Sample preparation

2.4.2. Physical analysis by magnetometry

2.4.3. Chemical analysis by ICP-MS

2.5. NPs status after exposure to *C. elegans*

2.5.1. Physical analysis by magnetometry

2.5.2. TEM analysis of internalized NPs

2.5.3. Excretion of ingested NMs

2.6. Qualitative analysis of oxidative stress

2.6.1. Sample preparation

2.6.2. Spectral optimization and data analysis

2.7. Photothermal effect

2.7.1. Sample preparation

2.7.2. Raman spectra analysis

2.8. Statistical analysis

2.9. Chapter conclusions

2.1. Introduction

The following parts show detailed protocols, including multiple material science techniques that we established or adopted to investigate interactions between inorganic nanoparticles (SPIONs, AuNPs) and *C. elegans*. The protocols and techniques are summarized in Table 1.

NPs in dispersion		Physicochemical characterization	Both NPs	C-SPIONs	AuNPs
Interactions between NPs and <i>C. elegans</i>	On <i>C. elegans</i>	Exposure condition	Acute exposure	Prolonged exposure	-
		Toxicity endpoints	Survival Progeny Lifespan Intestinal integrity Lipid content Locomotion Biodistribution	Chemotaxis	
		Uptake		Magnetometry ICP-MS	-
		Mechanism	Synchrotron FTIR	-	-
		Photothermal effects	-	-	Raman spectroscopy
		On NPs	NPs status		Magnetometry TEM

Table 1 Techniques used in the investigation of interactions between NPs and *C. elegans*.

2.2. Worms exposure conditions

Worms synchronization

C. elegans were cultured on nematode growth media (NGM) agar seeded with *E. coli*. Gravid worms were washed from NGM plates with M9 medium into a 1.5 mL centrifuge and cleaned with M9 medium for three rounds of centrifugation at 4400 rpm for 1 min to remove additional *E. coli*. The supernatant was removed, and a worm pellet was left at the bottom. The bleach solution is used to dissolve gravid worms to obtain a suspension containing only eggs²⁰⁴. To conduct the bleaching step, the worm pellet was dispersed into 900 μ L M9 medium and 100 μ L mixture of 5 M NaOH and NaClO with a ratio of 1:1. The resulting 1 mL solution was heavily vortexed around 4-6 mins related to the amount of worms. Then another three rounds of centrifugation at 5500 rpm for 1 min were performed to remove the basic solution. After the removal of the supernatant, the egg pellet was redispersed into 1 mL M9 medium and decanted into a 15 mL sterile falcon. Then, it was left under mild agitation overnight at room temperature. The next morning synchronized L1 staged worms were obtained.

Preparation of heat-killed *E. coli*

E. coli was incubated into the lysogeny broth (LB) medium at 37°C with mild agitation overnight. To collect solid *E. coli* from the resulting solution, three rounds of centrifugation at 6000 rpm for 15 min were

performed.

The obtained *E. coli* pellet dispersed into sterile MilliQ water was concentrated to an optical density measurement $OD_{600}=0.5$. The inactivation of *E. coli* was conducted by a heating process at 85°C for 30 min under mild agitation. To confirm the inactivation efficiency, several drops of inactivated *E. coli* solution were pipetted onto LB agar plates and incubated at 37°C overnight. No colonies formed around drops (shown in Figure 5). The obtained heat-killed *E. coli* was stored in the 4°C fridge and should be used within one week.

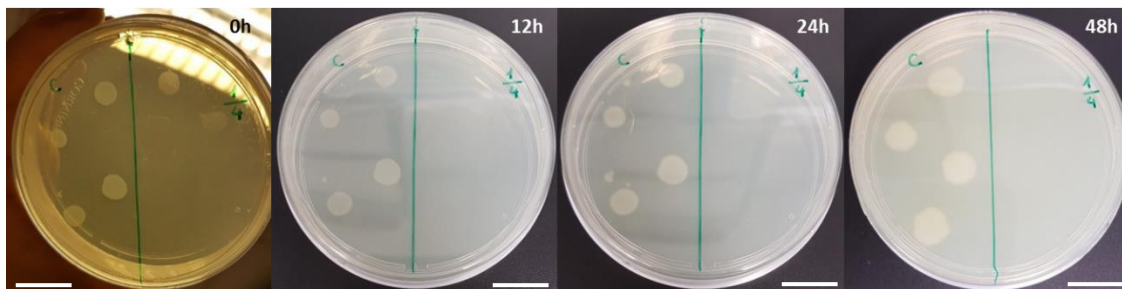


Figure 5 Confirmation of *E. coli* inactivation efficiency in 48 h, 4 drops of alive *E. coli* were put on the left part of the LB agar. 4 drops of heat-killed *E. coli* were put on the right part. The scale bar represents 20 mm.

Acute and prolonged exposure conditions

Young-adult staged worms exposed to NPs for 24 h was defined as the acute exposure^{57,76} (Figure 6). Synchronized L1 staged worms were transferred on the NGM agar plates seeded with *E. coli* and cultured at 20°C for 48 h to reach the young-adult stage which is based on the lifecycle of *C. elegans* at 20°C ²⁰⁵. Then, they were washed from plates with M9 medium (for exposure to SPIONs) or MilliQ water (for exposure to AuNPs) and cleaned by repeated rounds of centrifugation. With the removal of the supernatant, worms were redispersed in $500\ \mu\text{L}$ M9 medium or MilliQ water. A $5\ \mu\text{L}$ -pipette tip rinsed with $1\times$ phosphate-buffered saline (PBS) + 0.01% Triton X-100 (PBST) was utilized to aliquot worms on a glass slide. The estimated number of worms was based on the average number of worms from these drops. The acute exposure assay was conducted in the 96-well-plate with a final volume of $100\ \mu\text{L}$ containing around 15 worms with an additional $4\ \mu\text{L}$ of heat-killed *E. coli*.

Synchronized L1 larvae exposure to NPs for 72 h with *E. coli* was defined as the prolonged exposure^{57,76} (Figure 6). The same cleaning process and steps of estimating the number of worms were applied before conducting prolonged exposure in the 96-well-plates. In each well, around 15 worms were dispersed in the $100\ \mu\text{L}$ solution. $4\ \mu\text{L}$ of heat-killed *E. coli* was added every $24\ \text{h}$ ¹²⁴.

24-well-plate was used to prepare samples with a large population of worms for uptake quantification or assayed materials with a high propensity of aggregation. In each well, the volume of liquid was 1 mL containing 200 worms. The range of concentration was set depending on our previous published works and relative research^{59,101}. The concentrations applied were 100, 300, and $500\ \mu\text{g}/\text{mL}$ for SPIONs and AuNPs, respectively.

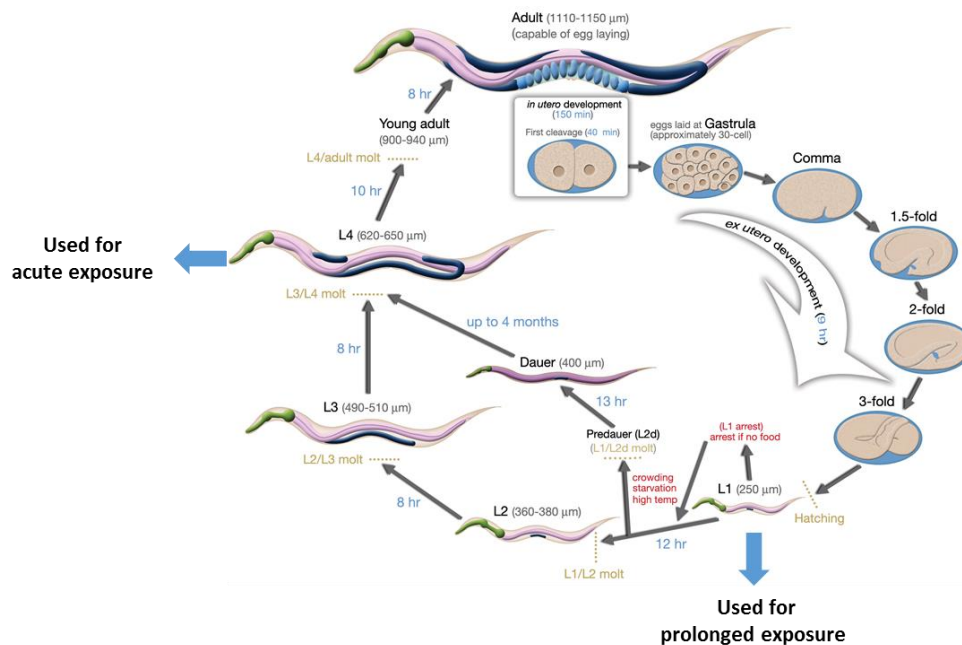


Figure 6 Schematic diagram of toxicological studies relevant to the different stages of *C. elegans* development, adapted from Wu⁵⁷.

2.3. Multiple toxicity endpoints

This part describes experimental details with the use of *C. elegans* in determining SPIONs' or AuNPs' toxicities by examining survival, progeny, lifespan, intestinal integrity, lipid content, locomotion behavior, chemotaxis and biodistribution²⁰⁴.

Survival and progeny assays

In the survival assay, for the acute exposure, synchronized young-adult worms were treated with varying concentrations of SPIONs or AuNPs in the 96-well-plate with a total volume of 100 μ L for 24 h with or without *E. coli*. For the prolonged exposure, synchronized L1-staged larvae were exposed to varying concentrations of SPIONs in the 96-well-plate with a total volume of 100 μ L for 72 h with *E. coli*. Worms in wells under the dissecting microscopy were defined as alive if they moved or responded to the gentle touch by a worm-picker⁷⁶.

To study the brood size, worms from control and treatment groups were dispensed onto a 24-well plate with NGM agar seeded with *E. coli* at 20°C. Every 24 h each worm was transferred into a new well. After 72 h, the number of offspring was counted as brood size. Twenty worms were checked per treatment.

Lifespan assay

Exposed worms were placed onto the NGM agar plate seeded with heat-killed *E. coli* containing 100 μ M Fluorodeoxyuridine (FUdR)²⁰⁶ to cease the progeny proliferation. The day of placement was defined as T=0 for the lifespan assay. The number of worms was scored every two days. If worms failed to respond to the

tapping on the plate or gentle touch on the head by a worm-picker, they were counted as dead. Worms that crawled on the wall of the plate or beneath the agar were not included in the final calculation of lifespan^{207,208}.

Intestinal integrity

The preparation followed reported protocols with minor modifications^{209,210}. Nile Red (Molecular Probes, Eugene, OR) dissolved in acetone with 0.5 mg/mL was stored at 4 °C as the stock solution. 150 µL of freshly prepared Nile red working solution (1 µg/mL) was in the incubation with nematodes under mild agitation for 0.5 h without light exposure. After multiple rounds of centrifugation with PBST to remove supernatant, worms were dispersed into 600 µL of PBST for 0.5 h in the dark, aiming to remove excess Nile red. Then, the same cleaning step was performed, and 50 µL of worm pellet was kept. Stained worms were mounted and immersed into 10 µL of 30 µM NaN₃ solution on the glass slide with an agarose pad. Images were taken with identical settings and exposure time²¹¹. Thirty nematodes were examined per treatment.

Lipid content

Oil Red O stock solution was prepared by dissolving 50 mg powder into 10 mL 100% isopropanol. The solution was 40 % diluted with water and filtered through a 0.2 µm filter, regarded as the working solution. 600 µL of freshly prepared Oil Red O working solution was incubated with worms already fixed by 4% paraformaldehyde for 2 h in the dark^{209,212,213}. Stained worms were mounted on the glass slide with an agarose pad. Images were taken with identical settings and exposure time. Thirty nematodes were examined per treatment.

Locomotion behavior

Fifteen nematodes per condition were transferred onto a new NGM agar without bacterial and recorded for 20s. A body bend was defined as every time the mid-body reaching a maximum bending angle in the opposite direction from the bend previously counted^{130,214}. Fifty worms in total were examined of each condition.

Chemotaxis

Exposed worms were collected and washed by centrifugation with CTX buffer²¹⁵ to remove the excess NaCl. With the removal of the supernatant, the worm pellet was pipetted onto the starvation agar plate and starved for 4 h. Then, starved worms were recollected with CTX buffer and the same cleaning step was performed to have a worm pellet. Around 100 worms were transferred onto the chemotaxis assay plate (Figure 7B) prepared in the method reported before^{216,217}. The worms were cultured on the plate for 1 h at 20°C. Afterward, under the microscope, the number of worms at each spot were counted for the chemotaxis index (CI) calculation, shown in (Figure 7A).

Bio-distribution assay

The bio-distribution assay was performed as described previously¹⁰¹. After exposure, worms were collected and fixed by 4% paraformaldehyde in MilliQ water for 2 h. To perform Prussian Blue staining, a freshly mixed Perl's solution was incubated with fixed worms without light exposure for 1 h. Then, worms were cleaned with MilliQ water and mounted on the glass slide for observation under the dissecting microscopy. The alimentary tract of worms was divided into four sections: pharynx, anterior gut, central gut, and posterior gut (Figure 8). The presence of SPIONs by detecting blue color in each section was counted. Results were expressed as the percentage of worms retaining SPIONs in certain sections and represented in the color map. Fifty nematodes were studied per treatment.

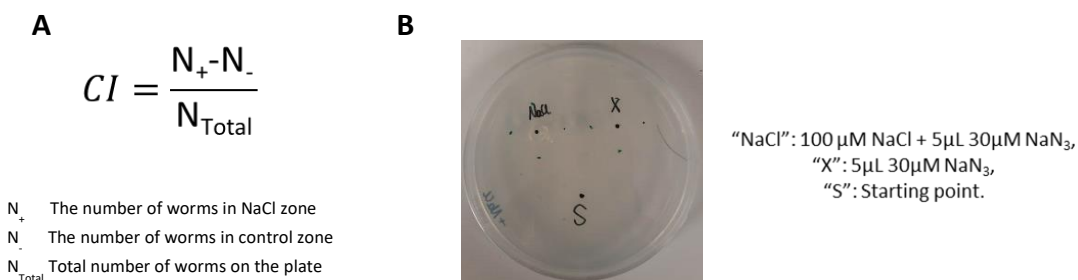


Figure 7 Chemotaxis assay (A) Chemotaxis index calculation equation, (B) Chemotaxis assay plate.

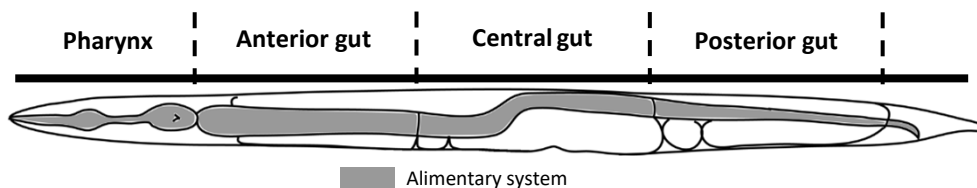


Figure 8 Anatomical evaluations of NPs biodistribution inside *C. elegans*.

2.4. NPs uptake in *C. elegans*

The uptake amount of SPIONs is determined by inductively coupled mass plasma spectrometry (ICP-MS) and Superconductive Quantum Interference Device (SQUID) which is specifically for SPIONs due to their magnetic properties.

2.4.1. Sample preparation

Around 8000 young adult worms were treated in the 24-well-plate for 24 h. Then, worms were thoroughly washed with MilliQ water by centrifugation. After discarding the supernatant, 100 μ L of concentrated worms containing SPIONs with a minimum amount of water was left as the pellet. Meanwhile, the total number of worms should be calculated. The iron content of the resulting solution was determined by ICP-MS with an Agilent 7500ce spectrometer¹⁵⁸.

The sample for magnetometry measurement was performed in the same steps. The worm pellet needed to be kept inside 60°C oven overnight to evaporate all the liquid and then put into a polycarbonate capsule

with a plastic speculum. The sample mass was determined by measuring the capsule before and after the addition of worms¹⁰¹.

2.4.2. Physical analysis by magnetometry

Superconductive Quantum Interference Device (SQUID) measurements were recorded on a magnetometer (Quantum Design MPMS5XL) to determine the magnetization of the SPIONs. Hysteresis loops were recorded at 5 K up to 5 Tesla. Due to the low magnetic signal determined by the small amount of SPIONs in samples, we needed to be precautious to handle sample preparations including removing SPIONs aggregation form the worm pellet, manipulating the capsule with plastic tweezers and filling the capsule tightly with cotton. We dried samples in the 1.5 mL centrifuge tube instead of the capsule, given that the capsule would be dissolved in liquid. Afterward, dried samples would be delivered into the capsule with plastic tweezers and compressed by a certain amount of cotton to make them stay firmly inside.

The subtraction of the diamagnetic signal by fitting the high magnetic field was made to the raw data (Figure 9A) to obtain the hysteresis curve (Figure 9B). The remanence magnetization value of worms containing SPIONs $M_{R(C. elegans)}$ (Figure 9C) was divided by the total number of worms to get the magnetization per worm (emu/worm). To assess the SPIONs uptake amount per worm, $M_{R(C. elegans)}$ was divided by the

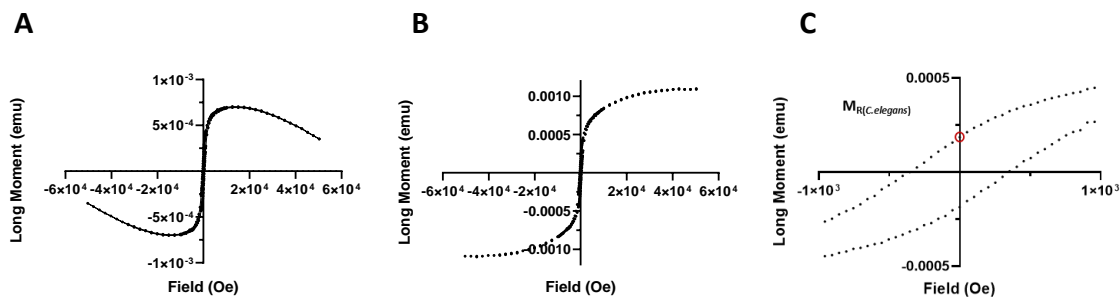


Figure 9 Magnetization measurements of *C. elegans* treated by SPIONs. (A) Raw data, (B) Hysteresis curve by making the subtraction of the diamagnetic signal, (C) Enlarged image of the curve to determine the $M_{R(C. elegans)}$ value.

2.4.3. Chemical analysis by ICP-MS

Given that inductively coupled mass plasma spectrometry (ICP-MS) was performed to measure SPIONs uptake, we adopted a protocol to make a thorough cleaning of the worm pellet¹⁰¹. The sample was dissolved and measured by technicians, and duplicate assays were performed to obtain a stable value of iron content. The completely metal content divided by the number of worms (pg Fe/ worm) was regarded as SPIONs uptake.

2.5. NPs status after exposure to *C. elegans*

2.5.1. Physical analysis by magnetometry

Samples were measured by zero-field-cooled/field-cooled magnetization (ZFC-FC) with measurement

settings (50 Oe applied field and 4-300 K). The blocking temperature $T_{B(C. elegans)}$ of internalized SPIONs shown in Figure 10B and the blocking temperature of original SPIONs $T_{B(SPIONs)}$ could be obtained. According to the Néel-Arrhenius equation (Figure 10A), the decrease could be calculated.

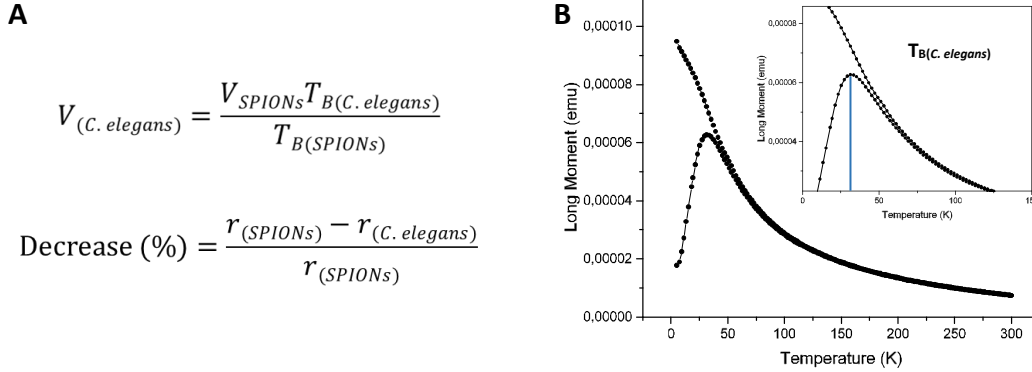


Figure 10 (A) Equations used to calculate the size decrease. V is the NP volume; T_B is the blocking temperature; r is the NP radius, (B) ZFC-FC measurement of internalized SPIONs at 4-300K.

2.5.2. TEM analysis of internalized NPs

After exposure upon SPIONs, worms were collected and washed with MilliQ water by centrifugation. Then a standard bleaching step was followed to dissolve *C. elegans* to obtain internalized SPIONs¹⁰¹. The resulting solution needed to be under the 14000 rpm centrifugation for 30 min to get a noticeable pellet. After removing the supernatant, the pellet was redispersed into the MilliQ water with 5 min sonication. Particle size distribution was analyzed by TEM.

2.5.3. Excretion of ingested NPs

C. elegans is a nematode that lives in the interstitial water containing dissolved or aggregated materials²¹⁸. Meanwhile, upon resumption of the abundance of *E. coli* in the normal culturing condition, treated worms could be stimulated to increase the pharynx pumping rate²¹⁹, and internalized NPs could be excreted fully within hours^{101,164}. To perform the excretion assay, treated worms were collected and washed thoroughly with MilliQ water several times. Then, worms were pipetted on a freshly prepared NGM agar plate seeded with *E. coli* for up to 12h. The excretion process was checked by observing worms under the stereomicroscope.

2.6. Qualitative analysis of oxidative stress

The role of oxidative stress induced by SPIONs or AuNPs was studied by applying synchrotron Fourier transform infrared microspectroscopy (SR- μ FTIR) with the MIRAS beamline at ALBA synchrotron (Barcelona, Spain). The degrees of lipid oxidation in *C. elegans* treated with and without SPIONs or AuNPs

were measured. Given that we have limited access to ALBA due to overbooking applications and restricted length of time for taking measurements²²⁰, we spent tremendous time establishing and optimizing the protocol of sample preparation, even though so far, we have been successfully granted with one project per year.

2.6.1. Sample preparation

The protocol of sample preparations was adopted from our published paper¹⁵⁹ with some modifications. Synchronized L3-staged worms were exposed in 50% M9 medium as control worms and to 500 $\mu\text{g}/\text{mL}$ SPIONs in 50% M9 medium or 100 $\mu\text{g}/\text{mL}$ AuNPs in MilliQ water as treated worms. After exposure, worms were collected into a 1.5 mL centrifuge tube and cleaned with MilliQ water thoroughly with multiple times' centrifugation (4400 rpm, 1 min). Then, around 50 worms per condition were aliquoted on the CaF_2 window into nine drops and dried in the vacuum condition at room temperature overnight. In this way, over-aggregation or overlaying of worms could be prevented during the vacuum drying process (shown in Figure 11).

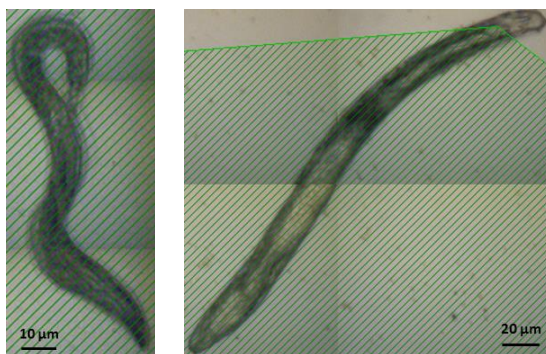


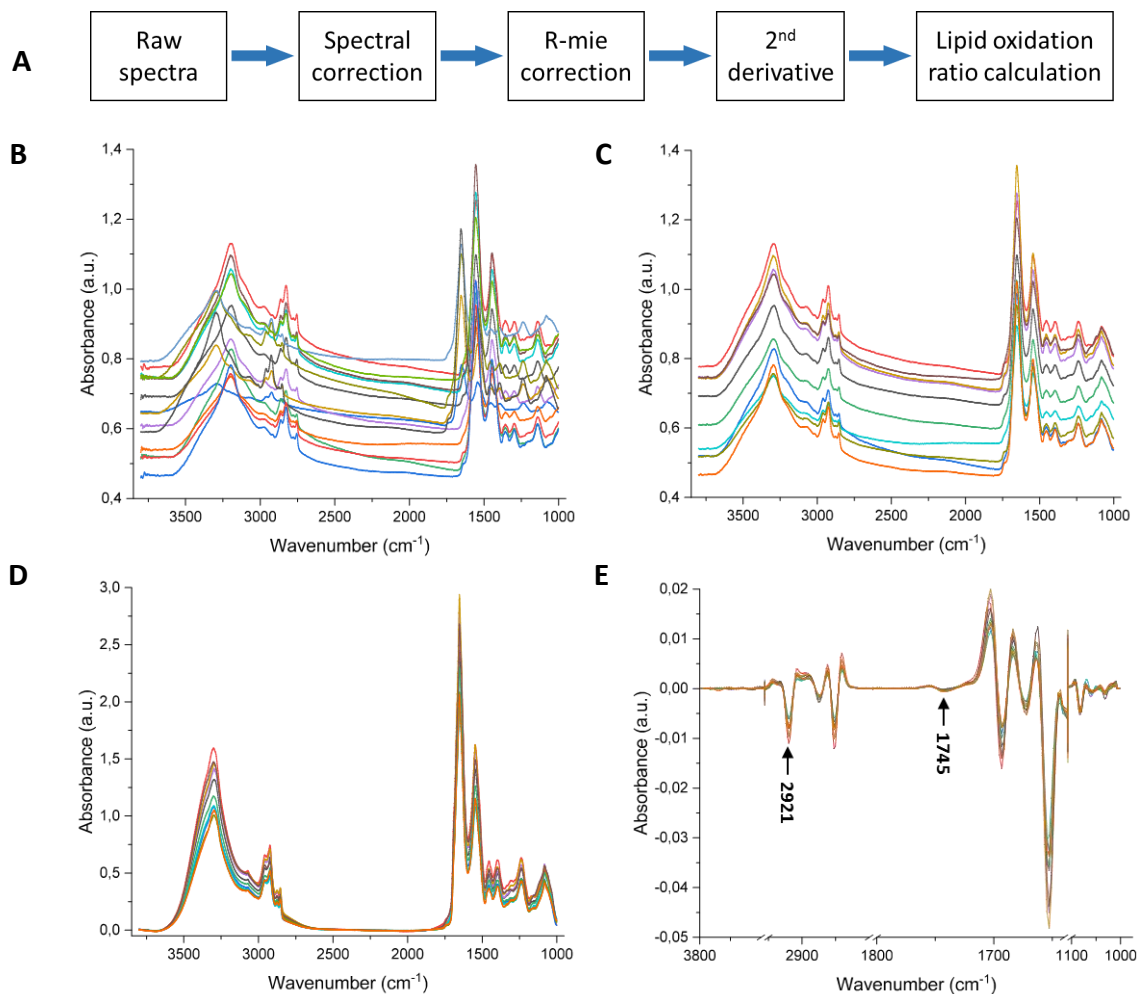
Figure 11 Visual images of *C. elegans* on the CaF_2 window for the SR- μFTIR measurement.

2.6.2. Spectral optimization and data analysis

SR- μFTIR experiments were performed with a Hyperion 3000 Microscope coupled to a Vertex 70 spectrometer (Bruker) equipped with a 36x magnification objective. The spectrum range was 650–4000 cm^{-1} and the spectra collection was done in transmission mode at 4 cm^{-1} spectral resolution. For the single-point measurement, a mercury cadmium telluride (MCT) detector was used with an aperture dimension of 10 $\mu\text{m} \times 10 \mu\text{m}$, and synchrotron light was used co-adding from 128-256 scans. Background spectra were collected from a clean area on each CaF_2 window every 30 s. A focal plane array (FPA) detector was used for imaging measurement using the internal source co-adding 256 scans²²¹.

FTIR data was analyzed with OPUS 7.5 (Bruker), Unscrambler 10.5, and Matlab R2010b (Mathworks). Spectra with signs of low signal to noise ratio or saturation were deleted. The remaining spectra were corrected for Resonant Mie Scattering (R-mie) by an open-source algorithm provided by Gardner group²²².

Matrigel was used as a reference spectrum, 10 iterations, a scattering particle diameter between 2-18 μm , and a refractive index 1.1-1.5. A second-order Savitsky-Golay derivative with 9 smoothing points and a polynomial order of two was applied to the corrected data. Lipid oxidation was determined by calculating the following ratio of each spectra, $\nu_s(\text{C}=\text{O})$ 1745 cm^{-1} / ($\nu_{\text{as}}(\text{CH}_2)$ 2921 cm^{-1})²²³. The scheme flow of spectral optimization was shown in Figure 12.



2.7. Photothermal effect

2.7.1. Sample preparation

The photothermal effect triggered by AuNPs was studied by applying Raman spectroscopy. Synchronized young-adult *C. elegans* were exposed to AuNPs in MilliQ water (treated worms) for 24 h. Then, treated worms were cleaned by centrifugation with MilliQ water to remove the excess AuNPs. Several drops of treated worms were aliquoted onto a clean glass slide on one side with an extra one drop of AuNPs on the

other side, shown in Figure 13.

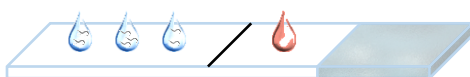


Figure 13 Sample preparation for photothermal effect study.

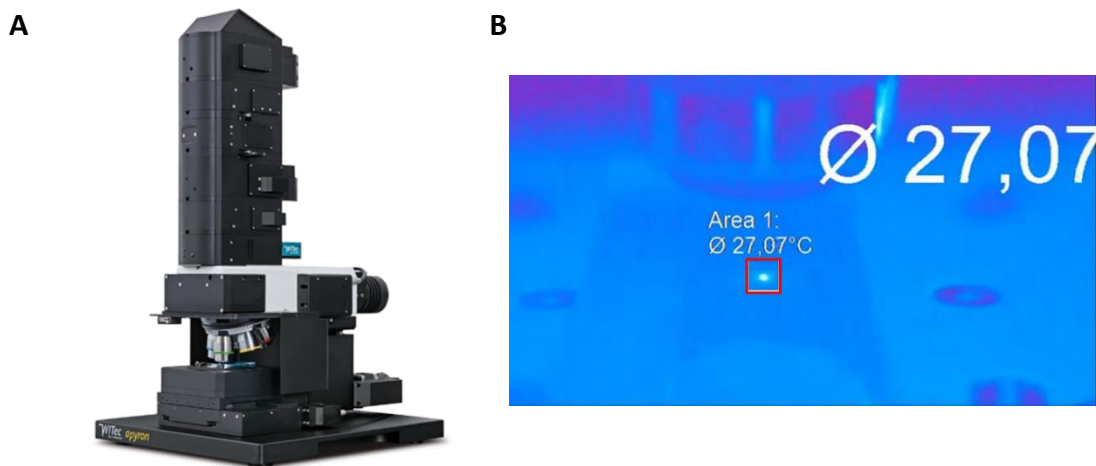


Figure 14 (A) Raman microscopy (apyron ∞ , WITec company), (B) The screenshot of the video recorded by the infrared camera. The red square showed the location where the temperature was monitored, within the chamber of the Raman microscope. The bright spot within the red square is the spot of laser irradiation. The value was the instant temperature of the red square.

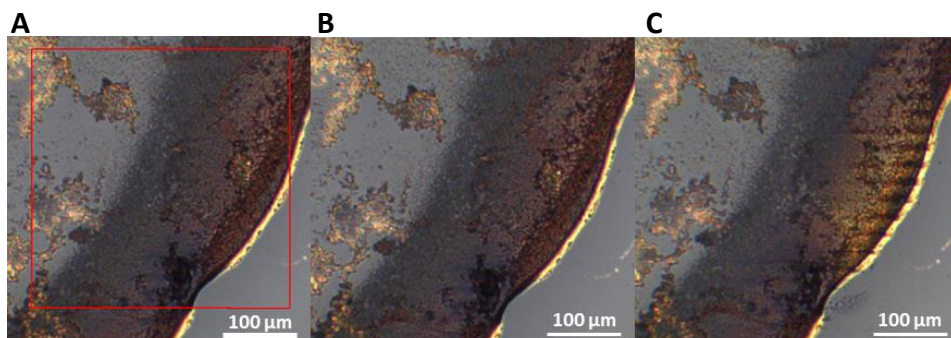


Figure 15 (A) The square zone with red boundary was set on the AuNPs, (B) The image of the zone before laser irradiation, (C) The image of the zone after laser irradiation.

2.7.2. Raman spectra analysis

AuNPs inside worms were under the irradiation using a 785 nm wavelength laser source at different power powers^{224,225} (apyron ∞ , WITec company) (Figure 14A). Three different irradiation modes were applied, namely “fix-point”, “line-scan”, and “large-scale-image-scan”. The “fix-point” mode was performed on one fixed position with stable or varied laser power. In the “line-scan” mode, 100 points per line with an integration time of 1.03 s was set. In the “large-scale-image-scan” mode, within the square zone, three line-scans of 100 points were applied with a scan speed of 103.3 s. A trail of “large-scale-image-scan” was

performed on the AuNPs, shown in Figure 15. An infrared camera was also set to record temperature variations surrounding the laser spot (Figure 14B). Raman spectra and mapping results were analyzed by Witec Project 4.1.

2.8. Statistical analysis

Prism 8.2 was used for the statistical analysis. Statistical significance between the two groups was assessed by T-test. For the multiple toxicity endpoint assays, statistical significance between more than two groups was assessed using ANOVA followed by the Tukey test. Three levels of statistical significance were considered in all cases: $p < 0.0332$ (*), $p < 0.0021$ (**), $p < 0.0002$ (***), and $p < 0.0001$ (****).

2.9. Chapter conclusion

From the material science technical viewpoint, SR- μ FTIR and Raman spectroscopy had been utilized to study changes in chemical compositions and physical properties. Notably, SR- μ FTIR, as a sensitive and non-destructive technique to study complex and intact nematodes, could advance our understanding of genotype-related toxicity mechanisms induced by nanoparticles.

From the biological viewpoint, multiple sublethal toxicity endpoints were applied to achieve a general study of molecular pathways triggered in *C. elegans* exposed upon nanoparticles.

To sum up, a collaborative network of material science and biological techniques could promote the research of nano-bio interaction between nanoparticles and *C. elegans*.

Chapter 3 Evaluation of SPIONs applying *C. elegans*. The influence of food availability and varied exposure durations

3.1. Introduction of superparamagnetic iron oxide nanoparticles

3.2. Aims

3.3. SPIONs synthesis and characterization

3.4. Toxicity analysis

3.4.1. Acute exposure

3.4.2. Prolonged exposure

3.5. Biodistribution of SPIONs

3.6. SPIONs uptake in *C. elegans*

3.6.1. Magnetometry

3.6.2. Inductively Coupled Plasma Mass Spectrometry (ICP-MS)

3.7. NPs status inside *C. elegans*

3.7.1. Zero Field Cooled/ Field Cooled Magnetometry (ZFC-FC)

3.7.2. Transmission electron microscopy (TEM)

3.8. Qualitative analysis of oxidative stress

3.8.1. Study of exposure duration

3.8.2. Study of genetic deficiency

3.8.3. FPA mapping

3.9. Chapter conclusions

3.1. Introduction of superparamagnetic iron oxide nanoparticles

Nanoscience has developed substantially in the past decade; a tremendous amount of research efforts has been extended into the development of nanoparticles' synthesis and their broad medical applications^{226,227}. Iron oxide nanoparticles (IONPs) have attracted great attention due to their intrinsic biocompatibility and their response to an external applied magnetic fields^{228,229}. IONPs can distort the magnetic field of their surrounding environment as a basis for enhanced contrast in magnetic resonance imaging (MRI)^{228,230}. Furthermore, with externally applied magnetic fields, we can achieve in the particle translation, rotation, and even energy dissipation in the form of heat²²⁸, leading to the applications in magnetically controlled drug delivery and magnetic hyperthermia^{227,228}. Superparamagnetic iron oxide nanoparticles (SPIONs) are excellent examples and are promising candidates for multiple bio-applications, as they possess properties of high biocompatibility, low toxicity, and non-immunogenicity^{226,231}. SPIONs can also be used in magnetically promoted cancer cell apoptosis²²⁷, magnetic separation²³², gene therapy, biosensors²²⁷, and treatment for iron-deficiency^{231,233}. So far, SPIONs have been clinically approved for anemia treatment and to be applied as MRI contrast agents, Ferumoxytol (trade name: Feraheme™)^{13,14} and Ferrotan®¹, respectively.

Regarding SPIONs' potential for drug delivery, studies of how they behave *in vivo* are required²³¹. The optimal administration route of NP-mediated drug delivery also needs to be considered²³⁴. The oral administration, as the most preferred administration route³⁸, is widely accepted by patients. The interactions between NPs and biomolecules in the gastrointestinal tract (GI) including food components and digestive enzymes^{42,43} would modify the *in vivo* fate and further affect their therapeutic efficacy^{33,42,44,45}.

In general, researchers study diverse toxicological profiles of different NPs through *in vitro* or *in vivo* assays⁵⁶. Simple non-mammalian models are typically used in the early stages of research which can minimize the cost and deliver answers to *in vivo* toxicological questions with relevance at the organism level^{77,235,236}. Among them, *Caenorhabditis elegans* (*C. elegans*) has been widely proved to be a powerful and valuable non-mammalian alternative toxicity assay model^{57-59,235}, with many advantages such as small size, short and prolific life cycle, ease of maintenance, transparency, etc^{59,61,66,67}. *C. elegans* can orally uptake NPs via the pharynx with food in the exposure system and transport them into the intestinal lumen which is a weakly acidic compartment of around pH 4.4⁷¹ containing digestive enzymes⁷². Together with the great diversity of toxicity endpoints, *C. elegans* is the our-choice model organism for rapid toxicity screening and studying the influence of food availability⁶⁵.

3.2. Aims

The aims were to study the influence of food supply on the interaction between SPIONs and *C. elegans* through measuring multiple sublethal endpoints, such as survival, reproduction, lifespan, etc. and using varied types of material science techniques for example TEM and Superconducting Quantum Interference

Devices (SQUID). This study also would evaluate the suitability of this animal model to study the interaction of food-NPs in a fast and reliable methodology.

3.3. SPIONs synthesis and characterization

SPIONs were synthesized by a fast microwave-assisted thermal decomposition method following previously reported protocols¹⁰¹. The synthesis was performed by colleagues from our group. Briefly, 0.35 mmol iron acetylacetonate $\text{Fe}(\text{acac})_3$ was dissolved into 4.5 mL benzyl alcohol in a microwave glass tube and vortexed for 2 minutes. The reaction tube was put into the microwave reactor (Figure 16A) and the following heating ramp was applied: 1) 5 min at 60 °C, 2) 10 min reaction at 180 °C, 3) cooling down to 50°C in 3 min using compressed nitrogen⁷⁷ (Figure 16B). After the reaction, the black solution was transferred into a 50 mL centrifugal tube, filled up to 40 mL with acetone, and centrifuged at 6000 rpm for 30 min to precipitate SPIONs. The supernatant was removed and the tube was refilled with acetone and centrifuged in the same condition. In the end, the obtained black pellet inside the tube was dispersed in 2 mL MilliQ water containing 5% sodium citrate Na_3Cit , and the tube was agitated overnight. After 12 h, the tube was filled with acetone and another round of centrifugation was applied to remove the extra Na_3Cit . After the removal of acetone, the SPIONs pellet was fully dried in the 60 °C oven overnight and kept in the tube tightly sealed with parafilm.

SPIONs were maintained in a monodisperse colloidal dispersion in aqueous media. SPIONs were characterized by TEM, DLS, and SQUID. SPIONs had a diameter of 5.8 ± 1.2 nm with a hydrodynamic mean diameter of 20 nm in MilliQ water and 36 nm in M9 medium. Electron diffraction rings confirmed the inverse spinel structure ($\gamma\text{-Fe}_2\text{O}_3$ or Fe_3O_4) of SPIONs. Superparamagnetic properties were confirmed, exhibiting a magnetization of 68 emu/g, the hysteresis loops at 5 K showed remanence. The characterization results are shown in Figure 17.

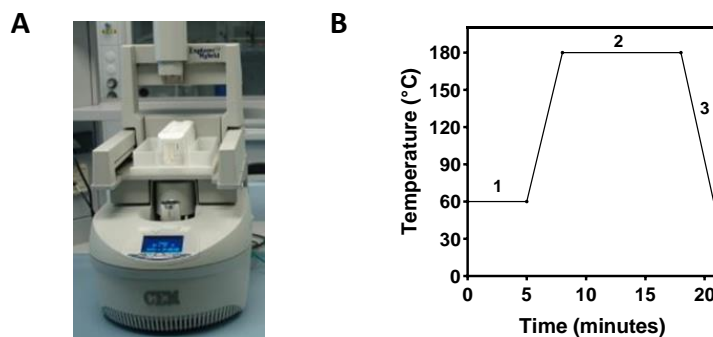


Figure 16 Microwave-assisted synthesis of SPIONs (A) The CEM Focused Microwave Synthesis System, (B) The temperature ramp indicating three steps: 1) 5 min at 60 °C, 2) 10 min reaction at 180 °C, 3) cooling down to 50°C in 3 min.

3.4. Toxicity analysis

C. elegans community has developed assays and standardized protocols, which are ideal for screening diverse NPs in any materials–chemistry laboratory⁶². Endpoints and standardized protocols are detailed in Chapter 2. The majority of these toxicity assays are designed to evaluate NPs influence on different systems of *C. elegans*, containing the alimentary system, reproductive system, neuronal system, and immune system^{62,68}. However, the choice of optimal endpoints for studying NPs' toxicities may rely on several factors, for instance, sensitivity, accuracy, and maneuverability, etc^{237,238}.

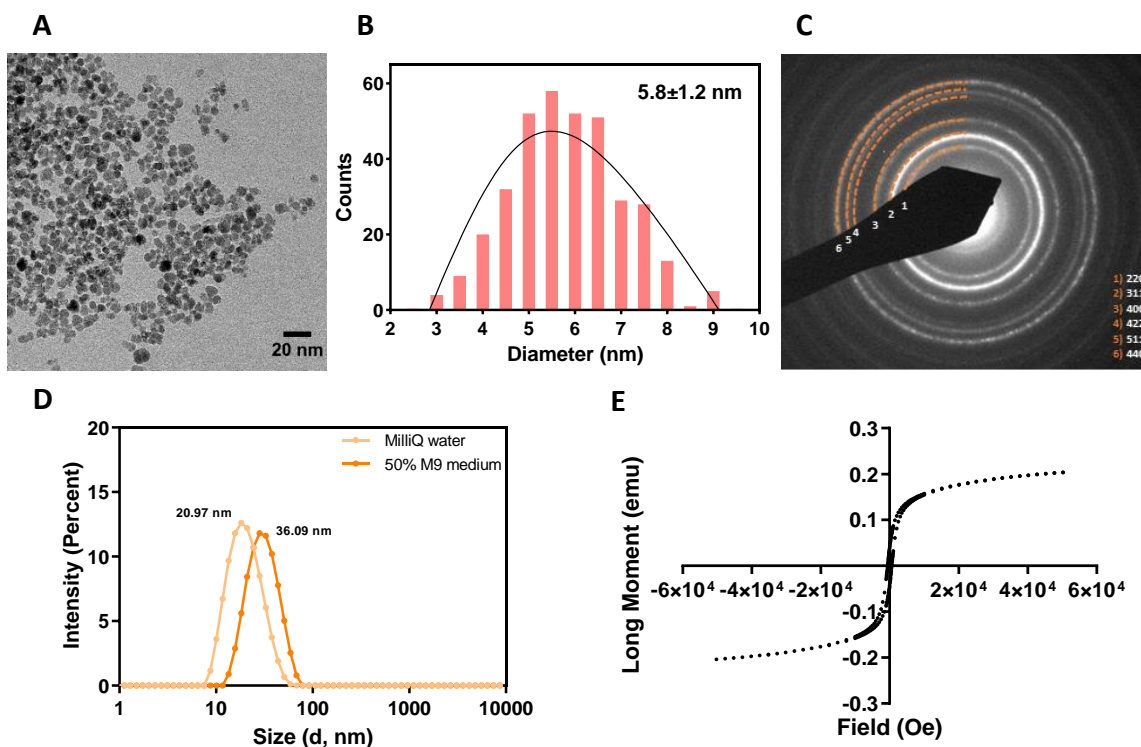


Figure 17 Structural characterization of SPIONs. (A) TEM image, (B) TEM size distribution, (C) SAED pattern indexed to an inverse spinel structure, (D) SPIONs stability in MilliQ water and M9 medium, (E) M(H) measurement at 300K up to 6 Tesla.

Generally, to study IONPs' toxicities in *C. elegans*, survival¹⁰¹ and mortality rate measurements are commonly performed for determining the overall fitness and lifespan of *C. elegans*⁶². The shortened lifespan is related to stress response from ROS production²³⁹ or free iron ions dissolved from IONPs^{208,239,240}. Behavioral (locomotion and chemotaxis)^{62,102} and reproductive (progeny) assays²³⁹ can serve as sensitive indicators of adverse effects from IONPs^{238,241}. The decreased reproduction correlates with endogenous stress like ROS induced by IONPs¹⁰². IONPs can also behave as a neurotoxin causing altered locomotive behaviors suggesting the possible dysfunction of the neural system^{102,171,242}.

C. elegans provides a platform for deciphering the homeostatic mechanisms of fat regulation in intact model organisms²⁴³. In addition, these metabolic responses are coordinately regulated by various endocrine signaling pathways, such as the insulin signaling pathway^{211,244}. On the other hand, *C. elegans* can be applied

as a promising model due to the high conservation of many proteins involved in iron homeostasis, including iron uptake (SMF-3), storage (FTN-1 and FTN-2, encoding ferritin, transcribed by *ftn-1* and *ftn-2*), and export (FPN-1.1, FPN-1.2, FPN-1.3, encoding ferroportin)^{211,245}.

In this chapter, I studied the influence of food availability on *C. elegans* after acute or prolonged exposure upon SPIONs. Synchronized young-adult staged worms exposed to SPIONs for 24 h and synchronized L1 larvae exposed to SPIONs for 72 h were defined as the acute and prolonged exposure, respectively^{57,76}. Previous reports showed that small silver nanoparticles (25 nm) could accumulate inside alive *E. coli* cells and exhibit detrimental effects on *C. elegans* through the food chain¹¹⁷. Thus, in order to avoid any interaction with our nanoparticles, SPIONs, we used heat-killed *E. coli*. After the exposure, survival, progeny, lifespan, intestinal integrity, lipid content, locomotion behavior, and chemotaxis were studied (shown in Figure 18).

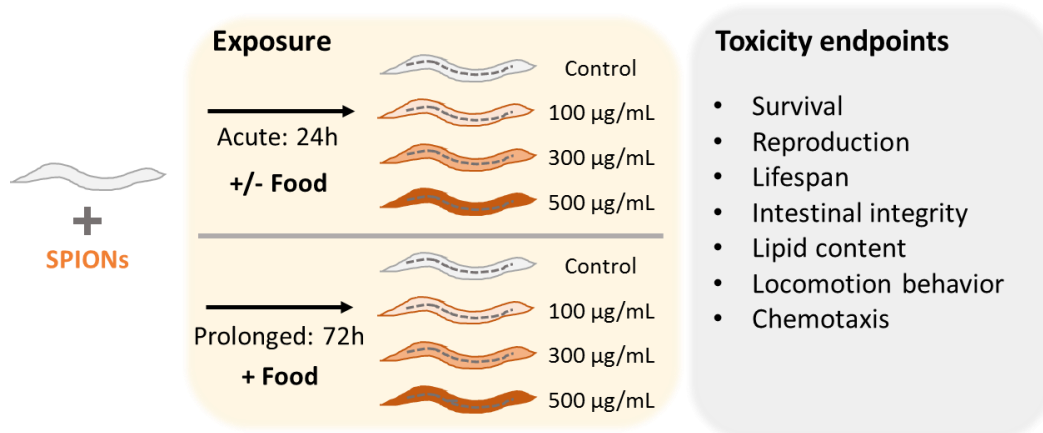


Figure 18 Graphical representations to describe the acute/prolonged exposure conditions and studies toxicity endpoints.

3.4.1. Acute exposure

In this section, multiple toxicity assays were performed with worms over a 24 h exposure to study acute toxicity of SPIONs. We evaluated and compared the toxicity of SPIONs with and without food.

Survival

Survival was calculated by counting worms defined as alive if they moved or responded to the gentle touch by a worm-picker⁷⁶ after 24 h exposure to SPIONs. We found that, with the presence of food, there was no mortality even at the highest concentration of 500 µg/mL (Figure 19A). If we compare this result to the exposure of SPIONs without food, we found a 45% increase in survival¹⁰¹, implying the protective role of the food in the acute exposure to SPIONs.

Reproduction

Reproduction was determined by counting the total number of offspring laid by exposed *C. elegans* after 72 h cultured on the NGM agar seeded with *E. coli*²⁰⁴. With the addition of food, there was a slight decrease

in reproduction percentage in worms exposed to 500 $\mu\text{g}/\text{mL}$ compared to the control group but with no significant difference (Figure 19B). Compared with 81% reproduction rate of 500 $\mu\text{g}/\text{mL}$ SPIONs exposure condition without food, it indicated a beneficial effect provided by food^{161,246}.

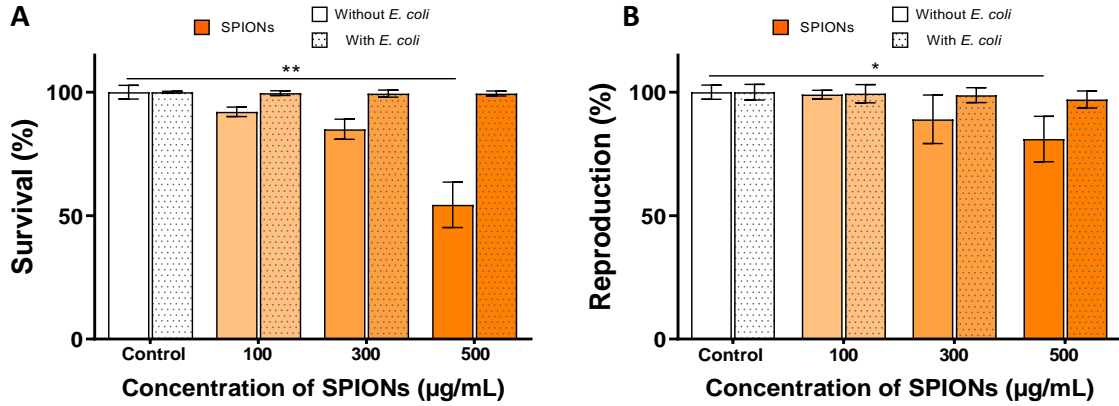


Figure 19 Effects of food availability on the survival (A) and reproduction (B) of *C. elegans* (n=3) exposed to increasing concentrations of SPIONs. Bars indicate the mean \pm S.E.M. p < 0.0332 (*), p < 0.0021 (**), p < 0.0002 (***).

Lifespan

Lifespan was assessed by measuring the longevity of treated worms under controlled conditions containing 100 μM Fluorodeoxyuridine (FUdR) to prevent additional progeny production and bagging^{206,247}. After acute exposure, a dose-dependence decrease of lifespan could be observed independently of the presence of food in the exposure condition (Figure 20). It indicated that exposure to SPIONs could result in a shortened lifespan. Besides, the addition of food couldn't decrease the detrimental effects of SPIONs on the lifespan of *C. elegans*.

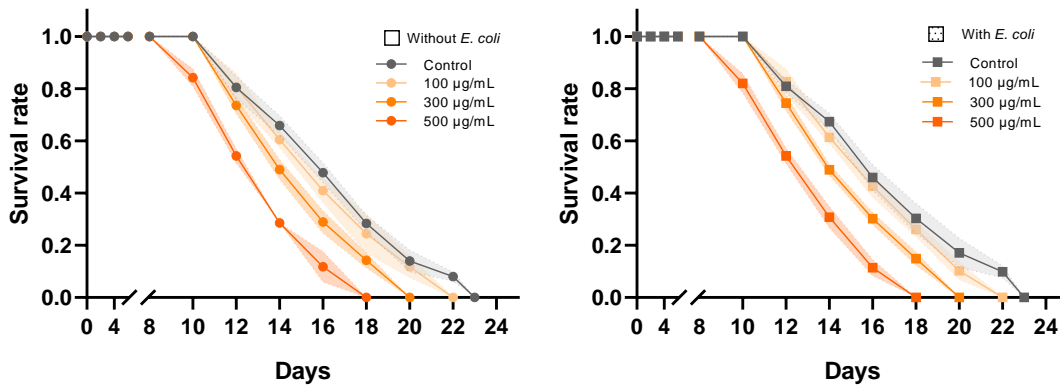


Figure 20 Effects of food availability on the lifespan of *C. elegans* after acute exposure upon SPIONs. (n=3). Bands represented SD.

Intestinal integrity

The intestine is the major site within the alimentary system of *C. elegans* under stress induced by NPs uptake through the ingestion process²⁰⁷. The disruption of intestinal integrity would allow NPs to translocate

into the secondary organs such as reproductive organs, possibly inducing reprotoxicity²⁴⁸ or transgenerational toxicity²⁴⁴. As shown in Figure 21, the relatively brighter parts because of Nile red staining within the whole worm represented the intestinal lumen. Intestinal integrity was determined by the comparison of relative fluorescent intensities from the intestine between control and treatment groups²⁴⁸ (Figure 21). If there was no difference discovered, it suggested that the intestinal integrity was still maintained after exposure. We found that acute exposure of SPIONs didn't impair the intestinal integrity regardless of food presence (Figure 22A), indicating that no severe deficit of intestinal structure was caused by SPIONs exposure.

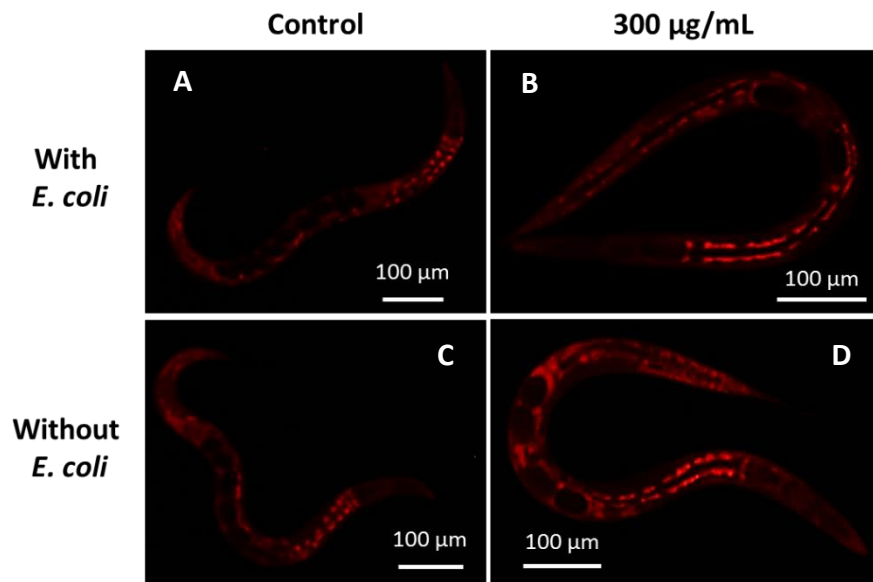


Figure 21 Nile red staining images of worms treated in control and 300 µg/mL SPIONs conditions.

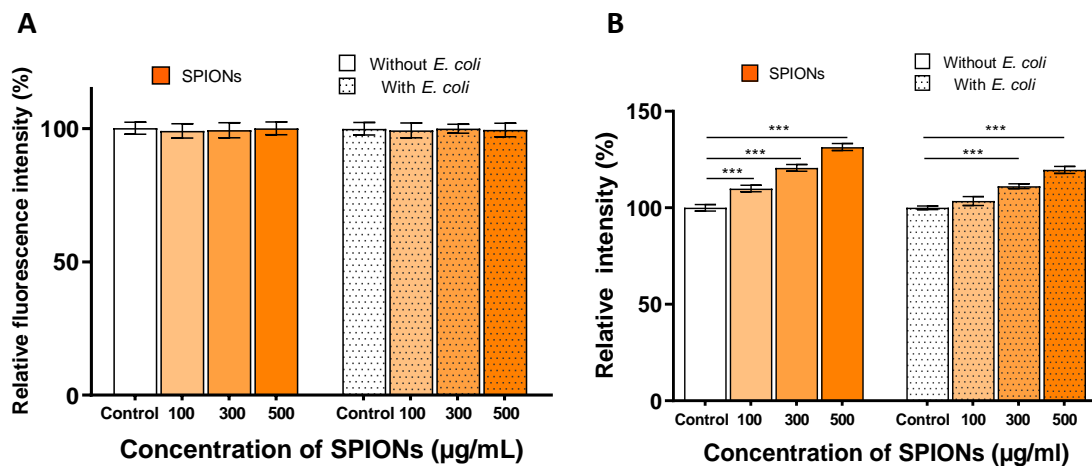


Figure 22 Effects of food availability on intestinal integrity (A) and lipid content (B) of *C. elegans* after acute exposure upon SPIONs (n=3). Bars indicate mean \pm S.E.M. $p < 0.0332$ (*), $p < 0.0021$ (**), $p < 0.0002$ (***)

Lipid content

Lipid content was investigated by applying Oil Red O to assess the fat store²¹³ of worms as the intensity of the stain is related to the amount of lipids in the animal. We compared the fat quantity of control and SPIONs-treated worms in the presence and absence of food. In both scenarios, there was a dose-dependence lipid accumulation tendency (Figure 22B). It might be correlated with findings of iron-promoted lipid accumulation proposed by Wang et al²¹¹. They demonstrated that, under iron overload, there was an iron-induced fat accumulation in *C. elegans*, indicated by increased size of lipid droplets (LDs) and abundance of large-sized LDs²¹¹. Moreover, the metabolic responses of worms are coordinately regulated by various endocrine pathways such as insulin signaling pathways²⁴³. However, the increment of relative intensities is lower when food is available, revealing an effect of food availability on the lipid metabolism of the worm.

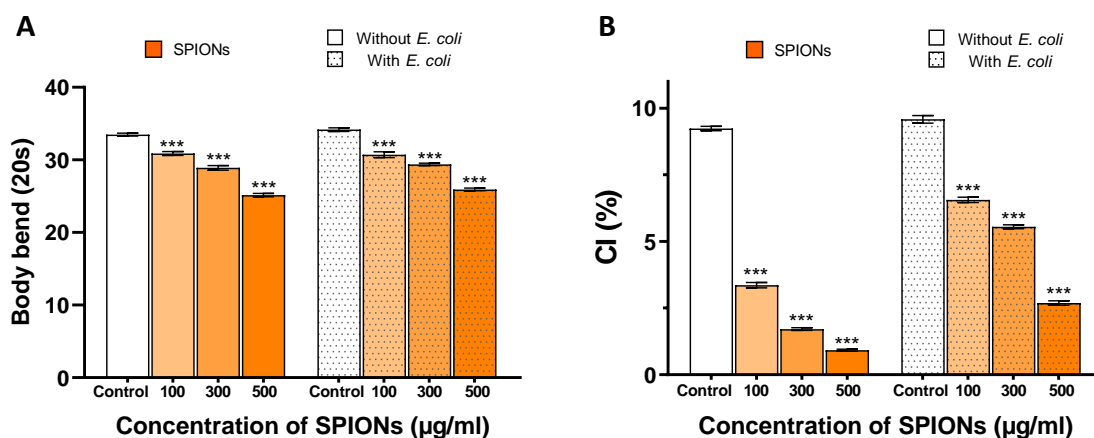


Figure 23 Effects of food availability on body bending frequency (A) and chemotaxis (B) of *C. elegans* after acute exposure upon SPIONs (n=3). Groups with and without food availability were separately analyzed. Bars indicate mean \pm S.E.M. $p < 0.0332$ (*), $p < 0.0021$.

Locomotion behavior

Locomotion behavior was studied by measuring the body bending frequency of worms after exposure to SPIONs. We found that it had a dose-dependent decrease in conditions of with or without food (Figure 23A). The body bending frequency decreased from 34 to 26 and 33 to 25 per 20 s in conditions with or without food availability, respectively. There was a significant difference between control and treatment groups suggesting some underlying neurotoxicity on the movement^{87,249}.

Chemotaxis index

The assay of chemotaxis towards sodium chloride was conducted to evaluate the potential neurotoxicity induced after exposure to SPIONs. From the results (Figure 23B), a decreased chemotaxis of worms exposed to higher concentrations of SPIONs was detected. It indicated that ASE neurons (ASEL and ASER)²⁵⁰, especially the ASEL neuron which is stimulated by the increases in the concentrations of NaCl²⁵¹ or neural

circuits⁸⁸, involved in the chemotaxis, might be dysregulated after SPIONs exposure. Moreover, with the presence of food, we found a relatively less decline in chemotaxis indicating a beneficial influence from food.

To sum up, we conducted a series of toxicity evaluation assays on *C. elegans* exposed to a range of SPIONs for 24 h with or without *E. coli*. Without food availability, exposure upon SPIONs induced lipid accumulation, shortened lifespan, locomotive deficits, and impaired chemotaxis consistent with others' work^{87,211,244}. However, the intestinal integrity was maintained. On the other hand, with food availability, no detrimental effects were observed on survival, reproduction, and intestinal integrity. Moreover, We detected reduced adverse influences chemotaxis, indicating that food played a beneficial role^{161,252}. But the equivalent level of lipid accumulation, locomotive deficits and shortened lifespan suggested that food could provide limited protections for worms.

3.4.2. Prolonged exposure

Survival

After 72 h exposure upon SPIONs, survival was determined by the same method mentioned above⁷⁶. We found that, with the daily addition of food, no severe effect happened to the survival (Figure 24A). L1 larvae of all treatment conditions developed to reach the adult stage (Figure 24C).

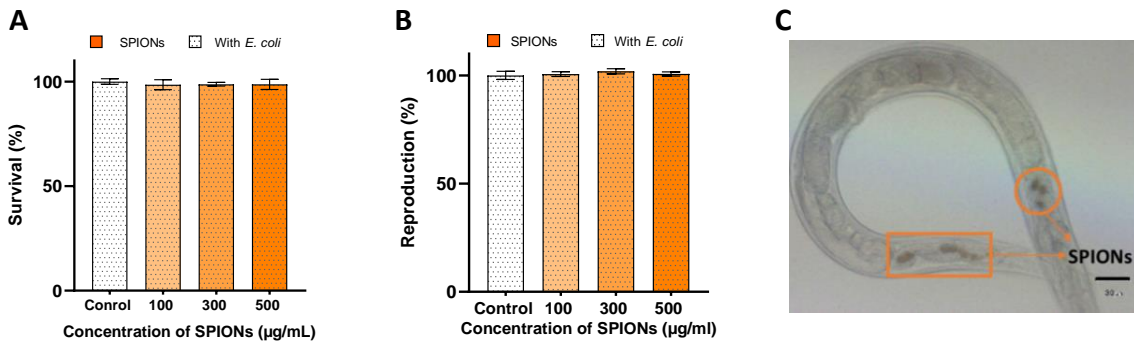


Figure 24 Effects of SPIONs on survival (A) and reproduction (B) of *C. elegans* after prolonged exposure with food availability (n=3). Bars indicate mean \pm S.E.M.(C) The L1 larva after prolonged exposure to SPIONs with *E. coli*. The scale bar represented 30 μ m.

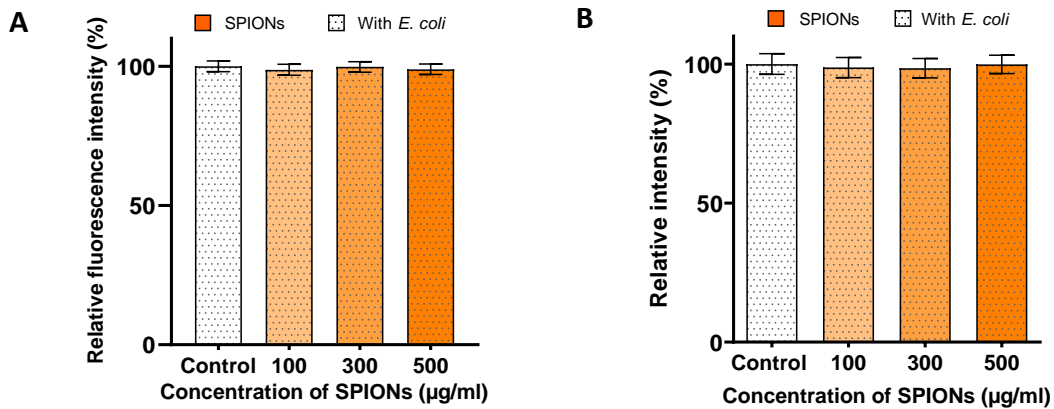


Figure 25 Effects of SPIONs on Nile red staining results (A) and Oil Red O staining results (B) of *C. elegans* after prolonged exposure with food availability (n=3). Bars indicate mean \pm S.E.M.

Reproduction

Reproduction was determined by counting the total number of offspring laid by treated *C. elegans* in 72 h cultured on the NGM agar seeded with *E. coli*²⁰⁴. As it's shown in Figure 24B, there was no significant difference in the reproduction percentage between control and treated worms, indicating that food exhibited protective effects^{116,252}.

Intestinal integrity

Intestinal integrity was evaluated by comparison of relative fluorescent intensities from the intestine stained by Nile red between control and treatment groups²⁴⁸. Compared with control worms, there was no enhancement in the relative fluorescent intensity of treated worms suggesting no effect on the intestinal integrity. The normal state of that in treated worms was still maintained (Figure 25A)²¹⁰.

Lipid content

The study of lipid content comparison was conducted by applying Oil Red O to assess the fat store²¹³. The lipid storage of treated and non-treated worms was relatively equivalent (Figure 25B), indicating that lipid accumulation was not induced.

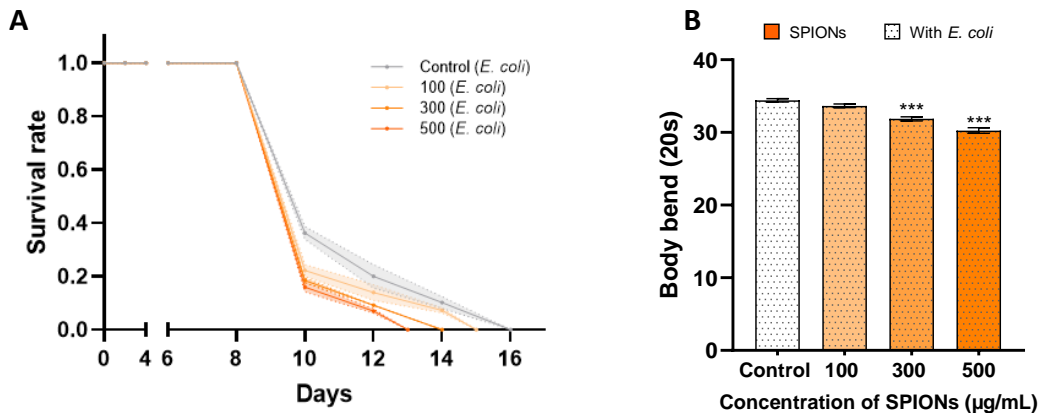


Figure 26 Effects of SPIONs on the lifespan (A) and body bending frequency (B) of *C. elegans* after prolonged exposure with food availability (n=3). Bars indicate mean \pm S.E.M. $p < 0.0332$ (*), $p < 0.0021$ (**), $p < 0.0002$ (***)

Lifespan

Lifespan was determined by the life expectancy of treated worms under control conditions containing 100 μM FUdR²⁰⁶. After prolonged exposure to different concentrations of SPIONs, we found a dose-dependent shortened lifespan (Figure 26A) that indicated a detrimental influence on *C. elegans* after the prolonged exposure to SPIONs.

Locomotion behavior

Locomotion behavior study was performed by measuring the body bending frequency of worms after prolonged exposure to SPIONs. As shown in Figure 26B, we found a dose-response decrease in body bending

frequency.

To summarize, with continuous uptake of food, L1 larvae survived and developed in a stressed environment. Prolonged exposure didn't impair the intestinal integrity or alter lipid storage. However, accumulated locomotive deficits occurred from the declined body bending frequency results and shortened lifespan might be explained by "trade-off" effects. It meant that energy providing by consumed food was more distributed for worms' growth than antioxidative defense against ROS under the long-term of iron stress condition^{159,207,246}.

Through the comparison of toxicity endpoints of worms separately treated in acute and prolonged exposure conditions with the presence of food, we found a similar extent of locomotive deficits and shorted lifespan except for the accumulated lipid content of worms after acute exposure (Table 2). It could be attributed to the notion that adult worms are more stress-resistant to deal with the toxicities from NPs compared with L1 larvae²⁵³. The adult nematodes could make flexible responses to defend or compensate for detrimental impacts on the whole-body system (a tendency of lipid accumulation). In general, L1-stage worms are more sensitive to the NP-induced toxicity^{59,100}. L1 larvae need to distribute more energy to assure that they could survive and develop in the toxic environment, especially in the varying nutritional conditions (same level of lipid content)^{254,255}. On the other hand, it might be correlated with the extended exposure time in the prolonged exposure condition. It had been reported that prolonged exposure upon NPs could induce adverse effects on locomotion behaviours^{176,256}.

		Survival	Decreased reproduction	Locomotive deficits	Shortened Lifespan	Lipid accumulation	Impaired Chemotaxis
Acute exposure	—	✓	✓	✓	✓	✓	✓
	+	↓	↓	=	=		↓
Prolonged exposure	+			✓	✓		✗

— Without food + With food ✓ Detected toxic effects = Equivalent toxic effects ↓ Decreased toxic effects

Table 2 The summary of diverse toxicity endpoints of *C. elegans* after acute or prolonged exposure upon SPIONs with and without food.

3.5. Biodistribution of SPIONs

We reported that, without the addition of food, after acute exposure, SPIONs were distributed primarily in the pharynx, closer to the entry portal⁷⁷, and the intestine¹⁰¹. Additionally, due to the continuous uptake of food and SPIONs, we expected a shifted gradient of more SPIONs observed in the intestinal area. Benefiting from the optical transparency of *C. elegans* and blue color from SPIONs stained by Prussian Blue, we confirmed the location of SPIONs inside *C. elegans*. Internalized SPIONs could be observed clearly under the microscope (Figure 27). Despite exposure upon different concentrations of SPIONs, we observed high percentages of worms with homogeneous distribution inside the intestinal cavity (Figure 28).

Before, we discovered that internalized SPIONs of treated worms could be fully excreted with the

resumption of food indicating that food availability could allow a continuous cycle of feeding-defecation¹⁰¹. George A. Lemieux et al. discovered that the pharyngeal pumping rate responded to a variety of external and internal cues, including food availability, food quality, and developmental state²⁵⁷. The pumping rate of young adults increases two times in the presence of a food source²¹⁹. Therefore, it is plausible that food availability could still facilitate the uptake of SPIONs, in agreement with previous studies²⁴⁶.

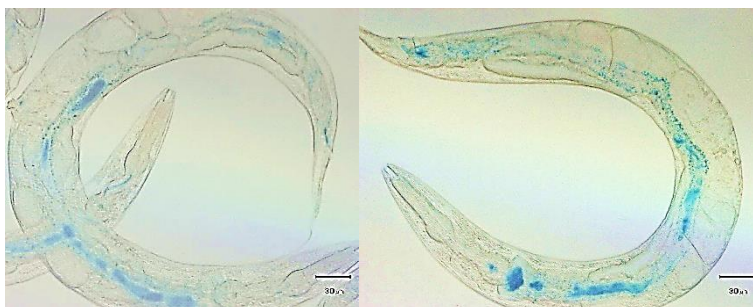


Figure 27 Prussian blue-stained worms after acute exposure to 500 µg/mL SPIONs with *E. coli*. Scale bar represents 30 µm.

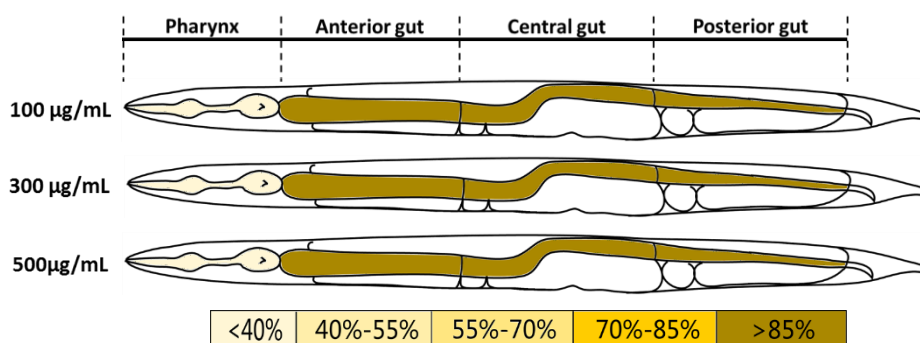


Figure 28 Biodistribution of SPIONs in *C. elegans* after acute exposure to varying concentrations of SPIONs with *E. coli* (50 worms per sample). The upper simplified graph showed the division of the alimentary system: pharynx, anterior gut, central gut, and posterior

3.6. SPIONs uptake in *C. elegans*

Several types of techniques have been applied to measure the iron content of *C. elegans* including inductively-coupled plasma mass spectrometry (ICP-MS)^{101,258}, atomic absorption spectrophotometry (AAS)²⁵⁹, liquid scintillation²⁶⁰ and colorimetric measurement¹¹⁹ related to specific properties of studied iron-containing materials.

In this part, we quantified the SPIONs uptake by conducting a physical approach SQUID magnetometry, self-established and validated¹⁰¹, and a chemical technique ICP-MS.

3.6.1. Magnetometry

Superconducting Quantum Interference Devices (SQUID) are the most powerful magnetic flux detectors allowing us to study magnetic properties of samples with very low magnetic moment⁵⁹. Thanks to the high

sensitivity, SQUID had been successfully utilized to quantify the uptake amount of SPIONs in biological samples, such as *C. elegans*¹⁰¹. The adapted SQUID measurement setting was performed to quantify the loading and study the status of SPIONs in *C. elegans* after the acute exposure to 500 µg/mL SPIONs with food availability. The remanence magnetization over the magnetic field was used to calculate the SPIONs uptake, while the magnetization over temperature, known as Zero Field Cooled Fielded Cooled (ZFC-FC), was applied to reveal their status inside worms. ZFC-FC analysis was presented in Section 2.5.1.

Given that the known total number of worms in samples and obtained remanence magnetization values (Figure 29), we found that the iron uptake per worm was around three times more than that of worms exposed to SPIONs without *E. coli*¹⁰¹ (Table 3), correlated with a well-accepted viewpoint that the dietary route could facilitate the uptake efficiency^{161,246,261} possibly stimulated by the presence of food²⁶².

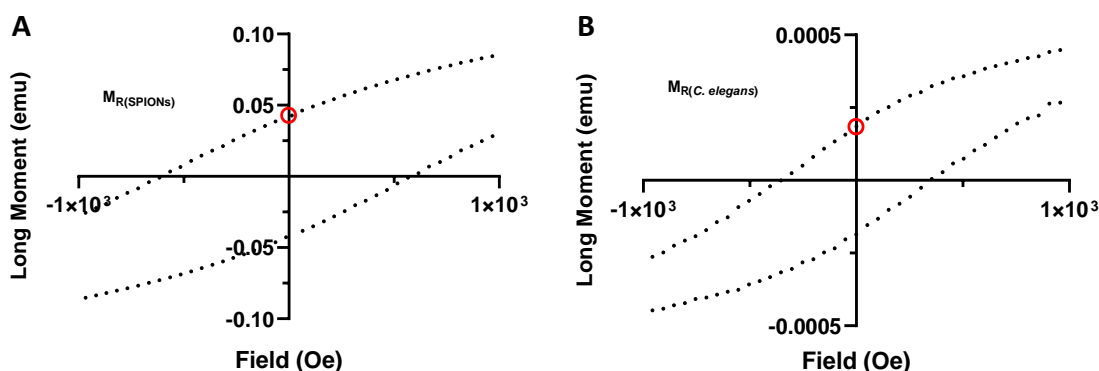


Figure 29 (A) Enlarged magnetic hysteresis of SPIONs at 5 K showing the remanence magnetization $M_R(\text{SPIONs})$, and (B) Enlarged magnetic hysteresis of treated worms at 5 K showing the remanence magnetization $M_R(C. elegans)$.

		Magnetometry (pg Fe/worm)	ICP-MS (pg Fe/worm)	Error (%)
SPIONs Acute exposure	With <i>E. coli</i>	411	406	1%
	Without <i>E. coli</i>	131	140	5%

Table 3 Comparison of the SPIONs uptake results by SQUIDS and ICP-MS. The relative error was indicated.

3.6.2. Inductively Coupled Plasma Mass Spectrometry (ICP-MS)

ICP-MS, a sensitive analytical tool, is used to provide the total mass of certain elements¹⁵⁷. To validate results from magnetometry, we conducted an ICP-MS measurement of worms with internalized SPIONs. The same batch of synthesized SPIONs was used in the sample preparation for SQUID and ICP-MS measurements. As shown in Table 3, iron uptake amount values obtained from both techniques with a small error indicated that they were in good agreement correlated with our previous findings¹⁰¹. This second technique confirmed the results with SQUID and validated the increased uptake efficiency of SPIONs in the presence of food.

3.7. NPs status inside *C. elegans*

The role of food availability in the exposure system is mostly considered as the energy source to mimic environmental conditions. Metal ion release from nanoparticles ingestion is mainly taken as the predominant factor which induces or contributes to toxic effects on *C. elegans*^{81,124,154}. However, as far as we know, the relationship between food presence and nanoparticles' structural modification is seldom addressed. Merely few studies have reported upgraded uptake efficiency of metal salts attributed to food existence^{162,218,262}. To look into the impact of food availability on the structural integrity of internalized SPIONs, after acute exposure, magnetometry measurement and Transmission electron microscope (TEM) analysis of excreted SPIONs were conducted.

3.7.1. Zero Field Cooled/ Field Cooled Magnetometry (ZFC-FC)

The maximum value of the plotted ZFC-FC curve is the blocking temperature (T_B). The size variation was evaluated by applying the Néel-Arrhenius equation with blocking temperatures of SPIONs and internalized SPIONs inside *C. elegans* (Figure 30). The sharp peak of the curve at the low temperature indicated that the paramagnetic component existed probably due to the presence of iron ions¹⁰¹. We found a 14% size decrease of SPIONs after 24 h inside *C. elegans* with the presence of food indicating the occurrence of partial digestion and released iron ions^{101,263}. This decrease seems to be related to the weakly acidic microenvironment and the abundance of digestive enzymes of *C. elegans* intestine⁷².

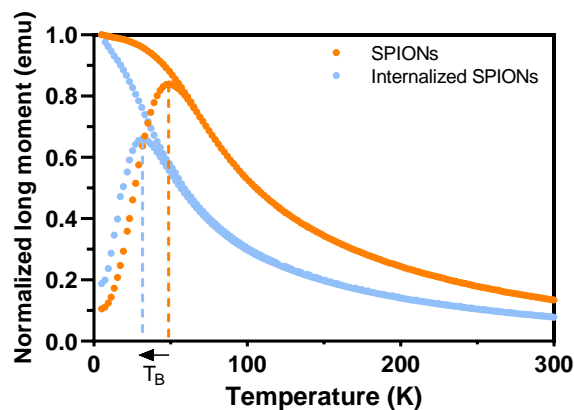


Figure 30 ZFC-FC graphs of synthesized SPIONs and internalized SPIONs inside *C. elegans*.

3.7.2. Transmission electron microscopy (TEM)

With the adapted bleaching method to dissolve *C. elegans*, internalized SPIONs were obtained and characterized by the TEM technique (Figure 31B). Through the size comparison of synthesized and internalized SPIONs (Figure 31A), we found a 13.7% size decrease consistent with our results from ZFC-FC measurement (Table 4).

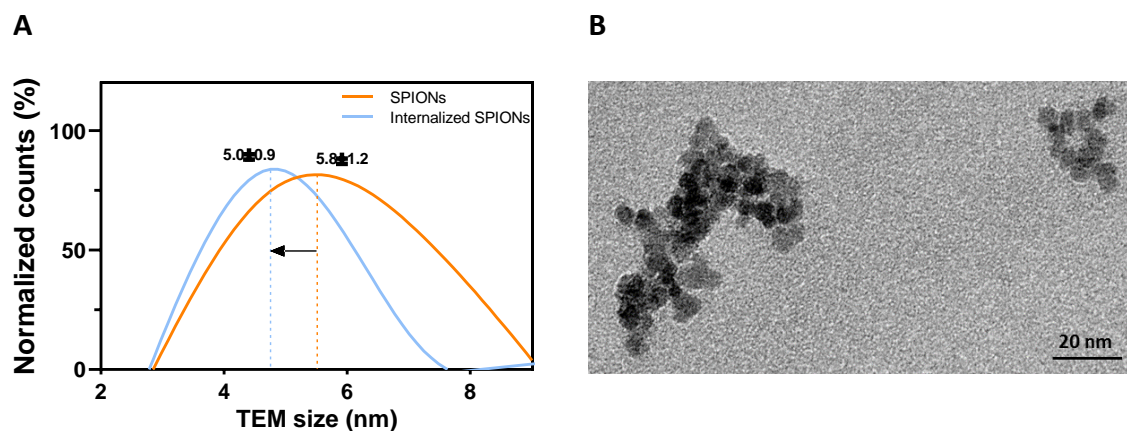


Figure 31 (A) Gaussian distribution of synthesized SPIONs and internalized SPIONs inside *C. elegans*, (B) TEM image of SPIONs after the recovery process.

		Decrease (%) NP size	
ZFC-FC	$T_{B(C. elegans)}$	$T_{B(SPIONs)}$	-
	31.2K	49.2K	14%
TEM	$D_{(C. elegans)}$	$D_{(SPIONs)}$	-
	5.0±0.9 nm	5.8±1.2 nm	13.7%

Table 4 Size decrease of internalized SPIONs and synthesized SPIONs estimated from ZFC-FC and TEM techniques.

In summary, a low extent of iron release occurred partially resulting from the long residence time of SPIONs in the intestinal microenvironment of low pH¹⁰¹. The presence of food could stimulate digestive enzymes to degrade the structure of SPIONs. The free iron ions released into the intestine may result in iron overload which disrupted the iron homeostasis^{244,245}. Iron homeostasis interruption could affect different biological pathways; among them, oxidative stress is one of them¹⁵⁹.

3.8. Qualitative analysis of oxidative stress

Reactive oxygen species (ROS) are naturally generated as byproducts during cellular metabolism²⁶⁴, including superoxide (O_2^-), hydroxyl radical ($\bullet OH$), and hydrogen peroxide (H_2O_2)²⁶⁵. In eukaryotes, SOD, a major enzyme, catalyzes the removal of O_2^- to protect against oxidative stress, containing cytosolic CuZn-SOD, extracellular CuZn-SOD, and Mn-SOD. In *C. elegans*, *sod-2* and *sod-3* each encode Mn-SOD^{159,264}. Iron is known to contribute to ROS production through Fenton and Fenton-like reactions^{266,267}. Thus, ROS production may be one of the main mechanisms of inducing toxicity in *C. elegans* exposed to SPIONs, especially high concentrations of SPIONs which could overwhelm antioxidant systems^{265,267}. Previously, by synchrotron Fourier Transform Infrared (SR- μ FTIR) microspectroscopy, we stated the presence of oxidative stress by identifying a higher level of lipid oxidation ration in treated worms¹⁵⁹. We conducted a general

research to study the effect of exposure durations and concentrations to better understand the kinetics and dynamics of SPIONs-induced oxidative stress *in vivo*, which is still poorly understood.

SR- μ FTIR microspectroscopy is a powerful and non-destructive²⁰⁰ technique that can potentially be applied to estimate chemical compositions of various materials, including intact nematodes⁶⁰. SR- μ FTIR microspectroscopy using synchrotron radiation (SR) source can help to improve the signal to noise ratio²⁶⁸, it allows the better spatial study of specific bands with high sensitivity²⁶⁹. Furthermore, Focal Plane Array (FPA) detectors pave a new avenue to let us obtain imaging of a relatively large sample area even the whole body and distributions of varied characteristic bands²⁰¹.

We exposed synchronized L1-staged worms to 100 and 500 μ g/mL SPIONs for 4 h as the short-term exposure and 24 h as the acute exposure, respectively. N2 wild-type and VC433 (*sod-3* deficiency) mutant worms were selected to investigate the oxidative effect induced by SPIONs treatment on the level of lipid oxidation.

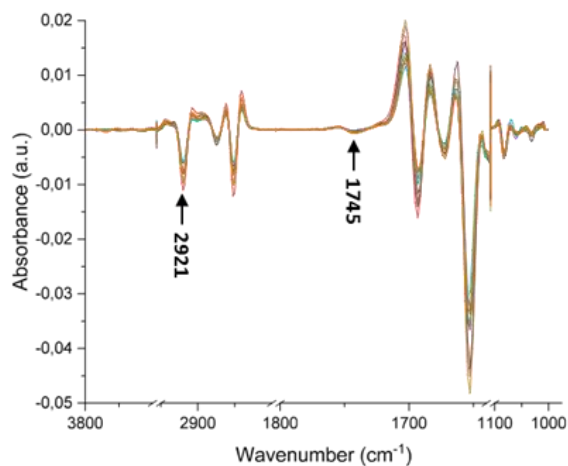


Figure 32 The peaks used for calculating lipid oxidation ratios are marked in the spectra with the application of the 2nd derivative. The peak 1745 cm^{-1} corresponded to the carbonyl group of the ester bond. The peak 2921 cm^{-1} corresponded to the asymmetric stretch from CH_2 .

3.8.1. Study of exposure time

It's reported that the peak 1745 cm^{-1} representing the absorption of the carbonyl group of the ester bond could serve as the indicator of lipid oxidation²⁶⁹. And the peak 2921 cm^{-1} corresponded to the asymmetric stretch from CH_2 ^{60,270} (Figure 32). The ratio (1745 cm^{-1} / 2921 cm^{-1}), associated with the increased aldehyde groups from the lipid oxidation^{271,272}, was selected to represent the level of lipid oxidation²⁶⁹. As shown in Figure 33, exposure to SPIONs induced increased ratios consistent with our previous findings¹⁵⁹. And we found a dose- and exposure-duration- (*sod-3* mutants) dependence increments. Another interesting discovery was that after 4 h exposure, the ratio was non-significantly different from that of worms after 24 h exposure upon either concentration indicating that the short-term exposure might be applied as the quick toxicity assay²⁶².

On the other hand, for the *sod-3* mutant, the increasing tendency of ratio followed a similar pattern (Figure 33). It suggested that long-time exposure and high concentrations of SPIONs could stimulate the lipid oxidation mostly. This discovery correlated with the wide-accepted opinion that exposure upon higher concentrations of NPs or longer exposure time could induce severer consequences in *C. elegans*⁵⁷.

3.8.2. Study of oxidative stress

Kregel and Zhang stated that, ascribed to bis-allylic structures of polyunsaturated fatty acids²⁷³, lipids were strongly sensitive to ROS oxidation²⁷⁴. Based on this, we planned to study if raised lipid oxidation ratios were related to lipids' sensitivities to oxidative stress. We made a cross-statistical analysis of wild-type worms and *sod-3* mutant in control and 24 h exposure conditions. As showed in Figure 33, the highest lipid oxidation ratio of *sod-3* mutant after exposure upon 500 µg/mL SPIONs for 24 h demonstrated that SPIONs-induced lipid oxidation was associated with the lack of oxidative-stress defense, *sod-3* deficiency.

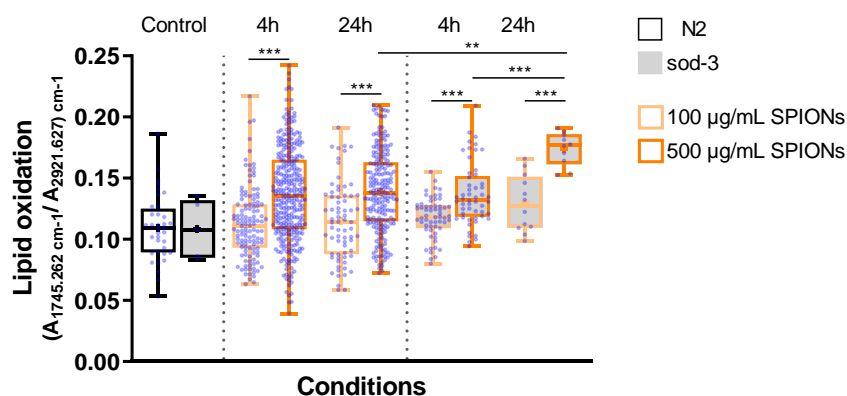


Figure 33 Box and whiskers plot of the lipid oxidation ratio ($1745 \text{ cm}^{-1} / 2921 \text{ cm}^{-1}$) of all spectra, for control, 4 h and 24 h exposure of wild-type and *sod-3* mutant worms to 100 µg/mL and 500 µg/mL SPIONs. $p < 0.0332$ (*), $p < 0.0021$ (**), $p < 0.0002$ (***)

Mn superoxide dismutase (MnSOD), located in the mitochondrial matrix²⁷⁵, expressed by *sod-2* and *sod-3* was among many stress-defense enzymes in *C. elegans*²⁷⁶. Additionally, Mn-SOD is under the regulation of *daf-2*²⁷⁶, the insulin receptor in the insulin/insulin-like signaling pathway (IIS), which regulates various key biological processes⁷⁶. After exposure, SPIONs could be taken up through cellular endocytosis^{159,277}, and released iron ions triggered oxidative stress to cause the mitochondrial damage²⁷⁷, inducing the up-regulation of *sod-3* expression¹⁵⁹. Furthermore, longer treatment time or exposure to the higher concentration of SPIONs would lead to more iron-induced oxidative stress leading to a higher level of lipid oxidation ratio (Figure 33).

3.8.3. FPA mapping

The Focal Plane Array (FPA) mapping images corresponding to *sod-3* mutants treated with 500 µg/mL SPIONs for 24 h were shown in Figure 35, based on the statistical analysis result showed in Figure 33. In

Figure 35, the distribution of the lipid oxidation ratio ($1745\text{ cm}^{-1} / 2921\text{ cm}^{-1}$) was shown. Dark blue color corresponded to the level of lipid oxidation measured in regions away from the worm, so the colors light blue, green, and red indicated a higher level of lipid oxidation than the control, in this order²⁶⁹. We found that within the whole worm, there were varying levels of lipid oxidation. Particularly, the green color in the head zone was indicative of the highest level of lipid oxidation. Meanwhile, we separately collected FTIR measurement points located in the head zone of worms in all 24 h treatment conditions and made a statistical analysis. We found that black dots shown in Figure 34 referring to SPIONs treatment conditions were within the upper part of the whole range above the mean value, especially for *sod-3* mutants consistent with the FPA mapping image (Figure 35). It suggested that the head part was more severely affected by oxidative stress which might be related to impaired chemotaxis of malfunctioned ASE neurons^{251,278}.

To sum up, we proposed that long-term exposure and/or exposure upon concentrated SPIONs resulted in elevated levels of lipid oxidation due to oxidative stress induced by the promoted release of iron ions. The head zone was relatively more heavily stressed where neurotoxicity potentially occurred.

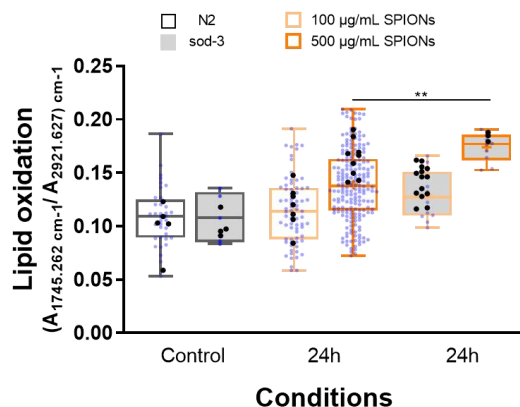


Figure 34 Merged Box and whiskers plots of the lipid oxidation ratio ($1745\text{ cm}^{-1} / 2921\text{ cm}^{-1}$) from the whole body and head zone of wild-type and *sod-3* worms exposed to $100\text{ }\mu\text{g/mL}$ and $500\text{ }\mu\text{g/mL}$ SPIONs for 24 h. $p < 0.0332$ (*), $p < 0.0021$ (**).

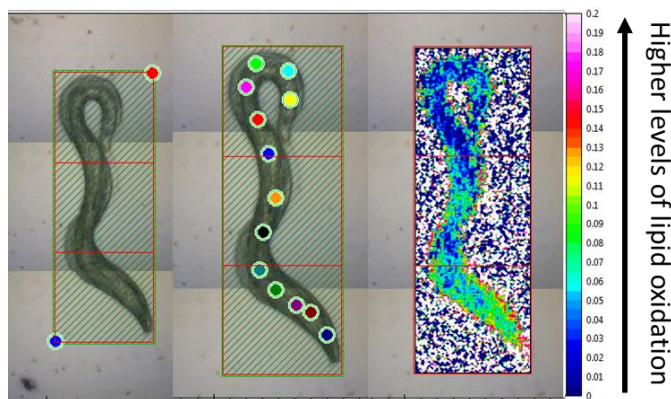


Figure 35 FTIR mapping of *sod-3* mutants treated with $500\text{ }\mu\text{g/mL}$ SPIONs for 24 h with the lipid oxidation ratio ($1745\text{ cm}^{-1} / 2921\text{ cm}^{-1}$). Dark blue color corresponds to the level of lipid oxidation measured in regions away from the worm. Color scale bar: dark blue means low, red means high.

3.9. Chapter conclusions

We studied the role of food availability in the acute or prolonged exposure upon citrate SPIONs up to 500 µg/mL. Multiple sublethal toxicity endpoints were measured and several material scientific techniques were applied.

In the acute exposure condition, with the presence of food, survival and reproduction were not affected even at the highest dose. The biodistribution study showed a higher percentage of worms with a more homogenous distribution of SPIONs within the intestine. Through SQUID, ICP-MS, and TEM, we found three times more uptake amount and a similar extent of size decrease of SPIONs.

The utilization of Nile red and Oil red O staining methods determined that the intestinal integrity was maintained, and a tendency of lipid accumulation was found. We assumed that it's induced by confirmed iron overload which promoted the overexpression of *ftn-1*^{159,207,211}. In addition, with the presence of food, there was a relatively slower growth of lipid content which might be due to consumed food to provide defense energy or tissue repair against the oxidative stress^{159,246,252,262}.

In the locomotion behavior study, we found a dose-dependent decrease in body bending frequency in conditions with or without food. It could be related to a continuous Fe influx rendering mitochondrion susceptible to the oxidative stress triggered by free Fe ions²⁴⁹. Meanwhile, it might also correspond to the neurotoxicological effects of Fe⁸⁷.

A dose-correspond decrease in lifespan was discovered. And the presence of *E. coli* didn't make any difference in the decreased tendency of lifespan. It correlated with the influence of *ftn-1* on lifespan under the iron stress condition^{207,266}. Moreover, *ftn-1* is exclusively expressed in the intestine which is the principle tract under stress from most NPs studied²⁰⁷, reinforcing the hypothesis that shortened lifespan was due to the regulation of *ftn-1*.

The SR-µFTIR study confirmed that elevated levels of lipid oxidation from longer exposure or higher dose of SPIONs performed was connected with *sod-3*, sensitivities to oxidative stress. Imaging the whole worm by FPA mapping, we found that in the head zone of worms, we found higher levels of lipid oxidation, and it was more stressed by oxidative stress which might explain for impaired chemotaxis towards NaCl under the control of ASE neurons^{251,278} regulated by *ins-1*^{278,279}.

On the other hand, after prolonged exposure, no detrimental effects were found on survival and reproduction. There was no structural deficit of the intestine and no increased lipid content detected. But we found a dose-dependent lifespan shortage and locomotive deficit. We assumed that the "trade-off" effect was involved²⁴⁶.

To summarize, *ftn-1*, responsible for the lipid accumulation and shortened lifespan, is under the regulation of *daf-16*^{245,280}, the downstream effector of *daf-2*. *sod-3* correlated with increased levels of lipid oxidation, and defective locomotion behavior is under the control of *daf-2*²⁷⁶. Combined with the *ins-1*, we propose a signaling cascade of *daf-2-sod-3-daf-16-ftn-1-ins-1* in response to SPIONs during acute exposure.

In addition, with food availability, increased uptake of SPIONs was observed which suggested that food intake allowed an enhanced oral bioavailability of SPIONs in *C. elegans*^{281,282}. It implied that the enhanced delivery capacity could be achieved in the oral administration of drugs, regarding SPIONs have been extensively studied as nanocarrier systems for drug delivery²⁸³.

Chapter 4 Evaluation of gold nanoparticles applying *C. elegans*. The influence of food availability

4.1. Introduction to the gold nanoparticles

4.2. Aims

4.3. Toxicity analysis

4.4. Biodistribution of AuNPs

4.5. Photothermal effect

4.5.1. Feasibility of performing laser irradiation (Preliminary trail)

4.5.2. Effects of laser irradiation conditions

4.6. Qualitative analysis of oxidative stress

4.6.1. Study of exposure duration

4.6.2. Study of genetic deficiency

4.7. Chapter conclusions

4.1 Introductions to the gold nanoparticles

Gold nanoparticles (AuNPs) are frequently studied materials due to their outstanding properties including ease of synthesis, surface modification, stability, low toxicity, and biocompatibility^{284,285}. Moreover, spherical AuNPs possess specific features such as size- and shape-related optoelectronic properties^{286,287} and large surface-to-volume ratio, rendering them as a potent tool in biotechnology^{288,289}. A broad range of surface functionalization and bioconjugations, together with great physical properties, make them promising for bioimaging applications²⁹⁰. Through modifications of their surface, we can produce highly sensitive and selective diagnostic agents^{288,290}. Due to the great developments of synthetic techniques and their high loading of drugs and genes as well as the controllable release, AuNPs also show promise in therapeutics^{288,291}. Also, AuNPs are proved to be outstanding drug carriers and photothermal therapy agents²⁹², especially in cancer treatment²⁹³.

As described earlier, multiple features of AuNPs such as biocompatibility, flexible functionality, a high loading capacity of drugs, and stability make them an interesting nanocarrier agent for drug delivery²⁹⁰. Additionally, ascribed to the ability to form stable complexes with DNA, small interfering RNA (siRNA) or drugs by covalent bonding²⁹³, AuNPs can easily penetrate and highly accumulate in the tumor site with drugs. Photothermal therapy (PTT) is a treatment method applied in cancer therapy with minimal invasiveness²⁹⁰, involving using electromagnetic radiation to generate heat for thermal ablation²⁹⁴ or optical hyperthermia²⁹⁵ of cancer cells²⁹³. Attributed to their unique physicochemical properties, for instance, absorption and scattering of electromagnetic radiation, AuNPs have gained interest to be applied as agents in the PTT²⁹⁶. In addition, the efficacy could be further enhanced by extra advantages of AuNPs contain a wide spectrum of absorption light (from UV to near-infrared) and higher absorption efficiency demanding lower laser power and shorter irradiation time^{293,297}. Particularly, the light within 700-900 nm called “biological transparency window” in the near-infrared (NIR) region can penetrate inside living tissues reaching a depth of a few centimeters²⁹⁸.

It's crucial to have a general understanding of the *in vivo* fate of AuNPs if they are to be applied as a therapeutic agent, especially as the drug delivery carriers and heat-generated agents destroying tumor tissues^{293,299}. Therefore, it's essential to perform toxicity assays with appropriate animal models based on varied research purposes. Among other parameters of AuNPs, including sizes, coatings, and electrical charges, the administration route of AuNPs has an impact on their pharmacokinetics, biodistributions, and toxicity profiles^{291,299}. In general, mice are the most frequently used animal model for studying the fate and toxicity of AuNPs. Meanwhile, the intravenous (IV) administration is widely applied to let mice expose to AuNPs other than oral, intraperitoneal, and intratracheal administrations^{299,300}. However, by intravenous injection, the excretion rate of AuNPs was lower compared with that of mice following oral administration which might result in serious medical complications³⁰¹. There have been some work studying toxicity profiles of AuNPs orally administered to mice but with controversial findings³⁰²⁻³⁰⁴. Zhang et al. reported that, among

the three applied administration routes, 13.5 nm AuNPs exhibited the highest toxicity through the oral and intraperitoneal routes compared with tail vein injection³⁰⁴. In contrast, Pokharkar et al. demonstrated that, after acute oral administration of chitosan-coated AuNPs with an average size of 50 nm, there was no death and treatment-related complications discovered in female mice³⁰³. MR Jo et al. and J Cancino-Bernardi et al. also reported that fourteen-day repeated and 48 h oral administration of AuNPs caused no adverse effects on mice, respectively^{305,306}. On the other hand, orally administered AuNPs have been investigated for the therapy of bacterial infections in the gastrointestinal (GI) tract in mice^{307–310}.

Regarding the fact that *in vivo* toxicity studies of AuNPs applying mice are time and cost consuming, we should find a simple and low-cost animal model³¹¹. In recent years, *Caenorhabditis elegans* (*C. elegans*) have received increased attention as the toxicity assay model to evaluate the toxicological profiles of different NPs^{57,59,76}. Meanwhile, including the simplicity and cost-effectiveness of the cultivation, the cellular complexity and conserved biochemical mechanisms between *C. elegans* and mammals make it a useful model to study the cellular and molecular processes^{59,236}. In addition, *C. elegans* offer an advantage to study the oral route of nanoparticles⁶². Together with assorted toxicity endpoints, *C. elegans* is the optimal model organism for rapid toxicity screening and studying the influence of food availability⁶⁵.

4.2 Aims

The aims were to study the role of food availability in the interaction between AuNPs and *C. elegans* through measuring multiple sublethal endpoints such as survival, reproduction, lifespan, etc. and using varied types of material science techniques, for instance, synchrotron Fourier Transform Infrared (SR- μ FTIR) and Raman spectroscopy.

4.3 Toxicity analysis

The interplay between NPs and *C. elegans*, measuring diverse lethal and sublethal endpoints, can be utilized to study the fate and toxicological profiles of NPs in a multicellular organism with different organ systems^{57,62}, including the alimentary system, reproductive system, neuronal system, and immune system^{62,68}. The most commonly applied exposure condition is oral exposure upon NPs for 24 h, defined as the acute exposure, in which nearly all types of endpoints can be used for toxicity evaluation of NPs^{57,61,76}. Besides, the choice of an optimal endpoint depends on not only several factors such as sensitivity, accuracy, and maneuverability, etc^{237,238}, but also types of toxicities including reprotoxicty and neurotoxicity^{57,63}.

Normally, to study AuNPs toxic effect on *C. elegans*, survival and brood size are commonly used to determine the fitness and reproduction success of *C. elegans*^{158,312}. The shortened lifespan is connected with the response to the oxidative stress¹⁵⁸ or certain gene expression¹²⁷. Locomotion behavior study can indicate if there are neurotoxic effects induced by AuNPs^{62,89,127}.

Therefore, I studied the influence of food availability on *C. elegans* after acute exposure upon 10 nm AuNPs. 10 nm AuNPs were purchased from Applied Nanoparticles (Barcelona, Spain) (shown in Figure 36).

Synchronized young-adult staged worms exposed to AuNPs for 24 h with the addition of heat-killed *E. coli*¹¹⁷. After the exposure, multiple toxicity endpoints, namely: survival, reproduction, lifespan, intestinal integrity, lipid content, and locomotion behavior were studied (shown in Figure 37).

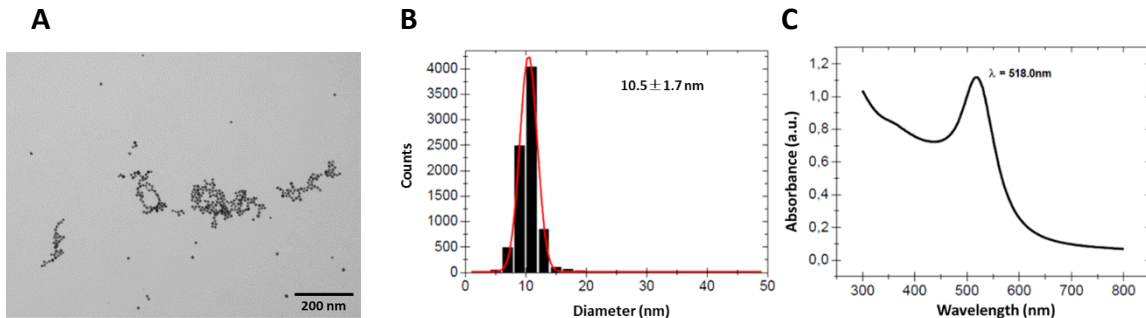


Figure 36 Structural characterization of 10 nm AuNPs. (A) TEM image, (B) TEM size distribution, (C) UV-vis spectrum.

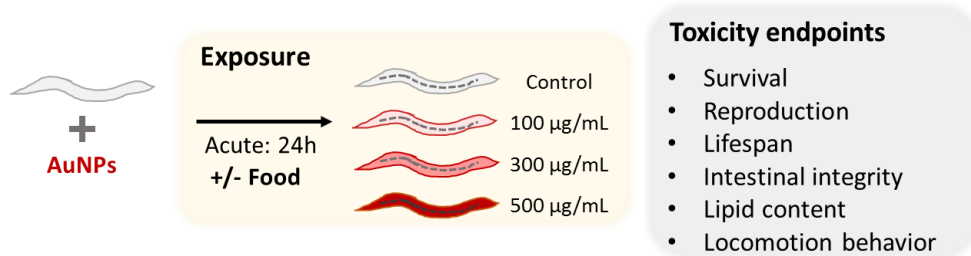


Figure 37 Graphical representations to describe the acute exposure condition and studies toxicity endpoints.

Survival

Survival was determined by the same method explained in section 3.4.1. For studying the role of food availability of *C. elegans* 24 h exposure upon 10 nm AuNPs, the same concentration range was performed, 0-500 µg/mL¹⁵⁸. As shown in Figure 38, with the presence of food, the survival rate at 100 µg/mL was close to 100%, not significantly different from that of the control condition. When worms were exposed to higher concentrations of AuNPs, the survival decreased but higher than that of treatment conditions without *E. coli* (75% VS 39%), suggesting the beneficial role of food.

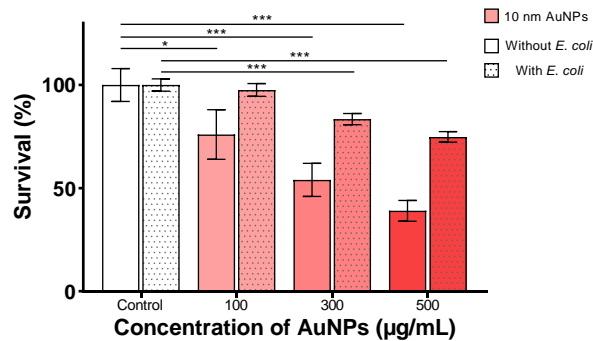


Figure 38 Effects of food availability on the survival exposed to increasing concentrations of AuNPs of *C. elegans* (n=3). Bars indicate the mean ± S.E.M. $p < 0.0332$ (*), $p < 0.0021$ (**), $p < 0.0002$ (***)

Reproduction

To assess the influence of food presence on the reproduction, a concentration of 100 $\mu\text{g}/\text{mL}$ was also chosen to compare with our previous work¹⁵⁸. We found that the reproduction rate is not affected by AuNPs exposure when food is available, but it declined to 60% in the absence of food¹⁵⁸ (Figure 39A). The lower reprotoxicity of AuNPs due to the presence of food may arise from the energy provided by ingesting food to defend oxidative stress^{158,252} or repair damaged reproductive integrity resulting in decrease reproduction rate¹¹⁷. It could also be that the presence of food forming a reversible “corona” around AuNPs reduced the interaction with intestinal cells³¹³.

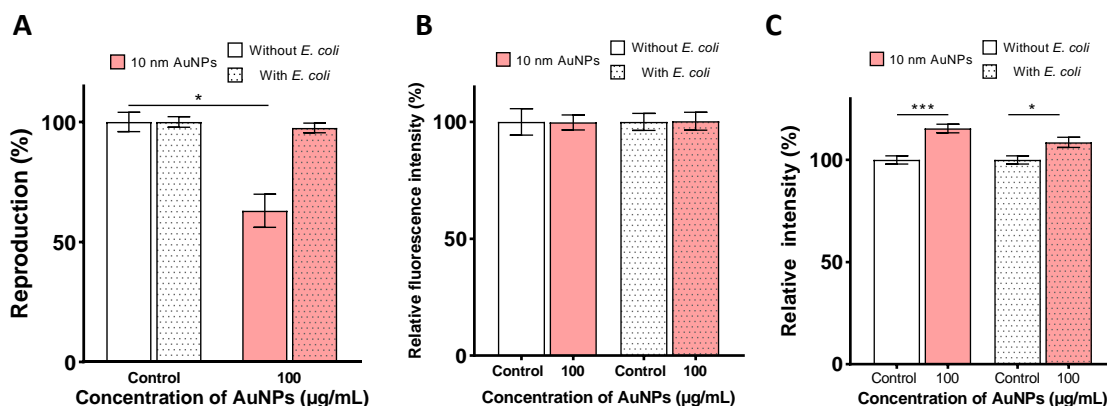


Figure 39 Effects of food availability on reproduction (A) intestinal integrity (B) and lipid content (C) of *C. elegans* after acute exposure upon 100 $\mu\text{g}/\text{mL}$ AuNPs (n=3). Bars indicate mean \pm S.E.M. $p < 0.0332$ (*), $p < 0.0021$ (**), $p < 0.0002$ (***)

Intestinal integrity

Intestinal integrity assay was performed to evaluate the structural status of the intestine through comparisons between control worms and treated worms²¹⁰. From Figure 39B, we discovered that, despite food presence, there was no statistical difference of relative fluorescent intensity of worms indicating no structural deficit. Thus, exposure to AuNPs does not affect the intestinal integrity regardless of food existence.

Lipid content

Lipid content was evaluated by measuring the color intensity of exposed worms stained by Oil Red O²¹³. We discovered an increased amount of lipid after exposure to AuNPs (Figure 39C). Food existence contributed relatively less to the lipid accumulation. It may be correlated with oxidative stress of causing a disruption in the pathway of utilizing lipid¹²⁷. On the other hand, taking advantage of food presence, treated worms might allocate more energy investment in anti-oxidative defense²⁴⁶, showing a relatively smaller increase than that of worms without food presence.

Locomotion behavior

Locomotion behavior was determined by the body-bending frequency of treated worms. As shown in Figure 40A, there was a dose-dependent decrease regardless of food presence, suggesting that AuNPs could have detrimental influences on the locomotion ability. Previous work showed that the impeded locomotion behavior of worms after exposure to AuNPs might be related to swollen muscle bellies on the ventral side⁸⁹ or neurons' growth of shorter axons¹²⁷.

Lifespan

Lifespan was assessed by measuring the longevity of treated worms under controlled conditions with 100 μM Fluorodeoxyuridine (FUDR) to stop progeny production and bagging^{206,247}. After acute exposure, we found a dose-dependence decrease of lifespan independently of the presence of food in the exposure condition (Figure 40B and 40C), suggesting that exposure to AuNPs could lead to a decreased lifespan. Besides, the addition of food couldn't protect *C. elegans* from detrimental effects of AuNPs on the lifespan. It correlated with others' findings that shortened lifespan of worms after exposure to AuNPs may be associated with loss of gene *acdh-1* activity¹²⁷ or inhibited functions of genes *abu-11* and *pqn-5*¹⁸⁵.

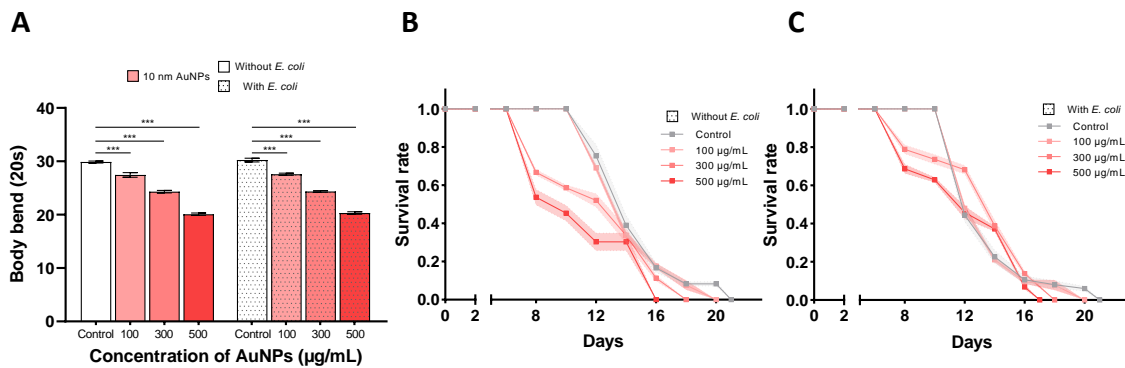


Figure 40 Effects of food availability on body bending frequency (A) and life span (B, C) of *C. elegans* after acute exposure upon AuNPs ($n=3$). Groups with and without food availability were separately analyzed. Bars indicate mean \pm S.E.M. $p < 0.0332$ (*), $p < 0.0021$ (**), $p < 0.0002$ (***) . Bands represented SD.

To summarize, we treated *C. elegans* with 10 nm citrate-AuNPs for 24 h with or without food to study the effects of food availability on survival, reproduction, intestinal integrity, lipid content, lifespan, and locomotion. After exposure, we observed the maintained intestinal integrity and an increase of lipid storage indicating disrupted metabolic pathways. We also found a dose-dependent declined body bending frequency, implying the neurotoxicity induced by AuNPs treatment. On the other hand, with food availability, we also discerned a lipid accumulation and impeded locomotion behavior combined with the discovery of lower lethality and no decreased progeny, suggesting limited beneficial effects provided by food. All these results suggested that acute exposure to 10 nm AuNPs may cause the dysregulation of metabolic pathways⁸⁹ and neurotoxicity related to oxidative stress¹²⁷.

4.4 Biodistribution of AuNPs

In the same methodology as for SPIONs, we evaluate the biodistribution of AuNPs observed by light microscopy in worms (Figure 41). We found that, with food availability, there was a gradient of AuNPs with a higher frequency of them being observed in the posterior compartment of the intestinal cavity (Figure 42) which correlated with previous findings⁷⁷. Additionally, exposure to more concentrated AuNPs could prompt relatively higher percentages of AuNPs confinement in the posterior region of worms which might be related to continuous uptake and ingestion of food facilitating the shifted distribution.



Figure 41 Worms after acute exposure to 500 µg/mL 10 nm AuNPs with *E. coli*. Scale bar represents 100 µm.

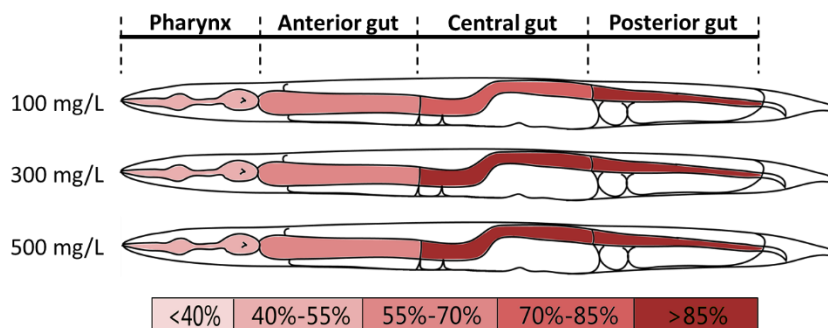


Figure 42 Biodistribution of 10 nm AuNPs in *C. elegans* after acute exposure to varying concentrations of AuNPs with *E. coli* (50 worms per sample). The upper simplified graph showed the division of the alimentary system: pharynx, anterior gut, central gut, and post gut. The lower color legend depicted the percentage of observed locations of AuNPs.

4.5 Photothermal effect

Raman spectroscopy combined with microscopy has been increasingly employed within biology. It can provide chemical and compositional information without much interference from water molecules³¹⁴. Taking advantage of the small-size, the excitation and scattering light could easily penetrate the whole body compared with other animal models³¹⁵. Moreover, its transparent structure allows us to detect distributions of nanoparticles and monitor laser-induced effects^{149,153,316}. Furthermore, a higher magnification of the Raman microscope could even enable us to obtain histological information^{315,317}.

AuNPs have been intensively studied in recent years which are attributed to not only their facile synthesis, easy surface modification, and biocompatibility but also their unique surface plasmon resonance (SPR)^{318,319}.

AuNPs could absorb light strongly typically in the visible light region and rapidly convert into heat offering photothermal applications^{320,321}, especially at the forefront of the cancer research.

Synchronized L3-staged wild-type worms were exposed to 150 nm AuNPs, purchased from the BBI solutions company, with 100 $\mu\text{g}/\text{mL}$ for 24 h. This chosen exposure condition was based on our previous findings that worms' survival and reproduction were not significantly affected^{77,158}. 785 nm was selected as the laser wavelength since it showed no damage to biological tissues³²². Multiple laser irradiation modes were conducted to investigate photothermal effects induced by AuNPs treatment.

4.5.1 Feasibility of performing laser irradiation (Preliminary trial)

Raman spectra of AuNPs and the glass substrate were obtained (Figure 43B) by a line-scan of the zone containing 150 nm AuNPs (Figure 43A). It showed that under the 785 nm laser irradiation, we could distinguish spectra attributed to AuNPs or the glass substrate, which might be useful for analysis of average Raman spectra obtained from complex biological samples, such as *C. elegans*. But we had to admit that the glass slide was not the appropriate choice as the substrate since it has a strong background fluorescence at most wavelength³¹⁴. Considering that it's a preliminary study, it's acceptable to use glass slides for sample preparation.

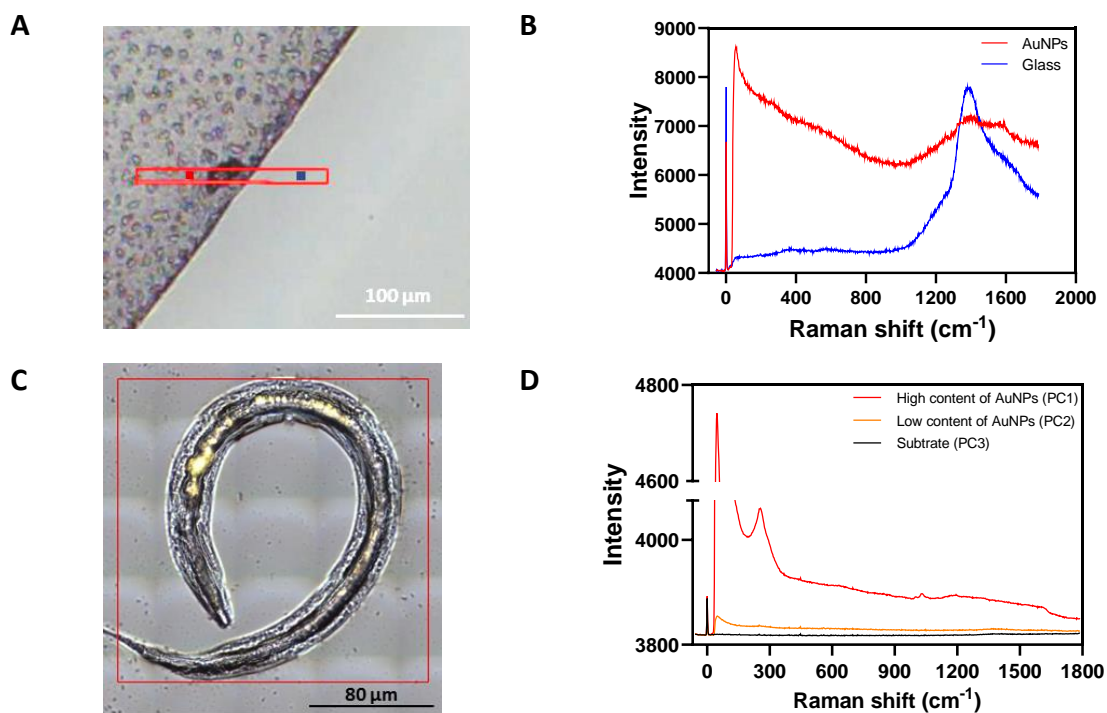


Figure 43 (A) A line-scan of 150 nm AuNPs on the glass slide. The red dot represented AuNPs, and the blue dot represented the glass. (B) Raman spectra of two locations showed in A. The colors of the spectra correspond to the colors of locations. (C) A white light image of *C. elegans* containing AuNPs. (D) Principle component analysis (PCA) was performed on the average spectra obtained from the large-scale-image-scan of the worm in C. 3 clusters were resolved and colored differently.

Then, we conducted a large-scale-image-scan of a worm treated with 150 nm AuNPs, showed in Figure 43C. The principal component analysis (PCA) applied to the average Raman spectra resulted in three main principal components (PCs) showed in Figure 43D. We assumed that it's related to varied contents of AuNPs within the worm^{323,324}, and the PC1 spectrum might be assigned to high loadings of AuNPs. To prove our hypothesis, we conducted line-scan and Raman mapping on positions of high or low content of AuNPs determined by visualization under the scope of the microscope (Figure 44A). As showed in Figure 44B, the average spectra of high and low accumulation of AuNPs were different. Raman mapping images obtained by performing the Z-axis profile of the whole worm could provide the projection of Raman intensity of AuNPs inside worms. They can be utilized to make a preliminary comparison of AuNPs content in different locations within one worm such as the pharynx and the posterior gut of the intestine by images colored by intensities³²⁵. As shown in Figure 44C and 44D, it illustrated varied contents of AuNPs inside the worm. We assumed that the spectral shape could be used as a maker to qualitatively estimate AuNPs loadings inside worms.

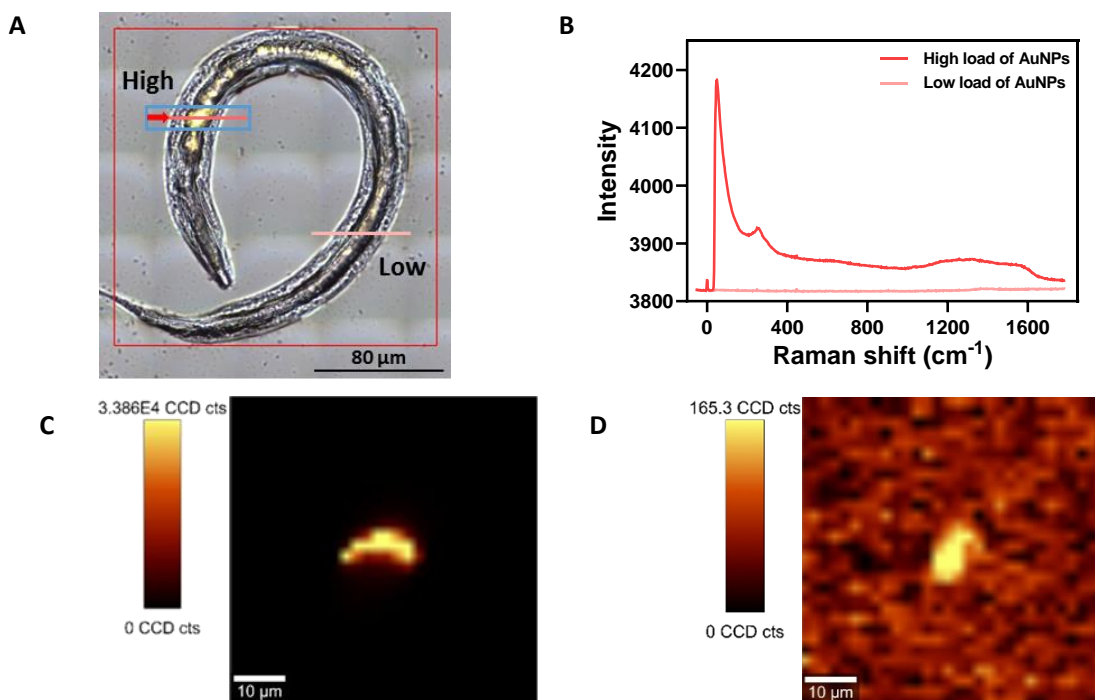


Figure 44 (A) Two positions of line-scan on the worm containing varied contents of AuNPs. (B) The average spectra of positions with high or low loadings of AuNPs. The colors of spectra corresponding to the colors were marked in 44A. (C) Raman mapping image of high loading of AuNPs with a Z-axis scan. (D) Raman mapping image of low loading of AuNPs with a Z-axis scan. The color scale bar illustrates the intensity of the band at 47 cm^{-1} .

For studying the potential photothermal effects, we performed the line-scan on the high accumulation of AuNPs with an infrared camera to monitor the temperature change. We observed that Raman spectral shape and the infrared temperature of the laser spot fluctuated at the same pace. When the laser spot

moved onto the center of the accumulated AuNPs, the brightest spot and highest temperature value appeared simultaneously (Figure 45). We successfully achieved a photothermal phenomenon of 150 nm AuNPs within *C. elegans* under the irradiation of the 785 nm laser.

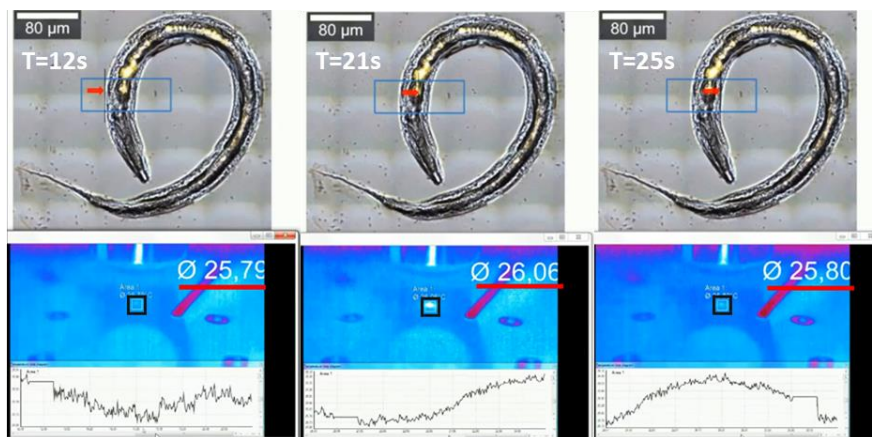


Figure 45 Snapshots of the video recording temperature variation during the line-scan irradiation.

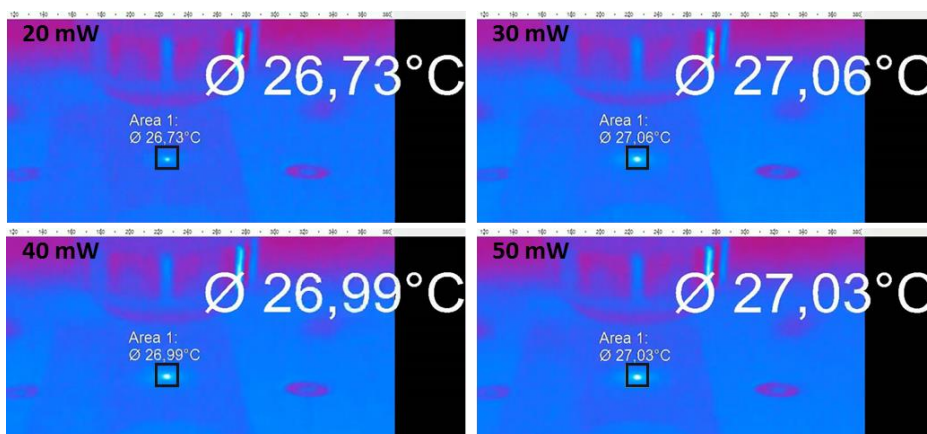


Figure 46 Snapshots of the video recording temperature variation during the pulsed irradiation on the fix-point with varied laser power.

4.5.2 Effects of laser irradiation conditions

Aiming to improve the photothermal efficiency, we performed a pulsed-laser on the same position of the worm containing 150 nm AuNPs with varied laser power (a range of 0-53.4 mW). Between each pulsed-laser irradiation of different powers, there was an interval of 15 seconds for cooling. The infrared camera was set to monitor the surrounding temperature of the laser spot. From Figure 47C, we observed the highest Raman intensity value when it's under the irradiation of 30 mW laser power. Meanwhile, the temperature fluctuated in the same pattern (Figure 46), reaching the highest point when a 30 mW laser was performed. Hence, we chose 30 mW as the efficient laser power for the following experiments.

Additionally, after the irradiation process, there was a structural damage on position 1, called “photoablation”³¹⁴ (Figure 47A). It was related to high sensitivity of samples, high laser power or prolonged

irradiation time which could burn samples once exposed^{314,326}. It reminded us that these variables were important to design and perform decisive Raman experiments for studies on the influence of AuNPs on *C. elegans*³¹⁵.

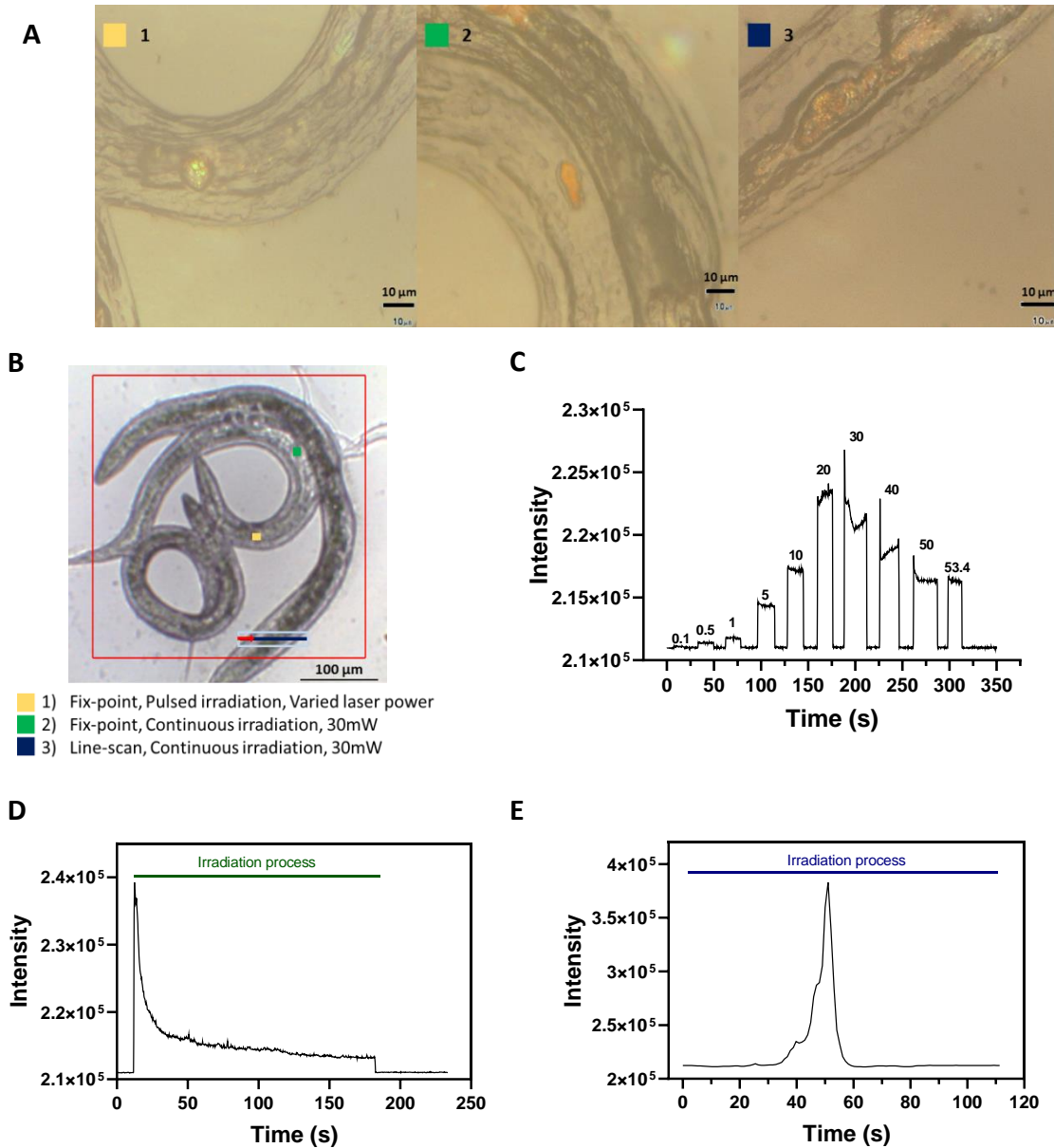


Figure 47 (A) A white light image of worms containing AuNPs with colored icons representing the irradiation positions. (B) The Raman intensity spectrum with time shifts of position 1. The laser power applied in each time interval was showed above the spectrum. (C) The Raman spectrum of continuous irradiation on position 2. (D) The Raman spectrum of line-scan under the continuous irradiation on position 3. (E) The enlarged reflected microscopy image of position 1, 2 and 3 after varied types of irradiation. Scale bar 10 μm .

To test this hypothesis, firstly, we performed continuous irradiation with the laser of 30 mW on the fixed position (Figure 47B). At the beginning of the irradiation process, Raman intensity values increased and reached the maximum value rapidly due to accumulated AuNPs. Then it plunged and decreased gradually

in the remaining irradiation process (Figure 47D). This spectral profile indicated that the laser power was too high. We also found a burned hole on the laser spot of the worm (Figure 47A). These results suggested that our choice of laser power was higher than needed. On the other hand, from the captured video of the irradiation process from the infrared camera (Figure 48), a bright spot could be visualized with a 0.45 °C increase implying the occurrence of photothermal phenomena.

Subsequently, a line-scan was performed across the worm to study the influence of irradiation time (Figure 47B). As shown in Figure 47E, intensity values increased when the laser moved close to accumulated AuNPs and declined when the laser moved away from AuNPs. Intensity values and temperature fluctuated in the same trend. Moreover, they reached the highest value when laser irradiated at the center of AuNPs inside *C. elegans* by the brightest spot showing up with a 1 °C increase of temperature (Figure 49). However, a photodamage was observed in the line-scan region (Figure 47A). These results demonstrated that we should reduce the irradiation time to maintain structural integrity

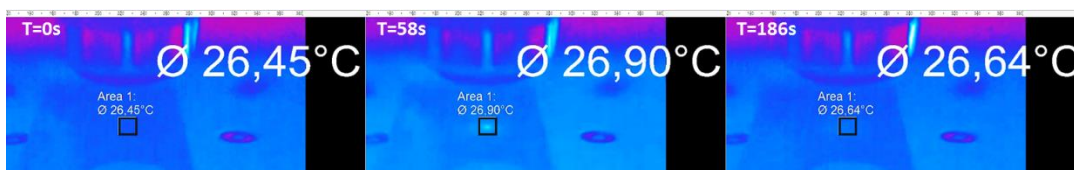


Figure 48 Snapshots of the video recording temperature variation during the continuous irradiation on the fix-point with the laser power of 30 mW.

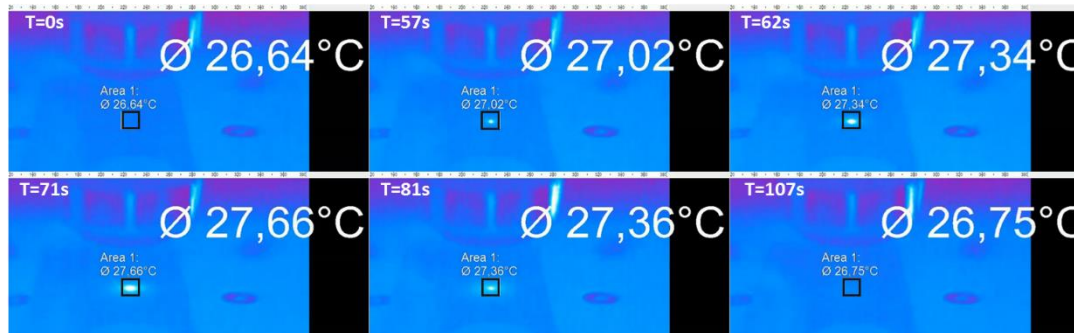


Figure 49 Snapshots of the video recording temperature variation during the continuous irradiation of line-scan with the laser power of 30 mW.

In summary, we successfully obtained the photothermal effects by employing Raman spectroscopy on *C. elegans* containing 150 nm AuNPs under the irradiation of the 785 nm laser. The choices of laser power, irradiation time, together with sample substrates, greatly impacted the resulting photothermal efficiency we expected³²⁶. On the other hand, *C. elegans* could be regarded as the testing platform permitting whole-body photothermal therapy to obtain optimized parameters before performed in a higher level of animal models like mice to be cost-effective¹⁴⁹.

4.6 Qualitative analysis of oxidative stress

We exposed synchronized L1-staged worms to 100 µg/mL 10nm or 150 nm AuNPs for 4 h as the short-term exposure and 24 h as the acute exposure, respectively. We aimed to study sizes' influences on the level

of lipid oxidation of N2 wild-type worms and VC433 (*sod-3*), a *sod-3* deficiency mutant, in terms of oxidative stress.

4.6.1 Study of exposure duration

The same ratio ($1745\text{ cm}^{-1} / 2921\text{ cm}^{-1}$) was selected to represent the level of lipid oxidation²⁶⁹. From Figure 50, exposure to 10 nm AuNPs for 24 h induced the highest ratio of lipid oxidation. On the other hand, for the *sod-3* mutant, the increasing tendency of ratio followed a similar pattern indicating that long exposure-time and small particles (10 nm) could stimulate the lipid oxidation mostly. Furthermore, we found a size- and exposure-duration- dependent increments of the ratio (Figure 50).

4.6.2 Study of oxidative stress

Kregel and Zhang reported that lipids were highly sensitive to ROS oxidation²⁷⁴. Subsequently, aiming to investigate if high sensitivities to oxidative stress were partially involved in escalated lipid oxidation ratios, we conducted a cross-statistical analysis of wild-type worms and *sod-3* mutant in control and 24 h exposure conditions. From Figure 50, we found that the highest lipid oxidation ratio corresponded to *sod-3* mutant after 24 h exposure to 10 nm AuNPs suggesting that AuNPs-induced lipid oxidation was related to *sod-3* expression. It correlated with our previous findings that a greater extent of oxidative stress can be triggered after exposure to smaller sized AuNPs¹⁵⁸.

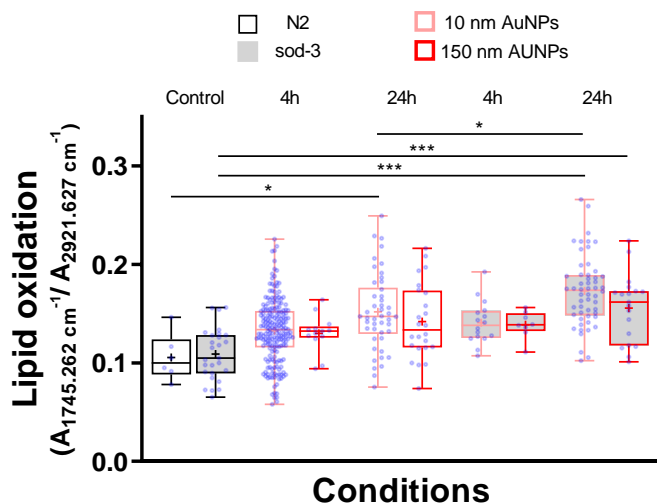


Figure 50 Box and whiskers plot of the lipid oxidation ratio ($1745\text{ cm}^{-1} / 2921\text{ cm}^{-1}$) of all spectra, for control, 4 h and 24 h exposure of wild-type (A) and *sod-3* mutant (B) worms to $100\text{ }\mu\text{g/mL}$ of 10 nm and 150 nm AuNPs. $p < 0.0332$ (*), $p < 0.0021$ (**), $p < 0.0002$ (***)

By qPCR, we previously discovered that after acute exposure to $100\text{ }\mu\text{g/mL}$ of citrate-AuNPs could trigger the up-regulation of *ftn-1*, encoding the iron storage protein FTN-1, which mainly occurred in the intestine of worms living in harsh conditions, for instance, exposure to metal nanomaterials or O_2 starvation^{327,328}. Moreover, this up-regulation would provide protective effects against oxidative injury³²⁷. It explained why

we detected a higher level of oxidative stress of escalated ratios of lipid oxidation and up-regulation of *ftn-1* of worms after exposure to AuNPs.

4.6.3 Focal Plane Array mapping

The Focal Plane Array (FPA) mapping images of *sod-3* mutants in control conditions, treated with 100 $\mu\text{g}/\text{mL}$ of 10 nm AuNPs for 4 h and 24 h, were shown with the distribution of the lipid oxidation ratio ($1745\text{ cm}^{-1} / 2921\text{ cm}^{-1}$), in Figure 51. Dark blue color corresponded to the level of lipid oxidation measured in regions away from the worm, so the colors light blue, green, and red indicated a higher level of lipid oxidation than the control, in this order²⁶⁹. We found that there was a relatively uniform increase in lipid oxidation within the whole worm. Additionally, for *sod-3* mutants, longer exposure triggered a higher level of lipid oxidation, which was in agreement with lipid oxidation ratios results shown in Figure 50.

To summarize, we proposed that long-term exposure to 10 nm AuNPs generated elevated levels of lipid oxidation due to oxidative stress might be due to smaller sizes with larger reactive surface areas.

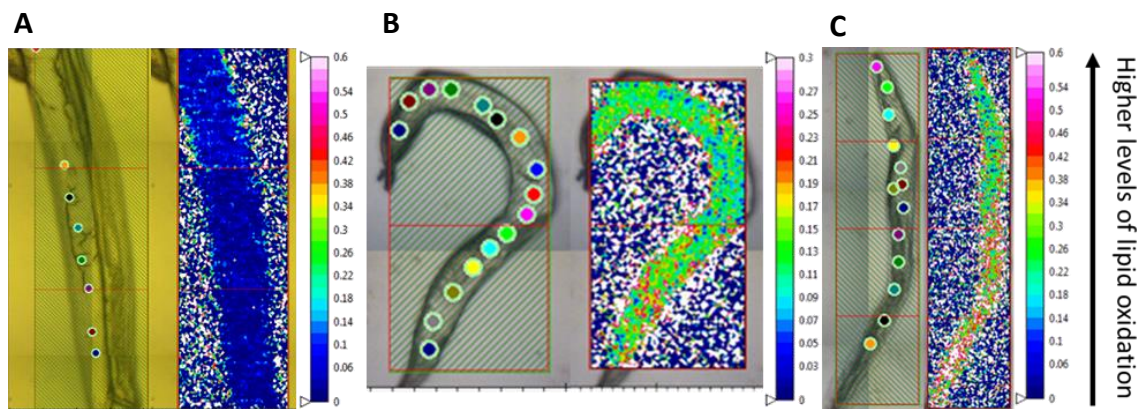


Figure 51 FTIR mapping of *sod-3* mutants in the control condition (A) and treated with 100 $\mu\text{g}/\text{mL}$ of 10 nm AuNPs for 4 h (B) and 24 h (C) with the lipid oxidation ratio ($1745\text{ cm}^{-1} / 2921\text{ cm}^{-1}$). Dark blue color corresponds to the level of lipid oxidation measured in regions away from the worm. Color scale bar: dark blue means low, red means high.

4.7 Chapter conclusions

We exposed *C. elegans* to 10 nm citrate-coated AuNPs with the presence of food. To study the role of food availability, we measured multiple sublethal toxicity endpoints and applied several material scientific techniques.

After 24 h exposure, with the addition of food, no mortality and reprotoxicity were found at the chosen working concentration (100 µg/mL) which were heavily affected in the absence of food condition. The intestinal integrity was maintained after the treatment, and accumulated lipid storage correlated with a disrupted pathway of utilizing lipid induced by oxidative stress⁸⁹. Additionally, a dose-dependent decrease of body bending frequency indicating locomotive deficits regardless of food presence was discovered. It might be due to swollen muscle bellies on the ventral side⁸⁹ or neurons' growth of shorter axons¹²⁷. And the decreased lifespan could be linked to inhibited functions of certain genes (acdh-1, abu-11 and pqn-5)^{127,185}.

In the biodistribution study, we found a distribution gradient of AuNPs, with a higher percentage in the posterior compartment of the intestinal cavity correlated with previous findings⁷⁷.

We irradiated *C. elegans* containing 150 nm AuNPs with 785 nm laser and observed photothermal phenomenon. To avoid causing "photoablation", experimental settings such as laser intensity, irradiation time need to be optimized. Taking advantage of the transparency and simplicity of *C. elegans*, it could pave a new avenue within "photothermal therapy" research.

Through the SR-µFTIR study, we confirmed that elevated levels of lipid oxidation were related to long exposure time, small size of AuNPs, and sensitivities to oxidative stress. Previous reports of cell culture showed that the increased ferritin levels triggered a greater extent of lipid oxidation³²⁹, indicating that the increase of lipid oxidation was also possible due to the over transcription of ftn-1 confirmed by previous discoveries¹⁵⁹. It suggested that ftn-1, responsible for iron homeostasis regulation, sod-3, defense against oxidative stress, were both involved in the process of a raised level of lipid oxidation after exposure to AuNPs, displaying the complex regulatory mechanism of AuNPs toxicity in *C. elegans*⁸⁸.

Chapter 5 Evaluation of Lutein's antioxidative effects and MOFs toxicity in *C. elegans*

5.1 Collaboration work in *C. elegans* research

5.2 The assessment of lutein in *C. elegans*

5.2.1 Aims

5.2.2 Lutein's antioxidative behaviors

5.2.3 Conclusions and future work

5.3 The assessment of MOFs in *C. elegans*

5.3.1 Aims

5.3.2 The effect of chitosan coating

5.3.3 Conclusions and future work

5.1. Collaboration work in *C. elegans* research

During the last decades, it's increasingly common to make toxicity assessments of diverse materials using different model animals; and *C. elegans* is one of the applied models⁵⁷. It has multiple advantages such as cost-effectiveness, small size, transparency, short lifespan, prolific lifecycle, genetic manipulability, etc^{59,62,68}. It can provide us toxicity data from a complete animal model containing alimentary, reproductive, neuromuscular systems^{63,68}. Furthermore, combined with collaborative work of employing other advanced techniques, a deeper understanding of tested materials' fates and their toxicity mechanisms inside *C. elegans* can be attained^{59,62,159}. In this chapter, I will describe two collaborative projects I participated about investigating lutein's antioxidative behaviors in newly established *C. elegans* disease models applying synchrotron Fourier transform infrared (SR- μ FTIR) microspectroscopy and studying the chitosan coating's influence on the *C. elegans*' uptake efficiency of metal-organic frameworks (MOFs) using high performance liquid chromatography (HPLC).

5.2. The assessment of lutein in *C. elegans*

Neurodegenerative diseases are a heterogeneous type of chronic illnesses including Huntington's disease (HD), Parkinson's disease (PD), Alzheimer's disease (AD), etc³³⁰. Researchers have proposed several molecular mechanisms that are involved in the pathogenesis of these diseases³³¹. And mitochondrial dysfunction has been considered as the potential candidate connecting these disorders³³⁰. Mitochondria play a crucial role in energy production in cells³³². The generation of ATP, cellular energy, is catalyzed by the oxidative phosphorylation (OXPHOS) system, which contains five complexes³³³. The mitochondrial complex I (CI), the first complex deficiency, is the most common cause of neurodegenerative diseases^{221,333}, including Leigh disease (LD)³³² and PD³³¹. The defects of CI activities are associated with increased production of reactive oxygen species (ROS)³³², decreased respiration, and lipid oxidation which could be improved by the administration of antioxidants³³⁰.

Unfortunately, because of the complexity and variety of these diseases, an appropriate treatment strategy for some specific disease is difficult to be developed. Therefore, there is a high demand for conducting preliminary trials in a suitable model organism^{221,332}. It has been reported that around 42% of human disease genes have homologs in *C. elegans*, whose genome was completely sequenced^{63,334}. Together with no ethical constraints, it could be a promising tool for studying underlying molecular pathways in some human neurodegenerative diseases^{62,334} and therapeutic efficacy of new drug³³⁵.

Lutein, one of the xanthophylls carotenoids (shown in Figure 52), highly accumulates in the macula of the retina^{336,337} and protects the retina from photo-oxidative damage through scavenging ROS and filtering blue light^{338,339}. But human cannot synthesize lutein de novo and need to orally intake it from the diet^{336,340}. Therefore, lutein has been commonly used as food additive³³⁶ and diet supplement for age-related macular degeneration (AMD)^{338,341} due to its anti-oxidative and anti-inflammatory properties^{339,342}.

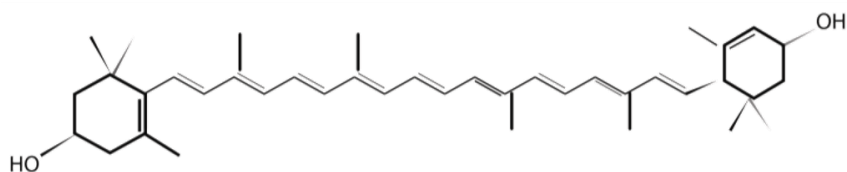


Figure 52 The chemical structure of lutein, adapted from Koushan K et al³⁴³.

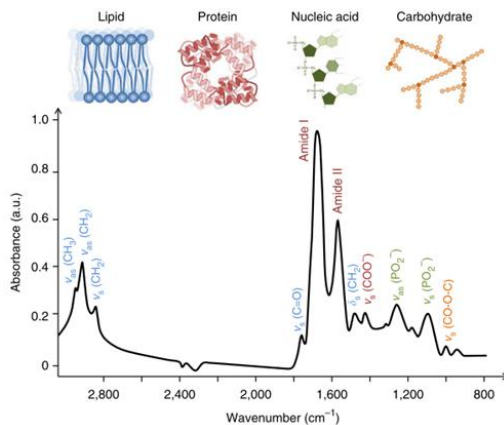


Figure 53 The spectrum showed biomolecular peak assignments from 3000–800 cm^{-1} . Adapted from Baker et al³⁴⁴.

Fourier transform infrared (FTIR) spectroscopy is a non-destructive technique offering possibilities of analyzing biochemical properties in different biological samples^{272,345} like *C. elegans*⁶⁰. FTIR spectra are representative of organic components in biological samples (shown in Figure 53). Thus, they can be applied as molecular signatures, for instance, lipid oxidation and protein conformation²⁷², of samples in various status^{346,347}. Another advantage is that no need of staining, homogenization and further manipulations is required before analysis^{272,346}. In addition, synchrotron radiation light based FTIR could achieve much-improved signal to noise ratio, better spatial resolution and much less acquisition time compared with that with conventional light²⁶⁸. Furthermore, the synchrotron FTIR technique has been performed to study neurodegenerative diseases such as AD³⁴⁸, PD³⁴⁹ and HD³⁵⁰.

5.2.1. Aims

In this part, we conducted research about lutein's anti-oxidative behaviors in *C. elegans* with complex I deficiency (*nuo-5* and *lpd-5*) by comparing the level of lipid oxidation and amide oxidation through synchrotron FTIR technique^{269,271}. Lipid oxidation, amide oxidation and lutein ratio were determined by calculating ratios for each spectrum^{221,351}, $V_s(\text{C}=\text{O}) 1745 \text{ cm}^{-1} / V_{as}(\text{CH}_2) 2921 \text{ cm}^{-1}$, $V_{as}(\text{C}=\text{O}) 1745 \text{ cm}^{-1} / V_s(\text{Amide}) 1654 \text{ cm}^{-1}$, and $V(\text{Lutein}) 1515 \text{ cm}^{-1} / V_{as}(\text{CH}_2) 2921 \text{ cm}^{-1}$.

5.2.2. Lutein's antioxidative behaviors

Freshly obtained eggs of wild-type N2, *nuo-5*, and *lpd-5* strains were put on the agar plates seeded with

E. coli (with or without lutein). Worms were collected at L3 stage (at 20°C). Sample preparation and spectral optimization are detailed in Chapter 2.6. As shown in Figure 54, we found reduced lipid and amide oxidation in *nuo-5* and *lpd-5* strains compared with that of control worms, indicating less oxidative damage. These results suggested that in these worms, they up-regulated their defense responses against oxidative stress.

Then, we studied if the uptake of lutein could contribute to protecting worms from oxidative stress. Firstly, by the lutein absorbance peak³⁵¹ of 1515.8 cm⁻¹, we detected the existence of lutein in worms, confirming that they uptake the drug (Figure 55C). Secondly, we compared the level of lipid oxidation or amide oxidation among N2, *nuo-5*, and *lpd-5* worms. There was no significant difference identified between with and without lutein in any type of worm (Figure 55A and 55B), suggesting that lutein failed to provide a protective response against oxidative stress. We assumed that ROS-triggered stress might be a minor part involved in the disease-related defects²²¹.

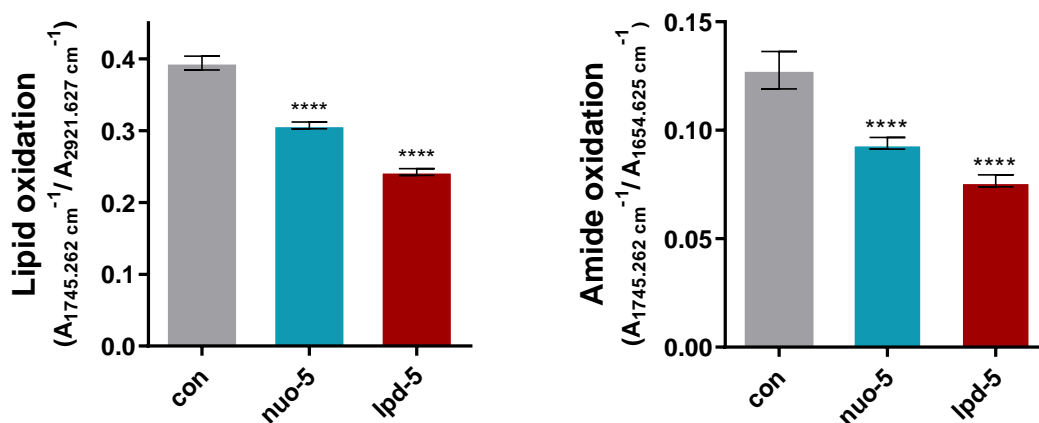


Figure 54 Bar plot of the lipid oxidation (1745 cm⁻¹/2921 cm⁻¹) and amide oxidation (1745 cm⁻¹/1654 cm⁻¹) of all spectra for control, *nuo-5*, and *lpd-5*. N=3, n=15-20. p < 0.0332 (*), p < 0.0021 (**), p < 0.0002 (***), and p < 0.0001 (****)

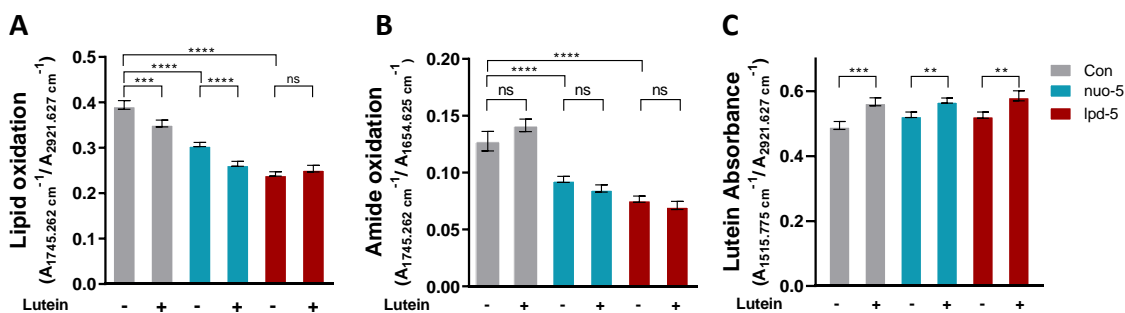


Figure 55 Bar plot of lipid oxidation (1745 cm⁻¹/2921 cm⁻¹), amide oxidation (1745 cm⁻¹/1654 cm⁻¹), and lutein absorbance (1515 cm⁻¹/2921 cm⁻¹) of all spectra for control, *nuo-5*, and *lpd-5*. N=3, n=15-20. p < 0.0332 (*), p < 0.0021 (**), p < 0.0002 (***), and p < 0.0001 (****) versus respective control conditions.

5.2.3. Conclusions and future work

To summarize, by SR-μFTIR method, we successfully detected the uptake of lutein. Moreover, through the statistical analysis of lipid oxidation and amide oxidation ratios in N2 and complex I deficiency (*nuo-5*

and lpd-5) worms, we obtained a deeper understanding of cellular defense against oxidative stress, indicating the great potential of applying *C. elegans* as the animal model for studying the molecular mechanism of neurodegenerative diseases. Moreover, we could investigate the potential therapeutic efficacy of medicine in established *C. elegans* models of human disease.

5.3. The assessment of MOFs in *C. elegans*

MOFs are composed of inorganic subunits (clusters, chains, or layers of transition metals, etc.) and organic polydentate ligands, with wide potentials in catalysis, gas storage and biomedical applications^{352–354}. Particularly, multiple strengths of MOFs including tunable porosity, adaptable structure, availability of functionalization, biodegradability make them promising bioplatfroms in biomedical applications^{352,354}. The frequently used metal ions in MOFs are iron, copper, zinc, cadmium, nickel, etc. Among them, iron-based MOFs are widely studied about their *in vitro* and *in vivo* toxicities owing to their lowest possibilities of inducing toxic effects on humans^{353–355}. Moreover, degraded components of iron-based MOFs within the human body, iron and organic linker could also be directly removed via urine and feces^{356,357}. In addition, coated with chitosan (CS), which a natural polymer with properties of biodegradability, biocompatibility, and non-toxicity³⁵⁸, the colloidal stability in complex media and cellular uptake were greatly improved³⁵⁹. Compared with extensive studies of MOFs' *in vitro* toxicities, there are quite a few *in vivo* toxicity researches³⁵⁵. Roja S et al. reported that MIL-127 (iron-based MOFs) (shown in Figure 56) was orally safe even at the high dose (1g/kg) in mice³⁶⁰. Considering the high cost and long term of performing *in vivo* toxicity assays in mice, we need to find an alternative model animal that is simple and cost-effective but with similar level cellular complexity, *C. elegans*²³⁶. *C. elegans* have various advantages such as small size, short lifespan, transparency, etc⁵⁷. More importantly, the intestine of *C. elegans* is a weakly acid microenvironment of pH around 4.4⁷¹ containing digestive enzymes to fully break up food particles⁷². These conserved alimentary features which are comparable to those of humans^{68,70} make *C. elegans* a good oral administration model⁶⁸ for studying MOFs' *in vivo* toxicities.

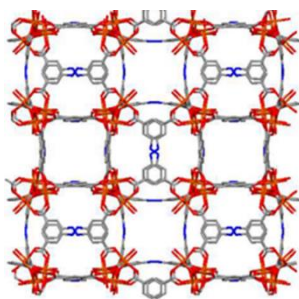


Figure 56 The structure of MIL-127 (Fe), adapted from Roja S et al³⁶⁰.

5.3.1. Aims

In this part, we performed an acute exposure of *C. elegans* upon MIL-127 and CS-MIL-127 in the low-ionic-strength simulated intestinal fluid (Lis-SIF) media. By measuring survival, we obtained preliminary toxicity of MIL-127 and CS-MIL-127. The CS coating's influence on the *C. elegans*' uptake efficiency of MOFs was studied by using HPLC.

5.3.2. The effect of chitosan coating

Survival

Survival was determined by counting worms defined as alive if they responded to the gentle touch by a worm-picker⁷⁶. We found that, after 24 h, there was no mortality even at the highest concentration (1000 µg/mL) of MIL127 or CS-MIL-127 (Figure 57A), suggesting that CS coating didn't interfere with MIL-127 toxicity. The MOFs uptake could also be clearly seen under the microscope (Figure 57B and 57C).

Uptake and excretion efficiency

In addition, combined with our collaborators' experiences of quantifying MOFs inside biological samples by the HPLC method³⁵⁷, we continued our research about how much MOFs was uptaken by *C. elegans* during the acute exposure and the role of CS coating in the uptake efficiency. Due to the measurement limitations of HPLC, around 2000 worms were treated with 1000 µg/mL of MIL-127 or CS-MIL-127 in the 24-well-plate for 24 h. After exposure, treated worms, aggregated MOFs settled at the bottom of the well, and the supernatant were separated from the mixture for HPLC measurement. Three replicates were independently performed for statistical purposes. We found that there was 0.07 ± 0.04 µg MIL-127 and 0.04 ± 0.01 µg CS-MIL-127 per worm, given that the average weight of adult worm is $4 \mu\text{g}$ ³⁶¹. It implied that CS coating didn't facilitate the uptake efficiency of MIL-127. Furthermore, we wondered if there was a potential influence of CS coating on the ability of exposed worms excreting uptake MOFs with the addition of *E. coli*. 2000 treated worms were cultured with *E. coli* in the same exposure condition for another 24 h which was taken as the excretion assay. The three aforementioned components in the mixture were separated. Determined by HPLC, there was 0.03 ± 0.01 µg MIL-127 and 0.03 ± 0.01 µg CS-MIL-127 per worm. Compared with the previous uptake amount of MIL-127 and CS-MIL-127, it suggested that CS coating decreased the excretion speed in



Figure 57 Effects of CS coating on the Survival (A) of *C. elegans* (n=3) exposed to increasing concentrations of MIL-127 and CS-MIL-127. Bars indicate the mean \pm S.E.M. (B) The worm after acute exposure to 500 µg/mL of MIL-127, (C) The worm after acute exposure to 500 µg/mL of CS-MIL-127. The scale bar represents 100 µm.

5.3.3. Conclusions and future work

In summary, we found that exposure to high concentrations of MIL-127 and CS-MIL-127 didn't induce lethality to worms. Although CS coating couldn't promote uptake efficiency, it extended the maintenance

time of MIL-127 inside worms by reducing the excretion rate. Additionally, we will conduct more types of toxicity assessments to obtain a general knowledge of potential toxicities of MIL-127 and CS-MIL-127.

Chapter 6 Conclusions

6.1 Conclusions

6.2 Future work

6.2.1 Exposure routes

6.2.2 Assayed materials

6.2.3 Advanced techniques

6.3 Prospects and challenges

6.1. Conclusions

1. We had performed the acute exposure (24 h) and prolonged exposure (72 h) of *C. elegans* to citrate-coated SPIONs to obtain a general understanding of their nano-bio interactions by measuring various toxicity endpoints such as lipid storage, lifespan, locomotion, etc. Moreover, we also studied the influence of food availability on SPIONs-induced toxicities in the acute exposure system.
 - a- We found that acute exposure to SPIONs could induce lipid accumulation, locomotive deficits, shortened lifespan, and impaired chemotaxis towards NaCl but with the maintained intestinal integrity. With the addition of food, there was a positive influence of food in causing no mortality and mitigating detrimental effects on lipid accumulation and chemotaxis. However, accumulated lipid content, damaged locomotion behaviors, and decreased lifespan could still be observed. There was also a more homogeneous biodistribution of SPIONs in the whole intestinal lumen. Additionally, combined with the application of SQUID and ICP-MS measurements, we discovered that food presence could improve the uptake efficiency of SPIONs. However, there was a similar level of iron ion release from SPIONs inside *C. elegans* proved by TEM and ZFC-FC magnetometry measurements compared with that of worms in the acute exposure condition without food existence. The free iron ions might be responsible for several sublethal toxicities detected on worms.
 - b- With the utilization of SR- μ FTIR, we discerned a dose- and exposure-time- related increase of lipid oxidation in *C. elegans*, related to worms' responses against oxidative stress triggered by SPIONs. Furthermore, a relatively higher level of lipid oxidation in the head zone was detected, especially in the FPA mapping image of *sod-3* deficiency mutant treated with 500 μ g/mL SPIONs for 24 h. It might be associated with neurotoxic symptoms.
 - c- After prolonged exposure to SPIONs, L1 larvae could develop normally even at the highest concentration of 500 μ g/mL. Although there were no harmful effects on reproduction, lipid content, and intestinal integrity, we still found a dose-dependence decreased lifespan and damaged locomotion behaviors.
2. We had conducted the acute exposure of *C. elegans* to citrate-coated 10 nm AuNPs with the addition of food to study the influence of food availability on AuNPs-induced toxicities by measuring various toxicity endpoints such as lipid storage, lifespan, locomotion, etc. We also investigated the potential of applying *C. elegans* as the model organism for photothermal therapy.
 - a. At the chosen concentration of 100 μ g/mL, with the presence of food, there was a positive influence on the survival and reproduction of *C. elegans*, but not on the intestinal integrity and lipid accumulation. In addition, exposure to higher concentrations of AuNPs (up to 500 μ g/mL), we detected locomotive deficits and decreased lifespan in both treatment conditions with and without food presence, indicating limited protective effects provided by food availability. In the biodistribution assay, with food availability, we discerned a higher frequency of AuNPs located in the posterior compartment

- of the intestinal lumen, especially exposed to concentrated AuNPs.
- b. By using Raman spectroscopy, we successfully discovered the photothermal phenomenon in *C. elegans* containing 150 nm AuNPs under the irradiation of the 785 nm laser. However, after the irradiation process, we also found photo-ablated damages on worms, indicating that we need to optimize the experimental settings such as the laser power and irradiation duration.
 - c. Through the SR- μ FTIR measurement of worms treated with 10 nm or 150 nm AuNPs for 4 or 24 h, we detected a size- and exposure-duration- dependent increase of lipid oxidation ratio. The highest level of lipid oxidation ratio was found in the *sod-3* deficiency mutant exposed to 10 nm AuNPs for 24 h, consistent with FPA mapping results, indicating that oxidative stress was involved in the toxicity mechanism of AuNPs.
3. We broadened the application range of SR- μ FTIR in studying lutein's anti-oxidative behaviors in *C. elegans* disease models (*nuo-5* and *lpd-5*) with mitochondrial dysfunction. Firstly, we confirmed worms' uptake of lutein by a higher lutein ratio of worms with lutein treatment compared with that of worms in the control condition. Secondly, through analyzing ratios of lipid oxidation and amide oxidation in disease models, together with our collaborators' other findings, we proposed that lutein behaved an anti-oxidant in ameliorating developmental, neuronal, and cellular dysfunction through indirect influences on the downstream processes rather than direct influences on the mitochondria²²¹.
 4. *C. elegans* was employed as an oral administration model in investigating MOFs' (MIL-127 and chitosan-coated MIL-127) *in vivo* toxicities. Meanwhile, chitosan's effect on *C. elegans*' uptake and excretion efficiency of MOFs was also studied using HPLC measurement. In the survival assay, both types of MOFs were not toxic to wild-type worms even at 1000 μ g/mL. Chitosan restrained the uptake but contributed to maintaining uptaken CS-MIL-127 inside worms by decreasing the excreting rate.

6.2 Future work

6.2.1. Exposure routes

The appropriate exposure route is one of the crucial factors in toxicity assessments of NPs⁷⁶. Previously, we intensively investigated SPIONs/AuNPs-induced toxicities in the acute exposure condition with or without food availability. We could study their environmental toxicities at an environment-relevant concentration through chronic exposure (> 72 h). Moreover, multigenerational exposure assays could also be performed to learn if there is transgenerational toxicity regarding their potential applications such as imaging agents and drug delivery^{7,84}.

6.2.2. Assayed materials

Based on our preliminary findings of MOFs' *in vivo* toxicities in *C. elegans*, we could investigate further by performing various toxicity assays such as reproduction, lifespan, and locomotion behaviors to obtain a

general understanding of MOFs-induced toxic effects. It will facilitate MOFs optimization for decreased toxicity and their green synthesis³⁶².

6.2.3. Advanced techniques

In this dissertation, we proposed several genes that might be involved in the toxicity mechanism of SPIONs/AuNPs. To validate it, we could study further in a toxicogenomic method by utilizing quantitative reverse transcription polymerase chain reaction (qRT-PCR), RNA interference (RNAi), or mutant assays.

6.3 Prospects and challenges

C. elegans, as an *in vivo* animal model, has been successfully utilized to evaluate NPs' toxicities⁵⁷, at the environmental level⁷⁶ and the preclinical level³⁶³. Various advanced material science techniques are also employed to acquire a deeper understanding of nano-bio interactions⁵⁹. To further the nanotoxicity study in *C. elegans*, genetic investigations including possible cellular uptake pathways and molecular mechanisms of NPs should be performed⁷⁷. The mutants from the Caenorhabditis Genetics Center and the *C. elegans* community could offer opportunities to precisely locate affected genes due to NPs treatment.

Regardless of multiple advantages provided by *C. elegans* applied in the ecotoxicity or as an oral administration model, several drawbacks still exist, especially compared with rodents which are the most generally used animal model for nanotoxicity studies^{57,76}. Meanwhile, good *C. elegans* practice and standardized toxicity tests are also essential to ensure the reliability and reproducibility of obtained toxicological results^{68,121,122}.

To summarize, we advocate that *C. elegans* can continuously fill in the knowledge gap between *in vitro* and *in vivo* nanotoxicity research. Moreover, combined with cross-disciplinary techniques, it could provide us valuable information for a better understanding of nano-bio interactions.

References:

- (1) Bisso, S.; Leroux, J. C. Nanopharmaceuticals: A Focus on Their Clinical Translatability. *Int. J. Pharm.* **2020**, *578*, 119098.
- (2) Boros, B. V.; Ostafe, V. Evaluation of Ecotoxicology Assessment Methods of Nanomaterials and Their Effects. *Nanomaterials* **2020**, *10* (4).
- (3) Ahmad, F.; Wang, X.; Li, W. Toxicity-Metabolomics of Engineered Nanomaterials: Progress and Challenges. *Adv. Funct. Mater.* **2019**, *29* (51), 1–24.
- (4) Foroozandeh, P.; Aziz, A. A. Insight into Cellular Uptake and Intracellular Trafficking of Nanoparticles. *Nanoscale Res. Lett.* **2018**, *13*.
- (5) Brohi, R. D.; Wang, L.; Talpur, H. S.; Wu, D.; Khan, F. A.; Bhattarai, D.; Rehman, Z. U.; Farmanullah, F.; Huo, L. J. Toxicity of Nanoparticles on the Reproductive System in Animal Models: A Review. *Front. Pharmacol.* **2017**, *8*, 1–22.
- (6) Anselmo, A. C.; Mitragotri, S. Nanoparticles in the Clinic. *Bioeng. Transl. Med.* **2016**, *1* (1), 10–29.
- (7) Thakor, A. S.; Jokerst, J. V.; Ghanouni, P.; Campbell, J. L.; Mittra, E.; Gambhir, S. S. Clinically Approved Nanoparticle Imaging Agents. *J. Nucl. Med.* **2016**, *57* (12), 1833–1837.
- (8) Azhdarzadeh, M.; Saei, A. A.; Sharifi, S.; Hajipour, M. J.; Alkilany, A. M.; Sharifzadeh, M.; Ramazani, F.; Laurent, S.; Mashaghi, A.; Mahmoudi, M. Nanotoxicology: Advances and Pitfalls in Research Methodology. *Nanomedicine* **2015**, *10* (18), 2931–2952.
- (9) Barenholz, Y. Doxil® - The First FDA-Approved Nano-Drug: Lessons Learned. *J. Control. Release* **2012**, *160* (2), 117–134.
- (10) Macdougall, L. C. Evolution of IV Iron Compounds over the Last Century. *J. Ren. Care* **2009**, *35* (SUPPL. 2), 8–13.
- (11) Borchard, G.; Flühmann, B.; Mühlebach, S. Nanoparticle Iron Medicinal Products - Requirements for Approval of Intended Copies of Non-Biological Complex Drugs (NBCD) and the Importance of Clinical Comparative Studies. *Regul. Toxicol. Pharmacol.* **2012**, *64* (2), 324–328.
- (12) Danielson, B. G. Structure, Chemistry, and Pharmacokinetics of Intravenous Iron Agents. *J. Am. Soc. Nephrol.* **2004**, *15* (SUPPL. 2), S93–S98.
- (13) Rosner, M. H.; Auerbach, M. Ferumoxytol for the Treatment of Iron Deficiency. *Expert Rev. Hematol.* **2011**, *4* (4), 399–406.
- (14) Auerbach M, Chertow G M, R. M. Ferumoxytol for the Treatment of Iron Deficiency Anemia. *Expert Rev. Hematol.* **2018**, *11* (10), 829–834.
- (15) Laurent, S.; Forge, D.; Port, M.; Roch, A.; Robic, C.; Vander Elst, L.; Muller, R. N. Magnetic Iron Oxide Nanoparticles: Synthesis, Stabilization, Vectorization, Physicochemical Characterizations and Biological Applications. *Chem. Rev.* **2008**, *108* (6), 2064–2110.
- (16) Na, H. Bin; Song, I. C.; Hyeon, T. Inorganic Nanoparticles for MRI Contrast Agents. *Adv. Mater.* **2009**, *21* (21), 2133–2148.
- (17) Wang, Y. X. J.; Hussain, S. M.; Krestin, G. P. Superparamagnetic Iron Oxide Contrast Agents: Physicochemical Characteristics and Applications in MR Imaging. *Eur. Radiol.* **2001**, *11* (11), 2319–2331.
- (18) Gupta, A. K.; Gupta, M. Synthesis and Surface Engineering of Iron Oxide Nanoparticles for Biomedical Applications. *Biomaterials* **2005**, *26* (18), 3995–4021.
- (19) Misselwitz, B. MR Contrast Agents in Lymph Node Imaging. *Eur. J. Radiol.* **2006**, *58* (3), 375–382.
- (20) Chen, B.; Li, Y.; Zhang, X.; Liu, F.; Liu, Y.; Ji, M.; Xiong, F.; Gu, N. An Efficient Synthesis of Ferumoxytol Induced by Alternating-Current Magnetic Field. *Mater. Lett.* **2016**, *170*, 93–96.
- (21) Wibroe, P. P.; Ahmadvand, D.; Oghabian, M. A.; Yaghmur, A.; Moghimi, S. M. An Integrated Assessment of Morphology, Size, and Complement Activation of the PEGylated Liposomal Doxorubicin Products Doxil®, Caelyx®, DOXOrubicin, and SinaDoxosome. *Journal of Controlled Release*. 2016, pp 1–8.
- (22) Peer, D.; Karp, J. M.; Hong, S.; Farokhzad, O. C.; Margalit, R.; Langer, R. Nanocarriers as an Emerging Platform for Cancer Therapy. *Nat. Nanotechnol.* **2007**, *2*, 751–760.
- (23) Anselmo, A. C.; Mitragotri, S. An Overview of Clinical and Commercial Impact of Drug Delivery

- Systems. *J. Control. Release* **2014**, *190*, 15–28.
- (24) Petros, R. A.; Desimone, J. M. Strategies in the Design of Nanoparticles for Therapeutic Applications. *Nat. Rev. Drug Discov.* **2010**, *9* (8), 615–627.
- (25) Dadfar, S. M.; Roemhild, K.; Drude, N. I.; von Stillfried, S.; Knüchel, R.; Kiessling, F.; Lammers, T. Iron Oxide Nanoparticles: Diagnostic, Therapeutic and Theranostic Applications. *Adv. Drug Deliv. Rev.* **2019**, *138*, 302–325.
- (26) Abadeer, N. S.; Murphy, C. J. Recent Progress in Cancer Thermal Therapy Using Gold Nanoparticles. *J. Phys. Chem. C* **2016**, *120* (9), 4691–4716.
- (27) Riley, R. S.; Day, E. S. Gold Nanoparticle-Mediated Photothermal Therapy: Applications and Opportunities for Multimodal Cancer Treatment. *Wiley Interdiscip. Rev. Nanomedicine Nanobiotechnology* **2017**, *9* (4).
- (28) Stern, J. M.; Kibanov Solomonov, V. V.; Sazykina, E.; Schwartz, J. A.; Gad, S. C.; Goodrich, G. P. Initial Evaluation of the Safety of Nanoshell-Directed Photothermal Therapy in the Treatment of Prostate Disease. *Int. J. Toxicol.* **2016**, *35* (1), 38–46.
- (29) Rastinehad, A. R.; Anastos, H.; Wajswol, E.; Winoker, J. S.; Sfakianos, J. P.; Doppalapudi, S. K.; Carrick, M. R.; Knauer, C. J.; Taouli, B.; Lewis, S. C.; Tewari, A. K.; Schwartz, J. A.; Canfield, S. E.; George, A. K.; West, J. L.; Halas, N. J. Gold Nanoshell-Localized Photothermal Ablation of Prostate Tumors in a Clinical Pilot Device Study. *Proc. Natl. Acad. Sci. U. S. A.* **2019**, *116* (37), 18590–18596.
- (30) Bobo, D.; Robinson, K. J.; Islam, J.; Thurecht, K. J.; Corrie, S. R. Nanoparticle-Based Medicines: A Review of FDA-Approved Materials and Clinical Trials to Date. *Pharm. Res.* **2016**, *33* (10), 2373–2387.
- (31) Feliu N, Docter D, Heine M, et al. In Vivo Degeneration and the Fate of Inorganic Nanoparticles. *Chem. Soc. Rev.* **2016**, *45* (9), 2440–2457.
- (32) Das, S.; Chaudhury, A. Recent Advances in Lipid Nanoparticle Formulations with Solid Matrix for Oral Drug Delivery. *AAPS PharmSciTech* **2011**, *12* (1), 62–76.
- (33) Chenthamara, D.; Subramaniam, S.; Ramakrishnan, S. G.; Krishnaswamy, S.; Essa, M. M.; Lin, F. H.; Qoronfleh, M. W. Therapeutic Efficacy of Nanoparticles and Routes of Administration. *Biomater. Res.* **2019**, *23* (1), 1–29.
- (34) Etheridge, M. L.; Campbell, S. A.; Erdman, A. G.; Haynes, C. L.; Wolf, S. M.; McCullough, J. The Big Picture on Nanomedicine: The State of Investigational and Approved Nanomedicine Products. *Nanomedicine Nanotechnology, Biol. Med.* **2013**, *9* (1), 1–14.
- (35) Arami H, Khandhar A, Liggitt D, et al. In Vivo Delivery, Pharmacokinetics, Biodistribution and Toxicity of Iron Oxide Nanoparticles. *Chem. Soc. Rev.* **2015**, *44* (23), 8576–8607.
- (36) Schaefer B, Meindl E, Wagner S, et al. Intravenous Iron Supplementation Therapy. *Mol. Aspects Med.* **2020**, 100862.
- (37) Bhandari S, Pereira D I A, Chappell H F, et al. Intravenous Irons : From Basic Science to Clinical Practice. *Pharmaceuticals* **2018**, *11* (3), 82.
- (38) Custodio, J. M.; Wu, C. Y.; Benet, L. Z. Predicting Drug Disposition, Absorption/Elimination/Transporter Interplay and the Role of Food on Drug Absorption. *Adv. Drug Deliv. Rev.* **2008**, *60* (6), 717–733.
- (39) Homayun, B.; Lin, X.; Choi, H. J. Challenges and Recent Progress in Oral Drug Delivery Systems for Biopharmaceuticals. *Pharmaceutics* **2019**, *11* (3).
- (40) Shreya, A. B.; Raut, S. Y.; Managuli, R. S.; Udupa, N.; Mutalik, S. Active Targeting of Drugs and Bioactive Molecules via Oral Administration by Ligand-Conjugated Lipidic Nanocarriers: Recent Advances. *AAPS PharmSciTech* **2019**, *20* (1).
- (41) Hua, S. Advances in Oral Drug Delivery for Regional Targeting in the Gastrointestinal Tract - Influence of Physiological, Pathophysiological and Pharmaceutical Factors. *Front. Pharmacol.* **2020**, *11* (April), 1–22.
- (42) Muraleetharan, V.; Mantaj, J.; Swedrowska, M.; Vllasaliu, D. Nanoparticle Modification in Biological Media: Implications for Oral Nanomedicines. *RSC Adv.* **2019**, *9* (69), 40487–40497.
- (43) McConnell, E. L.; Fadda, H. M.; Basit, A. W. Gut Instincts: Explorations in Intestinal Physiology and Drug Delivery. *Int. J. Pharm.* **2008**, *364* (2), 213–226.
- (44) Berardi, A.; Baldelli Bombelli, F. Oral Delivery of Nanoparticles - Let's Not Forget about the Protein Corona. *Expert Opin. Drug Deliv.* **2019**, *16* (6), 563–566.

- (45) Lichtenstein, D.; Ebmeyer, J.; Knappe, P.; Juling, S.; Böhmert, L.; Selve, S.; Niemann, B.; Braeuning, A.; Thünemann, A. F.; Lampen, A. Impact of Food Components during in Vitro Digestion of Silver Nanoparticles on Cellular Uptake and Cytotoxicity in Intestinal Cells. *Biol. Chem.* **2015**, *396* (11), 1255–1264.
- (46) Fleisher, D.; Li, C.; Zhou, Y.; Pao, L. H.; Karim, A. Drug, Meal and Formulation Interactions Influencing Drug Absorption after Oral Administration. Clinical Implications. *Clin. Pharmacokinet.* **1999**, *36* (3), 233–254.
- (47) Won, C. S.; Oberlies, N. H.; Paine, M. F. Mechanisms Underlying Food-Drug Interactions: Inhibition of Intestinal Metabolism and Transport. *Pharmacol. Ther.* **2012**, *136* (2), 186–201.
- (48) Boullata, J. I.; Hudson, L. M. Drug-Nutrient Interactions: A Broad View with Implications for Practice. *J. Acad. Nutr. Diet.* **2012**, *112* (4), 506–517.
- (49) Baxevanis, F.; Kuiper, J.; Fotaki, N. Fed-State Gastric Media and Drug Analysis Techniques: Current Status and Points to Consider. *Eur. J. Pharm. Biopharm.* **2016**, *107*, 234–248.
- (50) O’Shea, J. P.; Holm, R.; O’Driscoll, C. M.; Griffin, B. T. Food for Thought: Formulating Away the Food Effect – a PEARL Review. *J. Pharm. Pharmacol.* **2019**, *71* (4), 510–535.
- (51) McClements, D. J.; Xiao, H. Excipient Foods: Designing Food Matrices That Improve the Oral Bioavailability of Pharmaceuticals and Nutraceuticals. *Food Funct.* **2014**, *5* (7), 1320–1333.
- (52) Bordenave N, Hamaker B R, F. M. G. Nature and Consequences of Non-Covalent Interactions between Flavonoids and Macronutrients in Foods. *Food Funct.* **2014**, *5* (1), 18–34.
- (53) Delgado M C O, Tironi V A, A. M. C. Antioxidant Activity of Amaranth Protein or Their Hydrolysates under Simulated Gastrointestinal Digestion. *LWT - Food Sci. Technol.* **2011**, *44* (8), 1752–1760.
- (54) Lawless, E.; Griffin, B. T.; Mahony, A. O.; Driscoll, C. M. O. Exploring the Impact of Drug Properties on the Extent of Intestinal Lymphatic Transport - In Vitro and In Vivo Studies. *Pharm. Res.* **2015**, *32* (5), 1817–1829.
- (55) Di Maio S, C. R. L. Gastrointestinal Contents in Fasted State and Post-Lipid Ingestion : In Vivo Measurements and in Vitro Models for Studying Oral Drug Delivery. *J. Control. Release* **2011**, *151* (2), 110–122.
- (56) Jia, H. R.; Zhu, Y. X.; Duan, Q. Y.; Chen, Z.; Wu, F. G. Nanomaterials Meet Zebrafish: Toxicity Evaluation and Drug Delivery Applications. *J. Control. Release* **2019**, *311–312* (July), 301–318.
- (57) Wu, T.; Xu, H.; Liang, X.; Tang, M. *Caenorhabditis Elegans* as a Complete Model Organism for Biosafety Assessments of Nanoparticles. *Chemosphere* **2019**, *221*, 708–726.
- (58) Haegerbaeumer, A.; Höss, S.; Heininger, P.; Traunspurger, W. Is *Caenorhabditis Elegans* Representative of Freshwater Nematode Species in Toxicity Testing? *Environ. Sci. Pollut. Res.* **2018**, *25* (3), 2879–2888.
- (59) Gonzalez-Moragas, L.; Maurer, L. L.; Harms, V. M.; Meyer, J. N.; Laromaine, A.; Roig, A. Materials and Toxicological Approaches to Study Metal and Metal-Oxide Nanoparticles in the Model Organism: *Caenorhabditis Elegans*. *Mater. Horizons* **2017**, *4* (5), 719–746.
- (60) Bouyanfif A, Liyanage S, Hequet E, et al. Review of FTIR Microspectroscopy Applications to Investigate Biochemical Changes in *C. elegans* . *Vib. Spectrosc.* **2018**, *96*, 74–82.
- (61) Zhao, Y.; Wu, Q.; Li, Y.; Wang, D. Translocation, Transfer, and in Vivo Safety Evaluation of Engineered Nanomaterials in the Non-Mammalian Alternative Toxicity Assay Model of Nematode *Caenorhabditis Elegans*. *RSC Adv.* **2013**, *3* (17), 5741–5757.
- (62) Siddhardha, B.; Dyavaiah, M.; Kasinathan, K. *Model Organisms to Study Biological Activities and Toxicity of Nanoparticles*; 2020.
- (63) Avila, D.; Helmcke, K.; Aschner, M. The *Caenorhabditis Elegans* Model as a Reliable Tool in Neurotoxicology. *Hum. Exp. Toxicol.* **2012**, *31* (3), 236–243.
- (64) Brenner, S. The Genetics of *Caenorhabditis Elegans*. *Genetics* **1974**, *77* (1), 71–94.
- (65) Voogt, P. De. *Reviews of Environmental Contamination and Toxicology*; 2008; Vol. 237.
- (66) Hulme, S. E.; Whitesides, G. M. Chemistry and the Worm: *Caenorhabditis Elegans* as a Platform for Integrating Chemical and Biological Research. *Angew. Chemie - Int. Ed.* **2011**, *50* (21), 4774–4807.
- (67) Marsh, E. K.; May, R. C. *Caenorhabditis Elegans*, A Model Organism for Investigating Immunity. *Appl. Environ. Microbiol.* **2012**, *78* (7), 2075–2081.
- (68) Hunt, P. R. The *C. elegans* Model in Toxicity Testing. *J. Appl. Toxicol.* **2017**, *37* (1), 50–59.

- (69) Altun, Z.F. and Hall, D. . Alimentary System, Overview. In *In WormAtlas*; 2009.
- (70) Hafouri, S. G.; Hee, J. D. M. C. G. Bacterial Residence Time in the Intestine of *Caenorhabditis Elegans*. *Nematology* **2007**, *9* (1), 87–91.
- (71) Allman, E.; Johnson, D.; Nehrke, K.; York, N. Loss of the Apical V-ATPase α -Subunit VHA-6 Prevents Acidification of the Intestinal Lumen during a Rhythmic Behavior in *C. Elegans*. *Am. J. Physiol. Physiol.* **2009**, *297* (5), C1071–C1081.
- (72) Dimov, I.; Maduro, M. F. The *C. elegans* Intestine: Organogenesis, Digestion, and Physiology. *Cell Tissue Res.* **2019**, *377* (3), 383–396.
- (73) Thomas, J. H. Genetic Analysis of Defecation in *Caenorhabditis Elegans*. *Genetics* **1990**, *124* (4), 855–872.
- (74) Von Mikecz, A. Lifetime Eco-Nanotoxicology in an Adult Organism: Where and When Is the Invertebrate: *C. elegans* Vulnerable? *Environ. Sci. Nano* **2018**, *5* (3), 616–622.
- (75) Lints, R. and Hall, D. H. Reproductive System, Overview. In *In WormAtlas*; 2009.
- (76) Wang, D. *Nanotoxicology in Caenorhabditis Elegans*; 2018.
- (77) González Moragas, L. Evaluating Inorganic Nanoparticles in the Living Organism *Caenorhabditis Elegans*, 2016.
- (78) Sinis, S. I.; Gourgoulialis, K. I.; Hatzoglou, C.; Zarogiannis, S. G. Mechanisms of Engineered Nanoparticle Induced Neurotoxicity in *Caenorhabditis Elegans*. *Environ. Toxicol. Pharmacol.* **2019**, *67* (October 2018), 29–34.
- (79) Bono, M. De; Maricq, A. V. Neuronal Substrates of Complex Behaviors. *Annu. Rev. Neurosci* **2005**, *28*, 451–501.
- (80) Scharf, A.; Gührs, K. H.; Von Mikecz, A. Anti-Amyloid Compounds Protect from Silica Nanoparticle-Induced Neurotoxicity in the Nematode *C. elegans* . *Nanotoxicology* **2016**, *10* (4), 426–435.
- (81) Mashock, M. J.; Zanon, T.; Kappell, A. D.; Petrella, L. N.; Andersen, E. C.; Hristova, K. R. Copper Oxide Nanoparticles Impact Several Toxicological Endpoints and Cause Neurodegeneration in *Caenorhabditis Elegans*. *PLoS One* **2016**, *11* (12), 1–19.
- (82) Hisamoto, N.; Matsumoto, K. Signal Transduction Cascades in Axon Regeneration: Insights from *C. elegans* . *Curr. Opin. Genet. Dev.* **2017**, *44*, 54–60.
- (83) Ewbank, J. J. Evolution of the Innate Immune System : The Worm Perspective. *Immunol. Rev.* **2004**, *198* (1), 36–58.
- (84) KK.Jain. Future of Nanomedicine: Impact on Healthcare & Society. *Nanomedicine* **2015**.
- (85) Ganguly P, Breen A, P. S. C. Toxicity of Nanomaterials: Exposure, Pathways, Assessment, and Recent Advances. *ACS Biomater. Sci. Eng.* **2018**, *4* (7), 2237–2275.
- (86) Caito, S.; Aschner, M. *Neurotoxicity of Metals*; 2015; Vol. 131.
- (87) Chen, P.; Martinez-Finley, E. J.; Bornhorst, J.; Chakraborty, S.; Aschner, M. Metal-Induced Neurodegeneration in *C. elegans* . *Front. Aging Neurosci.* **2013**, *5*, 18.
- (88) Wang, D. Biological Effects, Translocation, and Metabolism of Quantum Dots in the Nematode *Caenorhabditis Elegans*. *Toxicol. Res. (Camb)*. **2016**, *5* (4), 1003–1011.
- (89) Bosch, S.; Botha, T. L.; Jordaan, A.; Maboeta, M.; Wepener, V. Sublethal Effects of Ionic and Nanogold on the Nematode *Caenorhabditis Elegans*. *J. Toxicol.* **2018**, *2018*.
- (90) Höss S, Bergtold M, Haitzer M, et al. Refractory Dissolved Organic Matter Can Influence the Reproduction of *Caenorhabditis Elegans* (Nematoda). *Freshw. Biol.* **2001**, *46* (1), 1–10.
- (91) Höss, S.; Jüttner, I.; Traunspurger, W.; Pfister, G.; Schramm, K. W.; Steinberg, C. E. W. Enhanced Growth and Reproduction of *Caenorhabditis Elegans* (Nematoda) in the Presence of 4-Nonylphenol. *Environ. Pollut.* **2002**, *120* (2), 169–172.
- (92) Fakhrollina, G.; Akhatova, F.; Kibardina, M.; Fokin, D.; Fakhrollin, R. Nanoscale Imaging and Characterization of *Caenorhabditis Elegans* Epicuticle Using Atomic Force Microscopy. *Nanomedicine Nanotechnology, Biol. Med.* **2017**, *13* (2), 483–491.
- (93) Akhatova, F.; Fakhrollina, G.; Khakimova, E.; Fakhrollin, R. Atomic Force Microscopy for Imaging and Nanomechanical Characterisation of Live Nematode Epicuticle: A Comparative *Caenorhabditis Elegans* and *Turbatrix Aceti* Study. *Ultramicroscopy* **2018**, *194*, 40–47.
- (94) Eom, H. J.; Choi, J. Clathrin-Mediated Endocytosis Is Involved in Uptake and Toxicity of Silica Nanoparticles in *Caenorhabditis Elegans*. *Chem. Biol. Interact.* **2019**, *311*, 108774.

- (95) Zanni, E.; De Bellis, G.; Bracciale, M. P.; Broggi, A.; Santarelli, M. L.; Sarto, M. S.; Palleschi, C.; Uccelletti, D. Graphite Nanoplatelets and *Caenorhabditis Elegans* : Insights from an *in Vivo* Model. *Nano Lett.* **2012**, *12* (6), 2740–2744.
- (96) Zhao, Y.; Wang, X.; Wu, Q.; Li, Y.; Wang, D. Translocation and Neurotoxicity of CdTe Quantum Dots in RMEs Motor Neurons in Nematode *Caenorhabditis Elegans*. *J. Hazard. Mater.* **2015**, *283*, 480–489.
- (97) Liu, J.; Liu, W.; Zhang, K.; Shi, J.; Zhang, Z. A Magnetic Drug Delivery System with “OFF–ON” State via Specific Molecular Recognition and Conformational Changes for Precise Tumor Therapy. *Adv. Healthc. Mater.* **2020**, *9* (3), 1–12.
- (98) Corsi A K, Wightman B, C. M. A Transparent Window into Biology: A Primer on *Caenorhabditis Elegans*. *Genetics* **2015**, *200* (2), 387–407.
- (99) Zhao, Y.; Wu, Q.; Tang, M.; Wang, D. The *in Vivo* Underlying Mechanism for Recovery Response Formation in Nano-Titanium Dioxide Exposed *Caenorhabditis Elegans* after Transfer to the Normal Condition. *Nanomedicine Nanotechnology, Biol. Med.* **2014**, *10* (1), 89–98.
- (100) Collin, B.; Oostveen, E.; Tsyusko, O. V.; Unrine, J. M. Influence of Natural Organic Matter and Surface Charge on the Toxicity and Bioaccumulation of Functionalized Ceria Nanoparticles in *Caenorhabditis Elegans*. *Environ. Sci. Technol.* **2014**, *48* (2), 1280–1289.
- (101) Gonzalez-moragas, L.; Yu, S. M.; Carezza, E.; Laromaine, A.; Roig, A. Protective Effects of Bovine Serum Albumin on Superparamagnetic Iron Oxide Nanoparticles Evaluated in the Nematode *Caenorhabditis Elegans*. *ACS Biomater. Sci. Eng.* **2015**, *1* (11), 1129–1138.
- (102) Wu, Q.; Li, Y.; Tang, M.; Wang, D. Evaluation of Environmental Safety Concentrations of DMSA Coated Fe₂O₃-NPs Using Different Assay Systems in Nematode *Caenorhabditis Elegans*. *PLoS One* **2012**, *7* (8).
- (103) Yu, S.; Rui, Q.; Cai, T.; Wu, Q.; Li, Y.; Wang, D. Close Association of Intestinal Autofluorescence with the Formation of Severe Oxidative Damage in Intestine of Nematodes Chronically Exposed to Al₂O₃-Nanoparticle. *Environ. Toxicol. Pharmacol.* **2011**, *32* (2), 233–241.
- (104) Piechulek, A.; von Mikecz, A. Life Span-Resolved Nanotoxicology Enables Identification of Age-Associated Neuromuscular Vulnerabilities in the Nematode *Caenorhabditis Elegans*. *Environ. Pollut.* **2018**, *233*, 1095–1103.
- (105) Ellegaard-Jensen L, Jensen K A, J. A. Nano-Silver Induces Dose-Response Effects on the Nematode *Caenorhabditis Elegans*. *Ecotoxicol. Environ. Saf.* **2012**, *80*, 216–223.
- (106) Yang, X.; Gondikas, A. P.; Marinakos, S. M.; Auffan, M.; Liu, J.; Hsu-Kim, H.; Meyer, J. N. Mechanism of Silver Nanoparticle Toxicity Is Dependent on Dissolved Silver and Surface Coating in *Caenorhabditis Elegans*. *Environ. Sci. Technol.* **2012**, *46* (2), 1119–1127.
- (107) Wang, H.; Wick, R. L.; Xing, B. Toxicity of Nanoparticulate and Bulk ZnO, Al₂O₃ and TiO₂ to the Nematode *Caenorhabditis Elegans*. *Environ. Pollut.* **2009**, *157* (4), 1171–1177.
- (108) Brinke, M.; Heininger, P.; Traunspurger, W. A Semi-Fluid Gellan Gum Medium Improves Nematode Toxicity Testing. *Ecotoxicol. Environ. Saf.* **2011**, *74* (7), 1824–1831.
- (109) Luo, X.; Xu, S.; Yang, Y.; Zhang, Y.; Wang, S.; Chen, S.; Xu, A.; Wu, L. A Novel Method for Assessing the Toxicity of Silver Nanoparticles in *Caenorhabditis Elegans*. *Chemosphere* **2017**, *168*, 648–657.
- (110) Williams, L.; Dusenbery, D. B. AQUATIC TOXICITY TESTING USING THE NEMATODE, CAENORHABDITIS ELEGANS. *Environ. Toxicol. Chem.* **1990**, *9*, 1285–1290.
- (111) Yang X, Jiang C, Hsu-Kim H, et al. Silver Nanoparticle Behavior, Uptake, and Toxicity in *Caenorhabditis Elegans*: Effects of Natural Organic Matter. *Environ. Sci. Technol.* **2014**, *48* (6), 3486–3495.
- (112) Starnes, D. L.; Unrine, J. M.; Starnes, C. P.; Collin, B. E.; Oostveen, E. K.; Ma, R.; Lowry, G. V.; Bertsch, P. M.; Tsyusko, O. V. Impact of Sulfidation on the Bioavailability and Toxicity of Silver Nanoparticles to *Caenorhabditis Elegans*. *Environ. Pollut.* **2015**, *196*, 239–246.
- (113) Collin B, Tsyusko O V, Starnes D L, et al. Effect of Natural Organic Matter on Dissolution and Toxicity of Sulfidized Silver Nanoparticles to *Caenorhabditis Elegans*. *Environ. Sci. Nano* **2016**, *3* (4), 728–736.
- (114) Carolin L. Schultz, Elma Lahive, Alan Lawlor, Alison Crossley, Victor Puntès, Jason M. Unrine, Claus Svendsen, and D. J. S. Influence of Soil Porewater Properties on the Fate And Toxicity of Silver Nanoparticles to *Caenorhabditis Elegans*. *Environ. Toxicol.* **2018**, *37* (10), 2609–2618.

- (115) Tyne, W.; Lofts, S.; Spurgeon, D. J.; Jurkschat, K.; Svendsen, C. A New Medium for Caenorhabditis Elegans Toxicology and Nanotoxicology Studies Designed to Better Reflect Natural Soil Solution Conditions. *Environ. Toxicol. Chem.* **2013**, *32* (8), 1711–1717.
- (116) Donkin, S. G.; Williams, P. L. Influence of Developmental Stage, Salts and Food Presence on Various End Points Using Caenorhabditis Elegans for Aquatic Toxicity Testing. *Environ. Toxicol. Chem.* **1995**, *14* (12), 2139–2147.
- (117) Luo X, Xu S, Yang Y, et al. Insights into the Ecotoxicity of Silver Nanoparticles Transferred from Escherichia Coli to Caenorhabditis Elegans. *Sci. Rep.* **2016**, *6*, 6465.
- (118) Kleiven, M.; Rossbach, L. M.; Gallego-Urrea, J. A.; Brede, D. A.; Oughton, D. H.; Coutris, C. Characterizing the Behavior, Uptake, and Toxicity of NM300K Silver Nanoparticles in Caenorhabditis Elegans. *Environ. Toxicol. Chem.* **2018**, *37* (7), 1799–1810.
- (119) Yang, Y. F.; Lin, Y. J.; Liao, C. M. Toxicity-Based Toxicokinetic/Toxicodynamic Assessment of Bioaccumulation and Nanotoxicity of Zerovalent Iron Nanoparticles in Caenorhabditis Elegans. *Int. J. Nanomedicine* **2017**, *12*, 4607–4621.
- (120) Handy, R. D.; Cornelis, G.; Fernandes, T.; Tsyusko, O.; Decho, A.; Sabo-Attwood, T.; Metcalfe, C.; Steevens, J. A.; Klaine, S. J.; Koelmans, A. A.; Horne, N. Ecotoxicity Test Methods for Engineered Nanomaterials: Practical Experiences and Recommendations from the Bench. *Environ. Toxicol. Chem.* **2012**, *31* (1), 15–31.
- (121) Scanlan, L. D.; Lund, S. P.; Coskun, S. H.; Hanna, S. K.; Johnson, M. E.; Sims, C. M.; Brignoni, K.; Lapasset, P.; Petersen, E. J.; Elliott, J. T.; Nelson, B. C. Counting Caenorhabditis Elegans: Protocol Optimization and Applications for Population Growth and Toxicity Studies in Liquid Medium. *Sci. Rep.* **2018**, *8* (1), 1–12.
- (122) Hanna, S. K.; Cooksey, G. A.; Dong, S.; Nelson, B. C.; Mao, L.; Elliott, J. T.; Petersen, E. J. Feasibility of Using a Standardized Caenorhabditis Elegans Toxicity Test to Assess Nanomaterial Toxicity. *Environ. Sci. Nano* **2016**, *3* (5), 1080–1089.
- (123) Hanna, S. K.; Montoro Bustos, A. R.; Peterson, A. W.; Reipa, V.; Scanlan, L. D.; Hosbas Coskun, S.; Cho, T. J.; Johnson, M. E.; Hackley, V. A.; Nelson, B. C.; Winchester, M. R.; Elliott, J. T.; Petersen, E. J. Agglomeration of Escherichia Coli with Positively Charged Nanoparticles Can Lead to Artifacts in a Standard Caenorhabditis Elegans Toxicity Assay. *Environ. Sci. Technol.* **2018**, *52* (10), 5968–5978.
- (124) Meyer, J. N.; Lord, C. A.; Yang, X. Y.; Turner, E. A.; Badireddy, A. R.; Marinakos, S. M.; Chilkoti, A.; Wiesner, M. R.; Auffan, M. Intracellular Uptake and Associated Toxicity of Silver Nanoparticles in Caenorhabditis Elegans. *Aquat. Toxicol.* **2010**, *100* (2), 140–150.
- (125) Contreras E Q, Puppala H L, Escalera G, et al. Size-Dependent Impacts of Silver Nanoparticles on the Lifespan, Fertility, Growth, and Locomotion of Caenorhabditis Elegans. *Environ. Toxicol.* **2014**, *33* (12), 2716–2723.
- (126) Ahn J M, Eom H J, Yang X, et al. Comparative Toxicity of Silver Nanoparticles on Oxidative Stress and DNA Damage in the Nematode, Caenorhabditis Elegans. *Chemosphere* **2014**, *108*, 343–352.
- (127) Hu C C, Wu G H, Lai S F, et al. Toxic Effects of Size-Tunable Gold Nanoparticles on Caenorhabditis Elegans Development and Gene Regulation. *Sci. Rep.* **2018**, *8* (1), 1–10.
- (128) Roh, J. Y.; Park, Y. K.; Park, K.; Choi, J. Ecotoxicological Investigation of CeO₂ and TiO₂ Nanoparticles on the Soil Nematode Caenorhabditis Elegans Using Gene Expression, Growth, Fertility, and Survival as Endpoints. *Environ. Toxicol. Pharmacol.* **2010**, *29* (2), 167–172.
- (129) Arnold, M. C.; Badireddy, A. R.; Wiesner, M. R.; Giulio, R. T. Di; Meyer, J. N. Cerium Oxide Nanoparticles Are More Toxic than Equimolar Bulk Cerium Oxide in Caenorhabditis Elegans. *Arch. Env. Contam Toxicol.* **2013**, *65* (2), 224–233.
- (130) Li, Y. Y.; Wang, W.; Wu, Q.; Li, Y. Y.; Tang, M.; Ye, B.; Wang, D. Molecular Control of TiO₂-NPs Toxicity Formation at Predicted Environmental Relevant Concentrations by Mn-SODs Proteins. *PLoS One* **2012**, *7* (9), 1–12.
- (131) Ratnasekhar, C.; Sonane, M.; Satish, A.; Krishna, M.; Mudiam, R. Metabolomics Reveals the Perturbations in the Metabolome of Caenorhabditis Elegans Exposed to Titanium Dioxide Nanoparticles. *Nanotoxicology* **2015**, *9* (8), 994–1004.
- (132) Wang, J.; Dai, H.; Nie, Y.; Wang, M.; Yang, Z.; Cheng, L.; Liu, Y.; Chen, S.; Zhao, G.; Wu, L.; Guang, S.; Xu, A. TiO₂ Nanoparticles Enhance Bioaccumulation and Toxicity of Heavy Metals in Caenorhabditis

- Elegans via Modification of Local Concentrations during the Sedimentation Process. *Ecotoxicol. Environ. Saf.* **2018**, *162*, 160–169.
- (133) Khare, P.; Sonane, M.; Nagar, Y.; Moin, N.; Ali, S.; Gupta, K. C. Size Dependent Toxicity of Zinc Oxide Nano-Particles in Soil Nematode *Caenorhabditis Elegans*. *Nanotoxicology* **2015**, *9* (4), 423–432.
- (134) Gupta, S.; Kushwah, T.; Vishwakarma, A.; Yadav, S. Optimization of ZnO-NPs to Investigate Their Safe Application by Assessing Their Effect on Soil Nematode *Caenorhabditis Elegans*. *Nanoscale Res. Lett.* **2015**, *10* (1), 303.
- (135) Kong L, Gao X, Zhu J, et al. Reproductive Toxicity Induced by Nickel Nanoparticles in *Caenorhabditis Elegans*. *Environ. Toxicol.* **2017**, *32* (5), 1530–1538.
- (136) Höss, S.; Fritzsche, A.; Meyer, C.; Bosch, J.; Meckenstock, R. U.; Totsche, K. U. Size- and Composition-Dependent Toxicity of Synthetic and Soil-Derived Fe Oxide Colloids for the Nematode *Caenorhabditis Elegans*. *Environ. Sci. Technol.* **2015**, *49* (1), 544–552.
- (137) Schultz, C. L.; Lahive, E.; Lawlor, A.; Crossley, A.; Puentes, V.; Unrine, J. M.; Svendsen, C.; Spurgeon, D. J. Influence of Soil Porewater Properties on the Fate and Toxicity of Silver Nanoparticles to *Caenorhabditis Elegans*. *Environ. Toxicol. Chem.* **2018**, *37* (10), 2609–2618.
- (138) Levard, C.; Hotze, E. M.; Colman, B.; Dale, A. L.; Yang, X.; Bone, A.; Brown, G. E.; Tanguay, R. L.; Richard, T.; Giulio, D.; Bernhardt, E.; Meyer, J.; Wiesner, M. R.; Lowry, G. V. Sulfidation of Silver Nanoparticles : Natural Antidote to Their Toxicity Sulfidation of Silver Nanoparticles : Natural Antidote to Their Toxicity. *ENVIRO* **2013**.
- (139) Starnes, D. L.; Lichtenberg, S. S.; Unrine, J. M.; Starnes, C. P.; Oostveen, E. K.; Lowry, G. V.; Bertsch, P. M.; Tsyusko, O. V. Distinct Transcriptomic Responses of *Caenorhabditis Elegans* to Pristine and Sulfidized Silver Nanoparticles. *Environ. Pollut.* **2016**, *213*, 314–321.
- (140) Yu S M, Gonzalez-Moragas L, Milla M, et al. Bio-Identity and Fate of Albumin-Coated SPIONs Evaluated in Cells and by the *C. elegans* Model. *Acta Biomater.* **2016**, *43*, 348–357.
- (141) Kim, J.; Shirasawa, T.; Miyamoto, Y. The Effect of TAT Conjugated Platinum Nanoparticles on Lifespan in a Nematode *Caenorhabditis Elegans* Model. *Biomaterials* **2010**, *31* (22), 5849–5854.
- (142) Arndt D A, Oostveen E K, Triplett J, et al. The Role of Charge in the Toxicity of Polymer-Coated Cerium Oxide Nanomaterials to *Caenorhabditis Elegans*. *Comp. Biochem. Physiol. Part C Toxicol. Pharmacol.* **2017**, *201*, 1–10.
- (143) Maurer L L, Yang X, Schindler A J, et al. Intracellular Trafficking Pathways in Silver Nanoparticle Uptake and Toxicity in *Caenorhabditis Elegans*. *Nanotoxicology* **2016**, *10* (7), 831–835.
- (144) O'Donnell B, Huo L, Polli J R, et al. From the Cover: ZnO Nanoparticles Enhanced Germ Cell Apoptosis in *Caenorhabditis Elegans*, in Comparison with ZnCl₂. *Toxicol. Sci.* **2017**, *156* (2), 336–343.
- (145) Ma H, Bertsch P M, Glenn T C, et al. Toxicity of Manufactured Zinc Oxide Nanoparticles in the Nematode *Caenorhabditis Elegans*. *Environ. Toxicol. Chem.* **2009**, *28* (6), 1324–1330.
- (146) Nie, Y.; Wang, J.; Dai, H.; Wang, J.; Wang, M.; Cheng, L.; Yang, Z.; Chen, S.; Zhao, G.; Wu, L.; Xu, A. UV-Induced over Time Transformation of AgNPs in Commercial Wound Dressings and Adverse Biological Effects on *Caenorhabditis Elegans*. *NanoImpact* **2020**, *17*, 100193.
- (147) Ma, H.; Kabengi, N. J.; Bertsch, P. M.; Unrine, J. M.; Glenn, T. C.; Williams, P. L. Comparative Phototoxicity of Nanoparticulate and Bulk ZnO to a Free-Living Nematode *Caenorhabditis Elegans*: The Importance of Illumination Mode and Primary Particle Size. *Environ. Pollut.* **2011**, *159* (6), 1473–1480.
- (148) Angelstorf, J. S.; Ahlf, W.; von der Kammer, F.; Heise, S. Impact of Particle Size and Light Exposure on the Effects of TiO₂ Nanoparticles on *Caenorhabditis Elegans*. *Environ. Toxicol. Chem.* **2014**, *33* (10), 2288–2296.
- (149) Foster S R, Galanzha E I, Totten D C, et al. Photoacoustically-Guided Photothermal Killing of Mosquitoes Targeted by Nanoparticles. *J. Biophotonics* **2014**, *7* (7), 465–473.
- (150) Fang-yen, C.; Avery, L.; Samuel, A. D. T. Two Size-Selective Mechanisms Specifically Trap Bacteria-Sized Food Particles in *Caenorhabditis Elegans*. *Proc. Natl. Acad. Sci. U. S. A.* **2009**, *106* (47), 1–4.
- (151) Nika, L.; Gibson, T.; Konkus, R.; Karp, X. Fluorescent Beads Are a Versatile Tool for Staging *Caenorhabditis Elegans* in Different Life Histories. *G3 Genes, Genomes, Genet.* **2016**, *6* (7), 1923–1933.
- (152) Gao, Y.; Liu, N.; Chen, C.; Luo, Y.; Li, Y.; Zhang, Z.; Zhao, Y. Mapping Technique for Biodistribution of

- Elements in a Model Organism, *Caenorhabditis Elegans*, after Exposure to Copper Nanoparticles with Microbeam Synchrotron Radiation X-Ray Fluorescence. *Anal. At. Spectrom.* **2008**, *23* (8), 1121–1124.
- (153) Iannarelli L, Giovannozzi A M, Morelli F, et al. Shape Engineered TiO₂ Nanoparticles in *Caenorhabditis Elegans*: A Raman Imaging Based Approach to Assist Tissue-Specific Toxicological Studies. *RSC Adv.* **2016**, *6* (74), 70501–70509.
- (154) Kim S W, Nam S H, A. Y. J. Interaction of Silver Nanoparticles with Biological Surfaces of *Caenorhabditis Elegans*. *Ecotoxicol. Environ. Saf.* **2012**, *77*, 64–70.
- (155) Pluskota A, Horzowski E, Bossinger O, et al. In *Caenorhabditis Elegans* Nanoparticle-Bio-Interactions Become Transparent: Silica-Nanoparticles Induce Reproductive Senescence. *PLoS One* **2009**, *4* (8).
- (156) Scharf A, Piechulek A, von M. A. Effect of Nanoparticles on the Biochemical and Behavioral Aging Phenotype of the Nematode *Caenorhabditis Elegans*. *ACS Nano* **2013**, *7* (12), 10695–10703.
- (157) Johnson M E, Hanna S K, Montoro Bustos A R, et al. Separation, Sizing, and Quantitation of Engineered Nanoparticles in an Organism Model Using Inductively Coupled Plasma Mass Spectrometry and Image Analysis. *ACS Nano* **2017**, *11* (1), 526–540.
- (158) Gonzalez-Moragas L, Berto P, Vilches C, et al. In Vivo Testing of Gold Nanoparticles Using the *Caenorhabditis Elegans* Model Organism. *Acta Biomater.* **2017**, *53*, 598–609.
- (159) Gonzalez-Moragas L, Yu S M, Benseny-Cases N, et al. Toxicogenomics of Iron Oxide Nanoparticles in the Nematode *C. elegans*. *Nanotoxicology* **2017**, *11* (5), 647–657.
- (160) Le Trequesser Q, Saez G, Devès G, et al. In Situ Titanium Dioxide Nanoparticles Quantitative Microscopy in Cells and in *C. elegans* Using Nuclear Microprobe Analysis. *Nucl. Inst. Methods Phys. Res. B* **2014**, *341*, 58–64.
- (161) Yu, Z. Y.; Zhang, J.; Yin, D. Q. Toxic and Recovery Effects of Copper on *Caenorhabditis Elegans* by Various Food-Borne and Water-Borne Pathways. *Chemosphere* **2012**, *87* (11), 1361–1367.
- (162) Offermann, K.; Matthäi, A.; Ahlf, W. Assessing the Importance of Dietborne Cadmium and Particle Characteristics on Bioavailability and Bioaccumulation in the Nematode *Caenorhabditis Elegans*. *Environ. Toxicol. Chem.* **2009**, *28* (6), 1149–1158.
- (163) Zhou, J. C.; Yang, Z. L.; Dong, W.; Tang, R. J.; Sun, L. D.; Yan, C. H. Bioimaging and Toxicity Assessments of Near-Infrared Upconversion Luminescent NaYF₄:Yb, Tm Nanocrystals. *Biomaterials* **2011**, *32* (34), 9059–9067.
- (164) Mohan, N.; Chen, C. S.; Hsieh, H. H.; Wu, Y. C.; Chang, H. C. In Vivo Imaging and Toxicity Assessments of Fluorescent Nanodiamonds in *Caenorhabditis Elegans*. *Nano Lett.* **2010**, *10* (9), 3692–3699.
- (165) Schultz, C. L.; Wamucho, A.; Tsyusko, O. V.; Unrine, J. M.; Crossley, A.; Svendsen, C.; Spurgeon, D. J. Multigenerational Exposure to Silver Ions and Silver Nanoparticles Reveals Heightened Sensitivity and Epigenetic Memory in *Caenorhabditis Elegans*. *Proc. R. Soc. B Biol. Sci.* **2016**, *283* (1832).
- (166) Kim S W, Kwak J I, A. Y. J. Multigenerational Study of Gold Nanoparticles in *Caenorhabditis Elegans*: Transgenerational Effect of Maternal Exposure. *Environ. Sci. Technol.* **2013**, *47* (10), 5393–5399.
- (167) Moon, J.; Kwak, J. I.; Kim, S. W.; An, Y. J. Multigenerational Effects of Gold Nanoparticles in *Caenorhabditis Elegans*: Continuous versus Intermittent Exposures. *Environ. Pollut.* **2017**, *220*, 46–52.
- (168) Fay, D. S. A Biologist's Guide to Statistical Thinking and Analysis. *WormBook* **2013**, 1–54.
- (169) Soria C, Coccini T, De Simone U, et al. Enhanced Toxicity of Silver Nanoparticles in Transgenic *Caenorhabditis Elegans* Expressing Amyloidogenic Proteins. *J. Protein Fold. Disord.* **2015**, *22* (4), 221–228.
- (170) Kim J, Takahashi M, Shimizu T, et al. Effects of a Potent Antioxidant, Platinum Nanoparticle, on the Lifespan of *Caenorhabditis Elegans*. *Mech. Ageing Dev.* **2008**, *129* (6), 322–331.
- (171) Kumar, S., Singh, R. K., Aman, A. K., Kumar, J., & Kar, M. Evaluation of Iron Oxide Nanoparticles (NPs) on Aging and Age Related Metabolism and Physiological Changes in *C. elegans*. *Int. J. Pharm. Sci. Res.* **2017**, *8*, 1000–1004.
- (172) Wu Q, Nouara A, Li Y, et al. Comparison of Toxicities from Three Metal Oxide Nanoparticles at Environmental Relevant Concentrations in Nematode *Caenorhabditis Elegans*. *Chemosphere* **2013**, *90* (3), 1123–1131.
- (173) Zhang H, He X, Zhang Z, et al. Nano-CeO₂ Exhibits Adverse Effects at Environmental Relevant

- Concentrations. *Environ. Sci. Technol.* **2011**, *45* (8), 3725–3730.
- (174) Negi, H.; Saikia, S. K.; Kanaujia, R.; Jaiswal, S.; Pandey, R. 3 β -Hydroxy-Urs-12-En-28-Oic Acid Confers Protection against ZnONPs Induced Adversity in *Caenorhabditis Elegans*. *Environ. Toxicol. Pharmacol.* **2017**, *53* (November 2016), 105–110.
- (175) Rui, Q.; Zhao, Y.; Wu, Q.; Tang, M.; Wang, D. Biosafety Assessment of Titanium Dioxide Nanoparticles in Acutely Exposed Nematode *Caenorhabditis Elegans* with Mutations of Genes Required for Oxidative Stress or Stress Response. *Chemosphere* **2013**, *93* (10), 2289–2296.
- (176) Li, Y.; Yu, S.; Wu, Q.; Tang, M.; Pu, Y.; Wang, D. Chronic Al₂O₃-Nanoparticle Exposure Causes Neurotoxic Effects on Locomotion Behaviors by Inducing Severe ROS Production and Disruption of ROS Defense Mechanisms in Nematode *Caenorhabditis Elegans*. *J. Hazard. Mater.* **2012**, *219*, 221–230.
- (177) Wu, Q.; Zhao, Y.; Li, Y.; Wang, D. Susceptible Genes Regulate the Adverse Effects of TiO₂-NPs at Predicted Environmental Relevant Concentrations on Nematode. *Nanomedicine Nanotechnology, Biol. Med.* **2014**, *10* (6), 1263–1271.
- (178) Roh J, Sim S J, Yi J, et al. Ecotoxicity of Silver Nanoparticles on the Soil Nematode *Caenorhabditis Elegans* Using Functional Ecotoxicogenomics. *Environ. Sci. Technol.* **2009**, *43* (10), 3933–3940.
- (179) Hu, C.; Hou, J.; Zhu, Y.; Lin, D. Multigenerational Exposure to TiO₂ Nanoparticles in Soil Stimulates Stress Resistance and Longevity of Survived *C. elegans* via Activating Insulin/IGF-like Signaling. *Environ. Pollut.* **2020**, *263*, 114376.
- (180) Lim, D.; Roh, J. Y.; Eom, H. J.; Choi, J. J. Y.; Hyun, J.; Choi, J. J. Y.; Lim D, Roh J, Eom H, et al. Oxidative Stress-Related PMK-1 P38 MAPK Activation as a Mechanism for Toxicity of Silver Nanoparticles to Reproduction in the Nematode *Caenorhabditis Elegans*. *Environ. Toxicol. Chem.* **2012**, *31* (3), 585–592.
- (181) Roh, J.; Eom, H.; Choi, J. Involvement of *Caenorhabditis Elegans* MAPK Signaling Pathways in Oxidative Stress Response Induced by Silver Nanoparticles Exposure. *Toxicol. Res.* **2012**, *28* (1), 19–24.
- (182) Chatterjee, N.; Eom, H. J.; Choi, J. Effects of Silver Nanoparticles on Oxidative DNA Damage-Repair as a Function of P38 MAPK Status: A Comparative Approach Using Human Jurkat T Cells. *Environ. Mol. Mutagen.* **2014**, *55* (2), 122–133.
- (183) Kim H, Jeong J, Chatterjee N, et al. JAKSTAT and TGF- β Activation as Potential Adverse Outcome Pathway of TiO₂ NPs Phototoxicity in *Caenorhabditis Elegans*. *Sci. Rep.* **2017**, *7* (7), 1–12.
- (184) Li, S. W.; Huang, C. W.; Liao, V. H. C. Early-Life Long-Term Exposure to ZnO Nanoparticles Suppresses Innate Immunity Regulated by SKN-1/Nrf and the P38 MAPK Signaling Pathway in *Caenorhabditis Elegans*. *Environ. Pollut.* **2020**, *256*, 113382.
- (185) Tsyusko, O. V.; Unrine, J. M.; Spurgeon, D.; Blalock, E.; Starnes, D.; Tseng, M.; Joice, G.; Bertsch, P. M. Toxicogenomic Responses of the Model Organism *Caenorhabditis Elegans* to Gold Nanoparticles. *Environ. Sci. Technol.* **2012**, *46* (7), 4115–4124.
- (186) Crone B, Aschner M, Schwerdtle T, et al. Elemental Bioimaging of Cisplatin in *Caenorhabditis Elegans* by LA-ICP-MS. *Metallomics* **2015**, *7* (7), 1189–1195.
- (187) Brinkhaus, S. G.; Bornhorst, J.; Chakraborty, S.; Wehe, C. A.; Niehaus, R.; Reifschneider, O. Elemental Bioimaging of Manganese Uptake in *C. elegans*. *Metallomics* **2014**, *6* (3), 617–621.
- (188) Wang J, Nie Y, Dai H, et al. Parental Exposure to TiO₂ NPs Promotes the Multigenerational Reproductive Toxicity of Cd in *Caenorhabditis Elegans* via Bioaccumulation of Cd in Germ Cells. *Environ. Sci. Nano* **2019**, *6* (5), 1332–1342.
- (189) Michelet, C.; Barberet, P.; Devès, G.; Bouguelmouna, B.; Bourret, S.; Delville, M. Quantitative Reconstruction of PIXE-Tomography Data for Thin Samples Using GUPIX X-Ray Emission Yields. *Nucl. Instruments Methods Phys. Res. Sect. B Beam Interact. with Mater. Atoms* **2015**, *348*, 92–99.
- (190) Polak N, Read D S, Jurkschat K, et al. Metalloproteins and Phytochelatin Synthase May Confer Protection against Zinc Oxide Nanoparticle Induced Toxicity in *Caenorhabditis Elegans*. *Comparative Biochem. Physiol. Part C Toxicol. Pharmacol.* **2014**, *160* (1), 75–85.
- (191) James S A, de Jonge M D, Howard D L, et al. Direct in Vivo Imaging of Essential Bioinorganics in *Caenorhabditis Elegans*. *Metallomics* **2013**, *5* (6), 627–635.
- (192) James S A, Roberts B R, Hare D J, et al. Direct in Vivo Imaging of Ferrous Iron Dyshomeostasis in

- Ageing *Caenorhabditis Elegans*. *Chem. Sci.* **2015**, *6* (5), 2952–2962.
- (193) Hare D J, Jones M W M, Wimmer V C, et al. High-Resolution Complementary Chemical Imaging of Bio-Elements in *Caenorhabditis Elegans*. *Metallomics* **2016**, *8* (2), 156–160.
- (194) James, S. A.; Hare, D. J.; Jenkins, N. L.; Jonge, M. D. De; Bush, A. I.; Mccoll, G. ΦXANES: In Vivo Imaging of Metal-Protein Coordination Environments. *Sci. Rep.* **2016**, *6*, 20350.
- (195) Ganio K, James S A, Hare D J, et al. Accurate Biometal Quantification per Individual *Caenorhabditis Elegans*. *Analyst* **2016**, *141* (4), 1434–1439.
- (196) Jones, M. W. M.; Phillips, N. W.; Abbey, B.; Hare, D. J.; Riessen, G. A. Van; Vine, D. J. Simultaneous Nanostructure and Chemical Imaging of Intact Whole Nematodes. *Chem. Commun.* **2019**, *55* (8), 1052–1055.
- (197) Essig, Y. J.; Webb, S. M.; Stürzenbaum, S. R. Deletion of Phytochelatin Synthase Modulates the Metal Accumulation Pattern of Cadmium Exposed *C. elegans*. *Int. J. Mol. Sci.* **2016**, *17* (2), 257.
- (198) Zhang, H.; He, X.; Bai, W.; Guo, X.; Zhang, Z. Ecotoxicological Assessment of Lanthanum with *Caenorhabditis Elegans* in Liquid Medium. *Metallomics* **2010**, *2* (12), 806–810.
- (199) Cagno, S.; Brede, D. A.; Nuyts, G.; Vanmeert, F.; Pacureanu, A.; Tucoulou, R.; Cloetens, P.; Falkenberg, G.; Janssens, K.; Salbu, B.; Lind, O. C. Combined Computed Nanotomography and Nanoscopic X-Ray Fluorescence Imaging of Cobalt Nanoparticles in *Caenorhabditis Elegans*. *Anal. Chem.* **2017**, *89* (21), 11435–11442.
- (200) Bouyanfif A, Liyanage S, Hewitt J E, et al. FTIR Imaging Detects Diet and Genotype-Dependent Chemical Composition Changes in Wild Type and Mutant *C. elegans* Strains. *Analyst* **2017**, *142* (24), 4727–4736.
- (201) Bouyanfif A, Liyanage S, Hequet E, et al. FTIR Microspectroscopy Reveals Fatty Acid-Induced Biochemical Changes in *C. elegans*. *Vib. Spectrosc.* **2019**, *102*, 8–15.
- (202) Sheng, M.; Gorzsás, A.; Tuck, S. Fourier Transform Infrared Microspectroscopy for the Analysis of the Biochemical Composition of *C. elegans* Worms. *Worm. Taylor Fr.* **2016**, *5* (1), e1132978.
- (203) K, T. The Biological Effects of Engineered Nanomaterials on Soil Organisms: Surface Coating and Age Matter, 2018.
- (204) Maurer, L. L.; Ryde, I. T.; Yang, X.; Meyer, J. N. *Caenorhabditis Elegans* as a Model for Toxic Effects of Nanoparticles: Lethality, Growth, and Reproduction. *Curr. Protoc. Toxicol.* **2015**, *66* (1), 20–10.
- (205) Altun, Z.F. and Hall, D. H. Introduction to *C. elegans* Anatomy. In *In WormAtlas*; 2009; p Introduction.
- (206) Solis, G. M.; Petrascheck, M. Measuring *Caenorhabditis Elegans* Life Span in 96 Well Microtiter Plates. *J. Vis. Exp.* **2011**, No. 49, 1–6.
- (207) Kim, Y. Il; Cho, J. H.; Yoo, O. J.; Ahnn, J. Transcriptional Regulation and Life-Span Modulation of Cytosolic Aconitase and Ferritin Genes in *C. elegans*. *J. Mol. Biol.* **2004**, *342* (2), 421–433.
- (208) Valentini, S.; Cabreiro, F.; Ackerman, D.; Alam, M. M.; Kunze, M. B. A.; Kay, C. W. M.; Gems, D. Manipulation of in Vivo Iron Levels Can Alter Resistance to Oxidative Stress without Affecting Ageing in the Nematode *C. elegans*. *Mech. Ageing Dev.* **2012**, *133* (5), 282–290.
- (209) Escorcia W, Ruter D L, Nhan J, et al. Quantification of Lipid Abundance and Evaluation of Lipid Distribution in *Caenorhabditis Elegans* by Nile Red and Oil Red O Staining. *J. Vis. Exp.* **2018**, *133*, e57352.
- (210) Zhao, Y.; Yu, X.; Jia, R.; Yang, R.; Rui, Q.; Wang, D. Lactic Acid Bacteria Protects *Caenorhabditis Elegans* from Toxicity of Graphene Oxide by Maintaining Normal Intestinal Permeability under Different Genetic Backgrounds. *Sci. Rep.* **2015**, *5*, 17233.
- (211) Wang, H.; Jiang, X.; Wu, J.; Zhang, L.; Huang, J.; Zhang, Y.; Zou, X.; Liang, B. Iron Overload Coordinately Promotes Ferritin Expression and Fat Accumulation in *Caenorhabditis Elegans*. *Genetics* **2016**, *203* (1), 241–253.
- (212) Deutsch, M. J.; Schriever, S. C.; Roscher, A. A.; Ensenuer, R. Digital Image Analysis Approach for Lipid Droplet Size Quantitation of Oil Red O-Stained Cultured Cells. *Anal. Biochem.* **2014**, *445* (1), 87–89.
- (213) O'Rourke E J, Soukas A A, Carr C E, et al. *C. elegans* Major Fats Are Stored in Vesicles Distinct from Lysosome-Related Organelles. *Cell Metab.* **2009**, *10* (5), 430–435.
- (214) Huang, C. W.; Li, S. W.; Hsiu-Chuan Liao, V. Chronic ZnO-NPs Exposure at Environmentally Relevant Concentrations Results in Metabolic and Locomotive Toxicities in *Caenorhabditis Elegans*. *Environ.*

- Pollut.* **2017**, *220*, 1456–1464.
- (215) Hukema, R. K.; Rademakers, S.; Jansen, G. Gustatory Plasticity in *C. elegans* Involves Integration of Negative Cues and NaCl Taste Mediated by Serotonin, Dopamine, and Glutamate. *Learn. Mem.* **2008**, *15* (11), 829–836.
- (216) Wu, T.; He, K.; Zhan, Q.; Ang, S.; Ying, J.; Zhang, S.; Zhang, T.; Xue, Y.; Tang, M. MPA-Capped CdTe Quantum Dots Exposure Causes Neurotoxic Effects in Nematode *Caenorhabditis Elegans* by Affecting the Transporters and Receptors of Glutamate, Serotonin and Dopamine at the Genetic Level, or by Increasing ROS, or Both. *Nanoscale* **2015**, *7* (48), 20460–20473.
- (217) Saeki, S.; Yamamoto, M.; Iino, Y. Plasticity of Chemotaxis Revealed by Paired Presentation of a Chemoattractant and Starvation in the Nematode *Caenorhabditis Elegans*. *J. Exp. Biol.* **2001**, *204* (10), 1757–1764.
- (218) Hoss S, Schlottmann K, T. W. Toxicity of Ingested Cadmium to the Nematode *Caenorhabditis Elegans*. *Environ. Sci. Technol.* **2011**, *45* (23), 10219–10225.
- (219) Srinivasan, S. Regulation of Body Fat in *Caenorhabditis Elegans*. *Annu. Rev. Physiol.* **2015**, *77* (1), 161–178.
- (220) Pascolo, L.; Bortot, B.; Benseny-Cases, N.; Gianoncelli, A.; Tosi, G.; Ruozi, B.; Rizzardi, C.; De Martino, E.; Vandelli, M. A.; Severini, G. M. Detection of PLGA-Based Nanoparticles at a Single-Cell Level by Synchrotron Radiation FTIR Spectromicroscopy and Correlation with X-Ray Fluorescence Microscopy. *Int. J. Nanomedicine* **2014**, *9* (1), 2791–2801.
- (221) Maglioni S, Schiavi A, Melcher M, et al. Lutein Restores Synaptic Functionality in a *C. elegans* Model for Mitochondrial Complex I Deficiency. *bioRxiv*, **2020**.
- (222) Bassan, P.; Kohler, A.; Martens, H.; Lee, J.; Byrne, H. J.; Dumas, P.; Gazi, E.; Brown, M.; Clarke, N.; Gardner, P. Resonant Mie Scattering (RMieS) Correction of Infrared Spectra from Highly Scattering Biological Samples. *Analyst* **2010**, *135* (2), 268–277.
- (223) Benseny-cases, N.; Álvarez-marimon, E.; Castillo-michel, H.; Cotte, M. Synchrotron-Based Fourier Transform Infrared Microspectroscopy (MFTIR) Study on the Effect of Alzheimer’s A β Amorphous and Fibrillar Aggregates on PC12 Cells. *Anal. Chem.* **2018**, *90* (4), 2772–2779.
- (224) Jaque, D.; Martínez Maestro, L.; Del Rosal, B.; Haro-Gonzalez, P.; Benayas, A.; Plaza, J. L.; Martín Rodríguez, E.; García Solé, J. Nanoparticles for Photothermal Therapies. *Nanoscale* **2014**, *6* (16), 9494–9530.
- (225) Wang, C.; Chen, J.; Talavage, T.; Irudayaraj, J. Gold Nanorod/Fe₃O₄ Nanoparticle “Nano-Pearl-Necklaces” for Simultaneous Targeting, Dual-Mode Imaging, and Photothermal Ablation of Cancer Cells. *Angew. Chemie - Int. Ed.* **2009**, *48* (15), 2759–2763.
- (226) Amin P, P. M. Magnetic Nanoparticles-a Promising Tool for Targeted Drug Delivery System. *Asian J. Nanosci. Mater.* **2020**, *3* (1), 24–37.
- (227) M., H. Magnetic Nanoparticles for Nanomedicine. *Magnetochemistry* **2020**, *6* (1), 3.
- (228) Savliwala S, Chiu-Lam A, Unni M, et al. *Nanoparticles for Biomedical Applications.*; Elsevier Inc., 2019.
- (229) Socoliuc, V.; Peddis, D.; Petrenko, V. I.; Avdeev, M. V.; Susan-Resiga, D.; Szabó, T.; Turcu, R.; Tombácz, E.; Vékás, L. Magnetic Nanoparticle Systems for Nanomedicine—A Materials Science Perspective. *Magnetochemistry* **2020**, *6* (1), 2.
- (230) Wang, Y.-X. J. Superparamagnetic Iron Oxide Based MRI Contrast Agents: Current Status of Clinical Application. *Quant. Imaging Med. Surg.* **2011**, *1* (1), 35–40.
- (231) Dulińska-Litewka J, Łazarczyk A, Hałubiec P, et al. Superparamagnetic Iron Oxide Nanoparticles-Current and Prospective Medical Applications. *Materials (Basel)*. **2019**, *12* (4).
- (232) Patil R M, Thorat N D, Shete P B, et al. Comprehensive Cytotoxicity Studies of Superparamagnetic Iron Oxide Nanoparticles. *Biochem. Biophys. Reports* **2018**, *13* (December 2017), 63–72.
- (233) Pietroiusti, A.; Magrini, A.; Campagnolo, L. New Frontiers in Nanotoxicology: Gut Microbiota/Microbiome-Mediated Effects of Engineered Nanomaterials. *Toxicol. Appl. Pharmacol.* **2016**, *299*, 90–95.
- (234) Yamanaka, Y. J.; Leong, K. W. Engineering Strategies to Enhance Nanoparticle-Mediated Oral Delivery. *J. Biomater. Sci. Polym. Ed.* **2008**, *19* (12), 1549–1570.
- (235) Zhao, Y.; Wu, Q.; Li, Y.; Nouara, A.; Jia, R.; Wang, D. In Vivo Translocation and Toxicity of Multi-

- Walled Carbon Nanotubes Are Regulated by MicroRNAs. *Nanoscale* **2014**, *6* (8), 4275–4284.
- (236) Kaletta, T.; Hengartner, M. O. Finding Function in Novel Targets: *C. elegans* as a Model Organism. *Nat. Rev. Drug Discov.* **2006**, *5* (5), 387–399.
- (237) Anderson G L, Boyd W A, W. P. L. Assessment of Sublethal Endpoints for Toxicity Testing With the Nematode *Caenorhabditis Elegans*. *Environ. Toxicol. Chem. An Int. J.* **2001**, *20* (4), 833–838.
- (238) Jiang, Y.; Chen, J.; Wu, Y.; Wang, Q.; Li, H. Sublethal Toxicity Endpoints of Heavy Metals to the Nematode *Caenorhabditis Elegans*. *PLoS One* **2016**, *11* (1), 1–12.
- (239) Ochoa JM, C. M. Investigation of the Toxicity of Amine-Coated, Carboxyl-Coated and Polyaniline-Coated FeO Magnetic Nanoparticles in *Caenorhabditis Elegans*. *J. Biosens. Bioelectron.* **2013**, *04* (05).
- (240) Contreras, E. Q. Investigating the Biological Impacts of Nanoengineered Materials in *Caenorhabditis Elegans* and in Vitro, 2012.
- (241) Anderson, G. L.; Cole, R. D.; Williams, P. L. Assessing Behavioral Toxicity with *Caenorhabditis Elegans*. *Environ. Toxicol. Chem.* **2004**, *23* (5), 1235–1240.
- (242) De Almeida Fagundez, D.; Câmara, D. F.; Salgueiro, W. G.; NoreMBERG, S.; Luiz Puntel, R.; Piccoli, J. E.; Garcia, S. C.; Da Rocha, J. B. T.; Aschner, M.; Ávila, D. S. Behavioral and Dopaminergic Damage Induced by Acute Iron Toxicity in *Caenorhabditis Elegans*. *Toxicol. Res. (Camb)*. **2015**, *4* (4), 878–884.
- (243) Lemieux, G. A.; Ashrafi, K. Insights and Challenges in Using *C. elegans* for Investigation of Fat Metabolism. *Crit. Rev. Biochem. Mol. Biol.* **2015**, *50* (1), 69–84.
- (244) Hu, Y. O.; Wang, Y.; Ye, B. P.; Wang, D. Y. Phenotypic and Behavioral Defects Induced by Iron Exposure Can Be Transferred to Progeny in *Caenorhabditis Elegans*. *Biomed. Environ. Sci.* **2008**, *21* (6), 467–473.
- (245) Anderson, C. P.; Leibold, E. A. Mechanisms of Iron Metabolism in *Caenorhabditis Elegans*. *Front. Pharmacol.* **2014**, *5*, 113.
- (246) Yu, Z.; Yin, D.; Hou, M.; Zhang, J. Effects of Food Availability on the Trade-off between Growth and Antioxidant Responses in *Caenorhabditis Elegans* Exposed to Sulfonamide Antibiotics. *Chemosphere* **2018**, *211*, 278–285.
- (247) Tank, E. M. H.; Rodgers, K. E.; Kenyon, C. Spontaneous Age-Related Neurite Branching in *Caenorhabditis Elegans*. *J. Neurosci.* **2011**, *31* (25), 9279–9288.
- (248) Wu, Q.; Yin, L.; Li, X.; Tang, M.; Zhang, T.; Wang, D.; Wu Q, Yin L, Li X, et al. Contributions of Altered Permeability of Intestinal Barrier and Defecation Behavior to Toxicity Formation from Graphene Oxide in Nematode *Caenorhabditis Elegans*. *Nanoscale* **2013**, *5* (20), 9934–9943.
- (249) Dixon, S. J.; Lemberg, K. M.; Lamprecht, M. R.; Skouta, R.; Zaitsev, E. M.; Gleason, C. E.; Patel, D. N.; Bauer, A. J.; Cantley, A. M.; Yang, W. S.; Morrison, B.; Stockwell, B. R. Ferroptosis: An Iron-Dependent Form of Nonapoptotic Cell Death. *Cell* **2012**, *149* (5), 1060–1072.
- (250) Bargmann, C. I.; Horvitz, H. R. Chemosensory Neurons with Overlapping Functions Direct Chemotaxis to Multiple Chemicals in *C. elegans*. *Neuron* **1991**, *7* (5), 729–742.
- (251) Suzuki, H.; Thiele, T. R.; Faumont, S.; Ezcurra, M.; Lockery, S. R.; Schafer, W. R. Functional Asymmetry in *Caenorhabditis Elegans* Taste Neurons and Its Computational Role in Chemotaxis. *Nature* **2008**, *454* (7200), 114–117.
- (252) Yu, Z. Y.; Zhang, J.; Yin, D. Q. Multigenerational Effects of Heavy Metals on Feeding, Growth, Initial Reproduction and Antioxidants in *Caenorhabditis Elegans*. *PLoS One* **2016**, *11* (4), 1–13.
- (253) Wu, Q.; Zhao, Y.; Li, Y.; Wang, D. Molecular Signals Regulating Translocation and Toxicity of Graphene Oxide in the Nematode *Caenorhabditis Elegans*. *Nanoscale* **2014**, *6* (19), 11204–11212.
- (254) Lemieux, G. A.; Ashrafi, K. Investigating Connections between Metabolism, Longevity, and Behavior in *Caenorhabditis Elegans*. *Trends Endocrinol. Metab.* **2016**, *27* (8), 586–596.
- (255) Zhao, Y. L.; Wang, D. Y. Formation and Regulation of Adaptive Response in Nematode *Caenorhabditis Elegans*. *Oxid. Med. Cell. Longev.* **2012**, 2012.
- (256) Wu, Q.; Wang, W.; Li, Y. Y.; Li, Y. Y.; Ye, B.; Tang, M.; Wang, D. Small Sizes of TiO₂-NPs Exhibit Adverse Effects at Predicted Environmental Relevant Concentrations on Nematodes in a Modified Chronic Toxicity Assay System. *J. Hazard. Mater.* **2012**, *243*, 161–168.
- (257) Lemieux, G. A.; Ashrafi, K. Neural Regulatory Pathways of Feeding and Fat in *Caenorhabditis Elegans*. *Annu. Rev. Genet.* **2015**, *49* (1), 413–438.
- (258) Rajan, M.; Anderson, C. P.; Rindler, P. M.; Romney, S. J.; Dos Santos, M. C. F.; Gertz, J.; Leibold, E. A.

- NHR-14 Loss of Function Couples Intestinal Iron Uptake with Innate Immunity in *C. elegans* through PQM-1 Signaling. *Elife* **2019**, *8*.
- (259) Zhao, Y.; Nancy, L. C. Requirements of Non-Haem Iron and Haem Iron in the Nematode *Caenorhabditis Elegans*. *Nematology* **2011**, *13* (7), 853–858.
- (260) Qi, B.; Han, M. Microbial Siderophore Enterobactin Promotes Mitochondrial Iron Uptake and Development of the Host via Interaction with ATP Synthase. *Cell* **2018**, *175* (2), 571-582.e11.
- (261) Lee, K. S.; Iwanir, S.; Kopito, R. B.; Scholz, M.; Calarco, J. A.; Biron, D.; Levine, E. Serotonin-Dependent Kinetics of Feeding Bursts Underlie a Graded Response to Food Availability in *C. elegans*. *Nat. Commun.* **2017**, *8* (1), 1–11.
- (262) Boyd, W. A.; Cole, R. D.; Anderson, G. L.; Williams, P. L. The Effects of Metals and Food Availability on the Behavior of *Caenorhabditis Elegans*. *Environ. Toxicol. Chem.* **2003**, *22* (12), 3049–3055.
- (263) Levy M, Luciani N, Alloyeau D, et al. Long Term in Vivo Biotransformation of Iron Oxide Nanoparticles. *Biomaterials* **2011**, *32* (16), 3988–3999.
- (264) Honda Y, H. S. Oxidative Stress and Life Span Determination in the Nematode *Caenorhabditis Elegans*. *Ann. N. Y. Acad. Sci.* **2002**, *959* (1), 466–474.
- (265) Abdal Dayem A, Hossain M K, Lee S B, et al. The Role of Reactive Oxygen Species (ROS) in the Biological Activities of Metallic Nanoparticles. *Int. J. Mol. Sci.* **2017**, *18* (1), 120.
- (266) Klang, I. M.; Schilling, B.; Sorensen, D. J.; Sahu, A. K.; Kapahi, P.; Andersen, J. K.; Swoboda, P.; Killilea, D. W.; Gibson, B. W.; Lithgow, G. J. Iron Promotes Protein Insolubility and Aging in *C. elegans*. *Aging (Albany, NY)*. **2014**, *6* (11), 975–991.
- (267) Paunovic J, Vucevic D, Radosavljevic T, et al. Iron-Based Nanoparticles and Their Potential Toxicity: Focus on Oxidative Stress and Apoptosis. *Chem. Biol. Interact.* **2020**, *316*, 108935.
- (268) Li, Y.; Li, Y. F.; Zhao, J.; Gao, Y.; Chen, C. Accumulation and Transformation of Nanomaterials in Ecological Model Organisms Investigated by Using Synchrotron Radiation Techniques. *J. Anal. At. Spectrom.* **2015**, *30* (10), 2038–2047.
- (269) Benseny-Cases, N.; Klementieva, O.; Cotte, M.; Ferrer, I.; Cladera, J. Microspectroscopy (MFTIR) Reveals Co-Localization of Lipid Oxidation and Amyloid Plaques in Human Alzheimer Disease Brains. *Anal. Chem.* **2014**, *86* (24), 12047–12054.
- (270) San-Blas, E.; Guerra, M.; Portillo, E.; Esteves, I.; Cubillán, N.; Alvarado, Y. ATR/FTIR Characterization of *Steinernema Glaseri* and *Heterorhabditis Indica*. *Vib. Spectrosc.* **2011**, *57* (2), 220–228.
- (271) Barraza-Garza G, Castillo-Michel H, de la Rosa L A, et al. Infrared Spectroscopy as a Tool to Study the Antioxidant Activity of Polyphenolic Compounds in Isolated Rat Enterocytes. *Oxid. Med. Cell. Longev.* **2016**, 2016.
- (272) Sanchez-Molina, P.; Kreuzer, M.; Benseny-Cases, N.; Valente, T.; Almolda, B.; González, B.; Castellano, B.; Perálvarez-Marín, A. From Mouse to Human: Comparative Analysis between Grey and White Matter by Synchrotron-Fourier Transformed Infrared Microspectroscopy. *Biomolecules* **2020**, *10* (8), 1–14.
- (273) Kregel K C, Z. H. J. An Integrated View of Oxidative Stress in Aging: Basic Mechanisms, Functional Effects, and Pathological Considerations. *Am. J. Physiol. Integr. Comp. Physiol.* **2017**, *292* (1), R18–R36.
- (274) Bouyanfif, A.; Liyanage, S.; Hequet, E.; Moustaid-Moussa, N.; Abidi, N. Fourier Transform Infrared Microspectroscopy Detects Biochemical Changes during *C. elegans* Lifespan. *Vib. Spectrosc.* **2019**, *102*, 71–78.
- (275) Back, P.; Braeckman, B. P.; Matthijssens, F. ROS in Aging *Caenorhabditis Elegans*: Damage or Signaling? *Oxid. Med. Cell. Longev.* **2012**, 2012.
- (276) Honda, Y.; Honda, S. The Daf-2 Gene Network for Longevity Regulates Oxidative Stress Resistance and Mn-superoxide Dismutase Gene Expression in *Caenorhabditis Elegans*. *FASEB J.* **1999**, *13* (11), 1385–1393.
- (277) Zhang, X.; Zhang, H.; Liang, X.; Zhang, J.; Tao, W.; Zhu, X.; Chang, D.; Zeng, X.; Liu, G.; Mei, L. Iron Oxide Nanoparticles Induce Autophagosome Accumulation through Multiple Mechanisms: Lysosome Impairment, Mitochondrial Damage, and ER Stress. *Mol. Pharm.* **2016**, *13* (7), 2578–2587.
- (278) Leinwand, S. G.; Yang, C. J.; Bazopoulou, D.; Chronis, N.; Srinivasan, J.; Chalasani, S. H. Circuit Mechanisms Encoding Odors and Driving Aging-Associated Behavioral Declines in *Caenorhabditis*

- Elegans. Elife* **2015**, *4* (September 2015), 1–26.
- (279) van der Heide, L. P.; Ramakers, G. M. J.; Smidt, M. P. Insulin Signaling in the Central Nervous System: Learning to Survive. *Prog. Neurobiol.* **2006**, *79* (4), 205–221.
- (280) Lee, S. S.; Kennedy, S.; Tolonen, A. C.; Ruvkun, G. DAF-16 Target Genes That Control *C. elegans* Life-Span and Metabolism. *Science* (80-.). **2003**, *300* (5619), 644–647.
- (281) Pathak, K.; Raghuvanshi, S. Oral Bioavailability: Issues and Solutions via Nanoformulations. *Clin. Pharmacokinet.* **2015**, *54* (4), 325–357.
- (282) McClements, D. J. Utilizing Food Effects to Overcome Challenges in Delivery of Lipophilic Bioactives: Structural Design of Medical and Functional Foods. *Expert Opin. Drug Deliv.* **2013**, *10* (12), 1621–1632.
- (283) Chee, C. F.; Leo, B. F.; Lai, C. W. *Superparamagnetic Iron Oxide Nanoparticles for Drug Delivery*; Elsevier Inc., 2018.
- (284) Długosz, O.; Szostak, K.; Staroń, A.; Pulit-Prociak, J.; Banach, M. Methods for Reducing the Toxicity of Metal and Metal Oxide NPs as Biomedicine. *Materials (Basel)*. **2020**, *13* (2).
- (285) Duncan, B.; Kim, C.; Rotello, V. M. Gold Nanoparticle Platforms as Drug and Biomacromolecule Delivery Systems. *J. Control. Release* **2010**, *148* (1), 122–127.
- (286) Hu, M.; Chen, J.; Li, Z. Y.; Au, L.; Hartland, G. V.; Li, X.; Marquez, M.; Xia, Y. Gold Nanostructures: Engineering Their Plasmonic Properties for Biomedical Applications. *Chem. Soc. Rev.* **2006**, *35* (11), 1084–1094.
- (287) Sau, T. K.; Rogach, A. L.; Jäckel, F.; Klar, T. A.; Feldmann, J. Properties and Applications of Colloidal Nonspherical Noble Metal Nanoparticles. *Adv. Mater.* **2010**, *22* (16), 1805–1825.
- (288) Yeh, Y. C.; Creran, B.; Rotello, V. M. Gold Nanoparticles: Preparation, Properties, and Applications in Bionanotechnology. *Nanoscale* **2012**, *4* (6), 1871–1880.
- (289) Nikezić, A. V. V.; Bondžić, A. M.; Vasić, V. M. Drug Delivery Systems Based on Nanoparticles and Related Nanostructures. *Eur. J. Pharm. Sci.* **2020**, *151* (May).
- (290) Elahi, N.; Kamali, M.; Baghersad, M. H. Recent Biomedical Applications of Gold Nanoparticles: A Review. *Talanta* **2018**, *184* (November 2017), 537–556.
- (291) Fratoddi, I.; Venditti, I.; Cametti, C.; Russo, M. V. Gold Nanoparticles and Gold Nanoparticle-Conjugates for Delivery of Therapeutic Molecules. Progress and Challenges. *J. Mater. Chem. B* **2014**, *2* (27), 4204–4220.
- (292) Luther, D. C.; Huang, R.; Jeon, T.; Zhang, X.; Lee, Y.-W.; Nagaraj, H.; Rotello, V. M. Delivery of Drugs, Proteins, and Nucleic Acids Using Inorganic Nanoparticles. *Adv. Drug Deliv. Rev.* **2020**.
- (293) Sztandera, K.; Gorzkiewicz, M.; Klajnert-Maculewicz, B. Gold Nanoparticles in Cancer Treatment. *Mol. Pharm.* **2019**, *16* (1), 1–23.
- (294) Murphy, C. J.; Thompson, L. B.; Alkilany, A. M.; Sisco, P. N.; Boulos, S. P.; Sivapalan, S. T.; Yang, J. A.; Chernak, D. J.; Huang, J. The Many Faces of Gold Nanorods. *J. Phys. Chem. Lett.* **2010**, *1* (19), 2867–2875.
- (295) MubarakAli D, Thajuddin N, Jeganathan K, et al. Plant Extract Mediated Synthesis of Silver and Gold Nanoparticles and Its Antibacterial Activity against Clinically Isolated Pathogens. *Colloids Surfaces B Biointerfaces* **2011**, *85* (2), 360–365.
- (296) Zou L, Wang H, He B, et al. Current Approaches of Photothermal Therapy in Treating Cancer Metastasis with Nanotherapeutics. *Theranostics* **2016**, *6* (6), 62.
- (297) Huang, X.; El-Sayed, I. H.; Qian, W.; El-Sayed, M. A. Cancer Cell Imaging and Photothermal Therapy in the Near-Infrared Region by Using Gold Nanorods. *J. Am. Chem. Soc.* **2006**, *128* (6), 2115–2120.
- (298) Dykman L A, K. N. G. Gold Nanoparticles in Biology and Medicine : Recent Advances and Prospects. *Acta Naturae (англоязычная версия)* **2011**, *3* (9), 34–55.
- (299) Arvizo, R. R.; Bhattacharyya, S.; Kudgus, R. A.; Giri, K.; Bhattacharya, R.; Mukherjee, P. Intrinsic Therapeutic Applications of Noble Metal Nanoparticles: Past, Present and Future. *Chem. Soc. Rev.* **2012**, *41* (7), 2943–2970.
- (300) Li, Y. F.; Chen, C. Fate and Toxicity of Metallic and Metal-Containing Nanoparticles for Biomedical Applications. *Small* **2011**, *7* (21), 2965–2980.
- (301) Bednarski, M.; Dudek, M.; Knutelska, J.; Nowiński, L.; Sapa, J.; Zygmunt, M.; Nowak, G.; Luty-Błocho, M.; Wojnicki, M.; Fitzner, K.; Teşiorowski, M. The Influence of the Route of Administration of Gold

- Nanoparticles on Their Tissue Distribution and Basic Biochemical Parameters: In Vivo Studies. *Pharmacol. Reports* **2015**, *67* (3), 405–409.
- (302) Hillyer, J. F.; Albrecht, R. M. Gastrointestinal Persorption and Tissue Distribution of Differently Sized Colloidal Gold Nanoparticles. *J. Pharm. Sci.* **2001**, *90* (12), 1927–1936.
- (303) Pokharkar, V.; Dhar, S.; Bhumkar, D.; Mali, V.; Bodhankar, S.; Prasad, B. L. V. Acute and Subacute Toxicity Studies of Chitosan Reduced Gold Nanoparticles: A Novel Carrier for Therapeutic Agents. *J. Biomed. Nanotechnol.* **2009**, *5* (3), 233–239.
- (304) Zhang, X. D.; Wu, H. Y.; Wu, D.; Wang, Y. Y.; Chang, J. H.; Zhai, Z. Bin; Meng, A. M.; Liu, P. X.; Zhang, L. A.; Fan, F. Y. Toxicologic Effects of Gold Nanoparticles in Vivo by Different Administration Routes. *Int. J. Nanomedicine* **2010**, *5* (1), 771–781.
- (305) Jo, M. R.; Bae, S. H.; Go, M. R.; Kim, H. J.; Hwang, Y. G.; Choi, S. J. Toxicity and Biokinetics of Colloidal Gold Nanoparticles. *Nanomaterials* **2015**, *5* (2), 835–850.
- (306) Cancino-Bernardi, J.; Marangoni, V. S.; Besson, J. C. F.; Cancino, M. E. C.; Natali, M. R. M.; Zucolotto, V. Gold-Based Nanospheres and Nanorods Particles Used as Theranostic Agents: An in Vitro and in Vivo Toxicology Studies. *Chemosphere* **2018**, *213*, 41–52.
- (307) Zhi, X.; Liu, Y.; Lin, L.; Yang, M.; Zhang, L.; Zhang, L.; Liu, Y.; Alfranca, G.; Ma, L.; Zhang, Q.; Fu, H.; Conde, J.; Ding, X.; Chen, D.; Ni, J.; Song, J.; Cui, D. Oral PH Sensitive GNS@ab Nanoprobes for Targeted Therapy of Helicobacter Pylori without Disturbance Gut Microbiome. *Nanomedicine Nanotechnology, Biol. Med.* **2019**, *20*, 102019.
- (308) Li, J.; Cha, R.; Zhao, X.; Guo, H.; Luo, H.; Wang, M.; Zhou, F.; Jiang, X. Gold Nanoparticles Cure Bacterial Infection with Benefit to Intestinal Microflora. *ACS Nano* **2019**, *13* (5), 5002–5014.
- (309) Cao, Z.; Chen, J.; Tran, J.; Chen, X.; Bacacao, B.; Bekale, L. A.; Santa Maria, P. Antimicrobial Gold Nanoclusters Eradicate Escherichia Coli Biofilms and Are Non-Toxic by Oral Administration. *ACS Appl. Bio Mater.* **2020**.
- (310) Zhu, S.; Jiang, X.; Boudreau, M. D.; Feng, G.; Miao, Y.; Dong, S.; Wu, H.; Zeng, M.; Yin, J. J. Orally Administered Gold Nanoparticles Protect against Colitis by Attenuating Toll-like Receptor 4- and Reactive Oxygen/Nitrogen Species-Mediated Inflammatory Responses but Could Induce Gut Dysbiosis in Mice. *J. Nanobiotechnology* **2018**, *16* (1), 1–18.
- (311) Moros, M.; Gonzalez-Moragas, L.; Tino, A.; Laromaine, A.; Tortiglione, C. *Invertebrate Models for Hyperthermia: What We Learned From Caenorhabditis Elegans and Hydra Vulgaris*; Elsevier Inc., 2019.
- (312) Tejada-Benitez L, O.-V. *Caenorhabditis Elegans, a Biological Model for Research in Toxicology[M]//Reviews of Environmental Contamination and Toxicology Volume 237*; 2016; Vol. 237.
- (313) Yang, S. T.; Liu, Y.; Wang, Y. W.; Cao, A. Biosafety and Bioapplication of Nanomaterials by Designing Protein-Nanoparticle Interactions. *Small* **2013**, *9* (9–10), 1635–1653.
- (314) Butler, H. J.; Ashton, L.; Bird, B.; Cinque, G.; Curtis, K.; Dorney, J.; Esmonde-White, K.; Fullwood, N. J.; Gardner, B.; Martin-Hirsch, P. L.; Walsh, M. J.; McAinsh, M. R.; Stone, N.; Martin, F. L. Using Raman Spectroscopy to Characterize Biological Materials. *Nat. Protoc.* **2016**, *11* (4), 664–687.
- (315) Drescher, D.; Kneipp, J. Nanomaterials in Complex Biological Systems: Insights from Raman Spectroscopy. *Chem. Soc. Rev.* **2012**, *41* (17), 5780–5799.
- (316) Schultz, C.; Powell, K.; Crossley, A.; Jurkschat, K.; Kille, P.; Morgan, A. J.; Read, D.; Tyne, W.; Lahive, E.; Svendsen, C.; Spurgeon, D. J. Analytical Approaches to Support Current Understanding of Exposure, Uptake and Distributions of Engineered Nanoparticles by Aquatic and Terrestrial Organisms. *Ecotoxicology* **2015**, *24* (2), 239–261.
- (317) Charan S, Chien F C, Singh N, et al. Development of Lipid Targeting Raman Probes for in Vivo Imaging of Caenorhabditis Elegans. *Chem. Eur. J.* **2011**, *17* (18), 5165–5170.
- (318) Huang, X.; El-Sayed, M. A. Gold Nanoparticles: Optical Properties and Implementations in Cancer Diagnosis and Photothermal Therapy. *J. Adv. Res.* **2010**, *1* (1), 13–28.
- (319) Huang, X.; Jain, P. K.; El-Sayed, I. H.; El-Sayed, M. A. Plasmonic Photothermal Therapy (PPTT) Using Gold Nanoparticles. *Lasers Med. Sci.* **2008**, *23* (3), 217–228.
- (320) Nam, J.; Won, N.; Jin, H.; Chung, H.; Kim, S. PH-Induced Aggregation of Gold Nanoparticles for Photothermal Cancer Therapy. *J. Am. Chem. Soc.* **2009**, *131* (38), 13639–13645.

- (321) Jain, P. K.; Huang, X.; El-Sayed, I. H.; El-Sayed, M. A. Noble Metals on the Nanoscale: Optical and Photothermal Properties and Some Applications in Imaging, Sensing, Biology, and Medicine. *Acc. Chem. Res.* **2008**, *41* (12), 1578–1586.
- (322) Altunbek, M.; Kuku, G.; Culha, M. Gold Nanoparticles in Single-Cell Analysis for Surface Enhanced Raman Scattering. *Molecules* **2016**, *21* (12), 1–18.
- (323) Ando, J.; Fujita, K.; Smith, N. I.; Kawata, S. Dynamic SERS Imaging of Cellular Transport Pathways with Endocytosed Gold Nanoparticles. *Nano Lett.* **2011**, *11* (12), 5344–5348.
- (324) Qian, X.; Peng, X. H.; Ansari, D. O.; Yin-Goen, Q.; Chen, G. Z.; Shin, D. M.; Yang, L.; Young, A. N.; Wang, M. D.; Nie, S. In Vivo Tumor Targeting and Spectroscopic Detection with Surface-Enhanced Raman Nanoparticle Tags. *Nat. Biotechnol.* **2008**, *26* (1), 83–90.
- (325) Bueno, J.; Lednev, I. K. Raman Microspectroscopic Chemical Mapping and Chemometric Classification for the Identification of Gunshot Residue on Adhesive Tape. *Anal. Bioanal. Chem.* **2014**, *406* (19), 4595–4599.
- (326) Chrimes, A. F.; Khoshmanesh, K.; Stoddart, P. R.; Mitchell, A.; Kalantar-zadeh, K. Microfluidics and Raman Microscopy: Current Applications and Future Challenges. *Chem. Soc. Rev.* **2013**, *42* (13), 5880.
- (327) Romero-Afrima, L.; Zelmanovich, V.; Abergel, Z.; Zuckerman, B.; Shaked, M.; Abergel, R.; Livshits, L.; Smith, Y.; Gross, E. Ferritin Is Regulated by a Neuro-Intestinal Axis in the Nematode *Caenorhabditis Elegans*. *Redox Biol.* **2020**, *28*, 101359.
- (328) Rodriguez, M.; Basten Snoek, L.; De Bono, M.; Kammenga, J. E. Worms under Stress: *C. elegans* Stress Response and Its Relevance to Complex Human Disease and Aging. *Trends Genet.* **2013**, *29* (6), 367–374.
- (329) Quach, T. K.; Chou, H. T.; Wang, K.; Milledge, G. Z.; Johnson, C. M. Genome-Wide Microarray Analysis Reveals Roles for the REF-1 Family Member HLH-29 in Ferritin Synthesis and Peroxide Stress Response. *PLoS One* **2013**, *8* (3).
- (330) Kwong, J. Q.; Beal, M. F.; Manfredi, G. The Role of Mitochondria in Inherited Neurodegenerative Diseases. *J. Neurochem.* **2006**, *97* (6), 1659–1675.
- (331) Monzio Compagnoni, G.; Di Fonzo, A.; Corti, S.; Comi, G. P.; Bresolin, N.; Masliah, E. The Role of Mitochondria in Neurodegenerative Diseases: The Lesson from Alzheimer’s Disease and Parkinson’s Disease. *Mol. Neurobiol.* **2020**, *57* (7), 2959–2980.
- (332) Frambach, S. J. C. M.; van de Wal, M. A. E.; van den Broek, P. H. H.; Smeitink, J. A. M.; Russel, F. G. M.; de Haas, R.; Schirris, T. J. J. Effects of Clofibrate and KH176 on Life Span and Motor Function in Mitochondrial Complex I-Deficient Mice. *Biochim. Biophys. Acta - Mol. Basis Dis.* **2020**, *1866* (6), 165727.
- (333) Koopman W J H, Beyrath J, Fung C W, et al. Mitochondrial Disorders in Children: Toward Development of Small-molecule Treatment Strategies. *EMBO Mol. Med.* **2016**, *8* (4), 311–327.
- (334) Markaki, M.; Tavernarakis, N. Modeling Human Diseases in *Caenorhabditis Elegans*. *Biotechnol. J.* **2010**, *5* (12), 1261–1276.
- (335) O’Reilly L P, Luke C J, Perlmutter D H, et al. *C. elegans* in High-Throughput Drug Discovery. *Adv. Drug Deliv. Rev.* **2014**, No. 69, 247–253.
- (336) Liu, C.; Chang, D.; Zhang, X.; Sui, H.; Kong, Y.; Zhu, R.; Wang, W. Oral Fast-Dissolving Films Containing Lutein Nanocrystals for Improved Bioavailability: Formulation Development, in Vitro and in Vivo Evaluation. *AAPS PharmSciTech* **2017**, *18* (8), 2957–2964.
- (337) Ranganathan, A.; Hindupur, R.; Vallikannan, B.; Ranganathan A, Hindupur R, V. B. Biocompatible Lutein-Polymer-Lipid Nanocapsules: Acute and Subacute Toxicity and Bioavailability in Mice. *Mater. Sci. Eng. C* **2016**, *69*, 1318–1327.
- (338) Liu R, Wang T, Zhang B, et al. Lutein and Zeaxanthin Supplementation and Association with Visual Function in Age-Related Macular Degeneration. *Invest. Ophthalmol. Vis. Sci.* **2015**, *56* (1), 252–258.
- (339) Bhat, I.; Yathisha, U. G.; Karunasagar, I.; Mamatha, B. S. Nutraceutical Approach to Enhance Lutein Bioavailability via Nanodelivery Systems. *Nutr. Rev.* **2020**, *0* (0), 1–16.
- (340) Yoo J, Baskaran R, Y. B. K. Self-Nanoemulsifying Drug Delivery System of Lutein: Physicochemical Properties and Effect on Bioavailability of Warfarin. *Biomol. Ther. (Seoul)*. **2013**, *21* (2), 173–179.
- (341) Sinha, S. Nanoparticles Loaded in Consumable Polymeric Oral Films : A Smart Dosage Form Design

- for Oral Administration. *GSC Biol. Pharm. Sci.* **2020**, *12* (01), 7–14.
- (342) Xue C, Rosen R, Jordan A, et al. Management of Ocular Diseases Using Lutein and Zeaxanthin : What Have We Learned from Experimental Animal Studies? *J. Ophthalmol.* **2015**, *2015*.
- (343) Koushan, K.; Rusovici, R.; Li, W.; Ferguson, L. R.; Chalam, K. V. The Role of Lutein in Eye-Related Disease. *Nutrients* **2013**, *5* (5), 1823–1839.
- (344) Baker, M. J.; Trevisan, J.; Bassan, P.; Bhargava, R.; Butler, H. J.; Dorling, K. M.; Fielden, P. R.; Fogarty, S. W.; Fullwood, N. J.; Heys, K. A.; Hughes, C.; Lasch, P.; Martin-Hirsch, P. L.; Obinaju, B.; Sockalingum, G. D.; Sulé-Suso, J.; Strong, R. J.; Walsh, M. J.; Wood, B. R.; Gardner, P.; Martin, F. L. Using Fourier Transform IR Spectroscopy to Analyze Biological Materials. *Nat. Protoc.* **2014**, *9* (8), 1771–1791.
- (345) Mamarelis, I.; Pissaridi, K.; Dritsa, V.; Kotileas, P.; Tsiligiris, V.; Tzilalis, V.; Anastassopoulou, J. Oxidative Stress and Atherogenesis. An FT-IR Spectroscopic Study. *In Vivo (Brooklyn)*. **2010**, *24* (6), 883–888.
- (346) Petibois, C.; Déléris, G. Chemical Mapping of Tumor Progression by FT-IR Imaging: Towards Molecular Histopathology. *Trends Biotechnol.* **2006**, *24* (10), 455–462.
- (347) Petibois, C.; Drogat, B.; Bikfalvi, A.; Déléris, G.; Moenner, M. Histological Mapping of Biochemical Changes in Solid Tumors by FT-IR Spectral Imaging. *FEBS Lett.* **2007**, *581* (28), 5469–5474.
- (348) Liao, C. R.; Rak, M.; Lund, J.; Unger, M.; Platt, E.; Albensi, B. C.; Hirschmugl, C. J.; Gough, K. M. Synchrotron FTIR Reveals Lipid around and within Amyloid Plaques in Transgenic Mice and Alzheimer's Disease Brain. *Analyst* **2013**, *138* (14), 3991–3997.
- (349) Szczerbawska-Boruchowska, M.; Dumas, P.; Kastyak, M. Z.; Chwiej, J.; Lankosz, M.; Adamek, D.; Krygowska-Wajs, A. Biomolecular Investigation of Human Substantia Nigra in Parkinson's Disease by Synchrotron Radiation Fourier Transform Infrared Microspectroscopy. *Arch. Biochem. Biophys.* **2007**, *459* (2), 241–248.
- (350) Bonda M, Perrin V, Vileno B, et al. Synchrotron Infrared Microspectroscopy Detecting the Evolution of Huntington's Disease Neuropathology and Suggesting Unique Correlates of Dysfunction in White versus Gray Brain Matter. *Anal. Chem.* **2011**, *83* (20), 7712–7720.
- (351) G. Britton, S. L.-J. and H. P. *Carotenoids. Volume 1B: Spectroscopy*; 1995.
- (352) Liu Y, Zhao Y, C. X. Bioengineering of Metal-Organic Frameworks for Nanomedicine. *Theranostics* **2019**, *9* (11), 3122.
- (353) Simon-Yarza, T.; Mielcarek, A.; Couvreur, P.; Serre, C. Nanoparticles of Metal-Organic Frameworks: On the Road to In Vivo Efficacy in Biomedicine. *Adv. Mater.* **2018**, *30* (37), 1–15.
- (354) Rojas, S.; Arenas-Vivo, A.; Horcajada, P. Metal-Organic Frameworks: A Novel Platform for Combined Advanced Therapies. *Coord. Chem. Rev.* **2019**, *388*, 202–226.
- (355) Pandey, Abhijeet, et al.; Pandey, A.; Dhas, N.; Deshmukh, P.; Caro, C.; Patil, P.; Luisa García-Martín, M.; Padya, B.; Nikam, A.; Mehta, T.; Mutalik, S. Heterogeneous Surface Architected Metal-Organic Frameworks for Cancer Therapy, Imaging, and Biosensing: A State-of-the-Art Review. *Coord. Chem. Rev.* **2020**, *409*, 213212.
- (356) Horcajada, P.; Chalati, T.; Serre, C.; Gillet, B.; Sebrie, C.; Baati, T.; Eubank, J. F.; Heurtaux, D.; Clayette, P.; Kreuz, C.; Chang, J. S.; Hwang, Y. K.; Marsaud, V.; Bories, P. N.; Cynober, L.; Gil, S.; Férey, G.; Couvreur, P.; Gref, R. Porous Metal-Organic-Framework Nanoscale Carriers as a Potential Platform for Drug Delivery and Imaging. *Nat. Mater.* **2010**, *9* (2), 172–178.
- (357) Baati, T.; Njim, L.; Neffati, F.; Kerkeni, A.; Bouttemi, M.; Gref, R.; Najjar, M. F.; Zakhama, A.; Couvreur, P.; Serre, C.; Horcajada, P. In Depth Analysis of the in Vivo Toxicity of Nanoparticles of Porous Iron(III) Metal-Organic Frameworks. *Chem. Sci.* **2013**, *4* (4), 1597–1607.
- (358) Dutta, P. K.; Duta, J.; Tripathi, V. S. Chitin and Chitosan: Chemistry, Properties and Applications. *J. Sci. Ind. Res. (India)*. **2004**, *63* (1), 20–31.
- (359) Hidalgo, T.; Giménez-Marqués, M.; Bellido, E.; Avila, J.; Asensio, M. C.; Salles, F.; Lozano, M. V.; Guillevic, M.; Simón-Vázquez, R.; González-Fernández, A.; Serre, C.; Alonso, M. J.; Horcajada, P. Chitosan-Coated Mesoporous MIL-100(Fe) Nanoparticles as Improved Bio-Compatible Oral Nanocarriers. *Sci. Rep.* **2017**, *7* (March), 1–14.
- (360) Rojas, Sara, et al. Metal-Organic Frameworks as Efficient Oral Detoxifying Agents. *J. Am. Chem. Soc.* **2018**, *14* (30), 9581–9586.
- (361) Gonzalez-Moragas, L.; Roig, A.; Laromaine, A. *C. elegans* as a Tool for in Vivo Nanoparticle

- Assessment. *Adv. Colloid Interface Sci.* **2015**, *219*, 10–26.
- (362) X, Y. Mechanisms of Silver Nanoparticle Toxicity in Laboratory Suspensions and Complex Environmental Media in *Caenorhabditis Elegans*, 2014.
- (363) Arya U, Das C K, S. J. R. *Caenorhabditis Elegans* for Preclinical Drug Discovery. *Curr. Sci.* **2010**, 1669–1680.

Curriculum vitae

Zhongrui Luo

Date of birth: 21/04/91

Current Professional address: Group of Nanoparticles and Nanocomposites, ICMAB, Campus UAB, 08193 Bellaterra, Barcelona, Spain.

Contact information: zluo@icmab.es// onewayluo@gmail.com

Education

- PhD in Material Science

Universitat Autònoma de Barcelona, Spain. Oct. 2016-Oct. 2020

Thesis title: “*In vivo* interactions between food availability and nanoparticles in *Caenorhabditis elegans*”

Director: Dr. Anna Laromaine.

- M.Sc. in Applied Chemistry

Yunnan University, China. Sep. 2013-Jul. 2016

Thesis title: “Synthesis of Ce-MIL-101 (Cr, Fe) and their catalysis in cyclohexane oxidation”

Tutor: Dr. Jiaqiang Wang

- B.Sc. in Biological engineering

Nanjing Agricultural University, China. Sep. 2009-Jul. 2013

Publications

- Maglioni, S., Schiavi, A., Melcher, M., Brinkmann, V., **Luo, Z.**, Raimundo, N., A Laromaine., JN Meyer., F Distelmaier., Ventura, N. (2020). Lutein restores synaptic functionality in a *C. elegans* model for mitochondrial complex I deficiency. *bioRxiv*.
- Luo, Z., L Gonzalez-Moragas., M Torras., A Laromaine. Protective role of food availability in *C. elegans* exposed to superparamagnetic iron oxide nanoparticles. *In preparation*.

Attendance of Conferences and Seminars

- VII Spanish Worm Meeting-Oral

“Evaluation of the nano-bio interaction between superparamagnetic iron oxide nanoparticles and *Caenorhabditis elegans*”

Barcelona, Spain. 28th-29th Mar. 2019

- 4th Scientific Meeting of BCN-b Students –Poster

“Evaluation of the nano-bio interaction between superparamagnetic iron oxide nanoparticles and *Caenorhabditis elegans*”

ICMAB and ICN2. 6th-7th Jun. 2019

- 3rd Scientific Meeting of BCN-b Students -Oral

“Evaluation of the nano-bio interactions between Au-NPs and *Caenorhabditis elegans*”

Barcelona 7th-8th Nov. 2017

- ICMAB Scientific School On Materials For Biomedical Applications (MATBIO2017)-Hands-on activities ICMAB. 19th-22nd Jun. 2017

- VI Spanish Worm Meeting-Poster

“Evaluation of the nano-bio interactions between Au-NPs and *Caenorhabditis elegans*”

Valencia. 9th-10th Mar. 2017

Grants and fellowships

- 4-year PhD scholarship 2016-2020: Awarded by Chinese Scholarship Council.
- Travel grant 2017: For the travel to VI Spanish Worm Meeting, Valencia, Spain. 2017; 150 €.

Participations in science projects

- ALBA synchrotron "Investigation Lutein tissues localization and oxidation in Lutein-treated *Caenorhabditis elegans* by synchrotron Fourier Transform Infrared Microscopy", Beam line BL01-MIRAS, A+ grade, 2018. PI Anna Laromaine.
- ALBA synchrotron "Investigation of tissue oxidation in nanoparticle-treated *Caenorhabditis elegans* by synchrotron Fourier Transform Infrared Microscopy", Beam line BL01-MIRAS, A+ grade, 2017. PI Anna Laromaine.
- Fundación l'Óreal, for women in Science "El uso de *Caenorhabditis elegans* (*C. elegans*) para facilitar la translación de nanopartículas (NPs) en la industria cosmética y de la alimentación, (Jan. 2017-Dec. 2017); 15.000€. PI Laromaine.
- MAT2015-64442-R MINECO, Engineering Bacterial Cellulose Nanocomposites (E-BCN), (1st Jan. 2016-31st Dec. 2018); 180.000 €. PI Laromaine
- Acción COST, Group of *C. elegans* New Investigators in Europe (GENIE), (2015-2019); BM1408. PI Laromaine.

Students' supervision

- Master student Gerrit Bredeck (Apr. 2018-Sep. 2018), University Düsseldorf

Project: "Evaluation of (bacterial) cellulose on *C. elegans*"

- Master student Genís Rabost (Oct. 2017-Mar. 2018), Universitat Autònoma de Barcelona

Projects: "Nanoparticles interactions with living organisms: *C. elegans* and SPIONs."

- Undergraduate student Maria Segarra (Mar. 2017-Sep. 2017), Universitat Autònoma de Barcelona

Projects: "Basic studies of *Caenorhabditis elegans*, Visualization of intestinal lumen Inactivation of food source Life cycle of mutant strains."

Technical skills

- Use of techniques such as Dynamic Light Scattering (DLS), Ultraviolet-visible spectroscopy (UV-Vis), Light microscopy (LM), optical microscopy, Synchrotron Fourier-transform infrared spectroscopy (FTIR).
- *C. elegans* culture techniques
- Biochemical staining methods

Languages

- Chinese: native speaker
- English: TOFEL 99 scores, 2016.